LPC REPORT NO. 57-

Structural Integrity Department / Research Division

THERMAL STRESS INVESTIGATION OF SOLID PROPELLANT GRAINS

VOLUME 1 - Theory and Experiment

by

J. JONES
J. E. FITZGERALD
E. FRANCIS

MAY 1963

This research was supported by the Space Systems Division, Air Force Systems Command, United States Air Force, Edwards Air Force Base, California, under Contract No. AF04 (611) - 8013.

Lockheed Propulsion Company

LPC Report No. 578-F

THERMAL STRESS
INVESTIGATION OF SOLID PROPELLANT GRAINS

VOLUME I - THEORY AND EXPERIMENT

by

J. Jones,
J. E. Fitzgerald
E. Francis

May 1963

Approved by:

J. E. Fitzgerald
Director of Research

This research was supported by the Space Systems Division, Air Force Systems Command, United States Air Force, Edwards Air Force Base, California, under Contract No. AF 04(611)-8013

CONTENTS

		Page
1	INTRODUCTION	1-1
2	THERMAL FIELD DETERMINATION	2-1
	2.1 GENERAL	2-1
	2.2 TEMPERATURE FIELDS IN CIRCULAR PORT GRAINS	2-3
	2.2.1 Biot's Approximation Method	2-3
	2.2.2 External Step Function Temperature Input	2-4
	2.2.3 Arbitrary External Temperature Variation	2-11
	2.3 PROPELLANT THERMAL PROPERTIES	2-14
	2.3.1 Conductivity, Specific Heat and Diffusivity	2-14
	2.3.2 Linear Expansion	2-16
	2.3.3 Heat Transfer Coefficients	2-16
	2.4 EXPERIMENTAL TEMPERATURE DISTRIBUTIONS IN CIRCULAR PROPELLANT GRAINS	2-20
	2.4.1 External Step Temperature Variation	2-20
	2.4.2 Arbitrary External Temperature Variation	2-20
	2.5 DISCUSSION	2-33
3	PROPELLANT VISCOELASTIC CHARACTERIZATION	3-1
	3.2 REDUCED VARIABLE CONCEPTS	3-2
	3.2.1 Basic Reduced Variable Relationships	3-3
	3.2.2 Reduced Variable Treatment for Linear Viscoelastic Materials	3-4
	3.2.3 Power Law Approximations to the Viscoelastic Stress-Strain Law	3-10
	3.3 PROPELLANT VISCOELASTIC DATA	3-13
	3.5 DISCUSSION	3-18

CONTENTS
(continued)

		Page
4	GRAIN THERMAL STRESS ANALYSIS	4-1
	4.1 BACKGROUND	4-1
	4.2 TRANSIENT THERMAL STRESS CALCULATIONS	4-2
	4.3 ELASTIC AND VISCOELASTIC LIMIT ANALYSIS	4-16
	4.4 PHOTOTHERMOVISCOELASTICITY	4-17
	4.4.1 University of Washington Subcontract Work	4-18
	4.5 DISCUSSION	4-28
	4.5.1 Transient Thermal Stress Computation	4-28
	4.5.2 Thermal Stress Accumulations	4-30
	4.5.3 Peak Thermal Stresses for Shock Cooling	4-30
	4.5.4 Photothermoviscoelasticity	4-31
5	GRAIN FAILURE ANALYSIS	5-1
	5.1 BACKGROUND	5-1
	5.2 MOTOR ANALOG EXPERIMENTS	5-2
	5.2.1 Rapid Monotonic Cooling Test	5-2
	5.2.2 Thermal Shock Experiments	5-9
	5.2.3 Cyclic Experiments	5-9
	5.3 DISCUSSION	5-14
	REFERENCES	5-16
	APPENDIX A THERMAL FIELD SOLUTIONS	A-1
	APPENDIX B ON THE THEORY OF PHOTOVISCO-ELASTICITY	B-1

TABLES

		Page
3-1	TEMPERATURE-TIME REDUCTION PARAMETERS	3-17
4-1	LIST OF SYMBOLS	4-3

FIGURES

		Page
2-1	Geometry and Related Coordinates	2-5
2-2	Transient Temperature Distribution for a Hollow Cylinder	2-7
2-3	Change of Inner Port Temperature with Time	2-10
2-4	Time-Temperature Distribution in a Hollow Cylinder (port insulated) with Zero Initial Temperature and a Suddenly Applied Surface Temperature, T_o	2-12
2-5	Temperature-Time Distribution for a Double Step Input	2-13
2-6	Cenco-Fitch Thermal Conductivity Apparatus	2-15
2-7	Quartz Tube Dilatometer	2-17
2-8	Heat Transfer Coefficient Test	2-19
2-9	Sealrite Casting Assembly (side view)	2-21
2-10	Sealrite Casting Assembly (top view)	2-22
2-11	Temperature versus Time in a Solid Cylinder Subjected to a Sudden Temperature Change at r = o	2-23
2-12	Temperature versus Time in a Solid Cylinder Subjected to a Sudden Temperature Change at r = 0.45 b	2-24
2-13	Temperature versus Time in a Solid Cylinder Subjected to a Sudden Temperature Change at r = 0.896	2-25
2-14	Temperature versus Time, r = o, Sequential Step Surface Temperature Variation	2-26
2-15	Temperature versus Time, r = 0.466, Sequential Step Surface Temperature Variation	2-27
2-16	Temperature versus Time at r = 0.896, Sequential Step Surface Temperature Variation	2-28
2-17	Liquid Bath Temperature versus Time	2-30
2-18	Temperature versus Time, r = 0.890b, Continuous Surface Temperature Variation	2-31
2-19	Temperature versus Time, r = 0.45b, Continuous Surface Temperature Variation	2-32

FIGURES
(continued)

		Page
3-1	Spring and Dashpot Analog	3-4
3-2	Parallel Assemblages of Model Analog	3-6
3-3	Constant Rate Master Curve, Polycarbutene-R Propellant	3-14
3-4	Log a_T versus Temperature, Polycarbutene Propellant, Constant Strain Rate Data	3-12
4-1	Hoop Stress at Port versus Time for Step, Step with a Jog, and Cyclic Thermal Inputs	4-6
4-2	Case-Grain Interface Pressure versus Time for Step, Step with a Jog, and Cyclic Thermal Inputs	4-7
4-3	Hoop Strain at Port versus Time for Step, Step with a Jog, and Cyclic Thermal Inputs	4-8
4-4	Hoop Stress at Port versus Temperature for Stairstep Thermal Inputs	4-9
4-5	Peak Port Hoop Stress versus Temperature Step and Grain O.D. to I.D. Ratio	4-11
4-6	Peak Port Hoop Stress versus Temperature Step and Grain O.D. to I.D. Ratio	4-12
4-7	Case-Grain Interface Pressure versus Temperature Step and Grain O.D. to I.D. Ratio	4-13
4-8	Case-Grain Interface Pressure versus Temperature Step and Grain O.D. to I.D. Ratio	4-14
4-9	Peak Thermal Stress Scale Factor versus Grain Outer Diameter Ratio	4-15
4-10	Plane Polariscope for Transient Loadings	4-21
4-11	Mechanical and Optical Creep Test	4-22
4-12	Mechanical Creep	4-23
4-13	Optical Creep	4-24
4-14	Diffused Light Polariscope for Material Characterizations	4-25
4-15	Material Calibration Apparatus	4-26

FIGURES
(continued)

		Page
5-1	5-inch Diameter by 14-inch Long Circular Port Analog Motor	5-3
5-2	Port Diameter Measurement Taken Using a Mueller Gage	5-4
5-3	Analog Motor Test Data, Motor No. 1	5-5
5-4	Analog Motor Test Data, Motor No. 2	5-6
5-5	Analog Motor Test Data, Motor No. 3	5-7
5-6	Analog Motor Test Data, Motor No. 4	5-8
5-7	Analog Motor Experiments Shock Cooling	5-10
5-8	Shock Heating Experiment, 4 by 14-inch Analog Motors	5-11
5-9	Cyclic Conditioning Test, 4 by 14-inch Analog Motor	5-12
A-1	Penetration Depth versus Time	A-2
A-2	Outer Surface Temperature Distribution for Various Times	A-5
A-3	Time-Temperature Variation in a Hollow Cylinder with Zero Initial Temperature and a Suddenly Applied Surface Temperature, T_o, on the Inner Port (outer surface insulated)	A-7
A-4	Time-Temperature Distribution of a Hollow Cylinder with Zero Initial Temperature and a Suddenly Applied Surface Temperature, T_o, on the Outer and Inner Surfaces	A-9
B-1	General Plane Wave	B-7
B-2	Plane Wave Propagating Along One Principal Axis, Case 1	B-8
B-3	Directions of Plane Waves	B-10
B-4	Principal Axes	B-21

Section 1

INTRODUCTION

The purpose of this program was to conduct an investigation of the effects of an arbitrary thermal input on the behavior of a case-bonded solid propellant rocket grain. The following paragraphs list some of the specific tasks that were carried out under this program.

(1) Development of a usable technique for the prediction of the transient temperature distribution through a case-bonded propellant grain subjected to arbitrary time-dependent thermal inputs. This was done using Biot's approximation solution to the Fourier heat conduction equation and the predictions obtained therefrom were confirmed in a series of motor experiments. The theory and experimental results are presented in Volume I.

(2) Development of a usable technique for the determination of stress and strain in a case-bonded real viscoelastic propellant grain subjected to the above arbitrary thermal inputs. This task (reported in Volume II) was accomplished with Purdue University under subcontract; Purdue conducted the theoretical study and Lockheed Propulsion Company carried out the computer programing and solution (Volume I) with the assistance of the Mathematical Section of the Lockheed-California Company and their IBM 7090 facility.

(3) Determination of the pertinent viscoelastic and thermal characterizations of propellant materials for use as described in items (1) and (2) above. This determination was made at LPC for typical rubber-base propellants. The methods used and the results obtained are reported in Volume I.

(4) Determination of applicable failure criteria for thermal cycling and, using analog motors, the confirmation of these criteria. The results are contained in Volume I.

(5) Reduction to engineering practice of the above analytical methods, using limit analysis as well as engineering methods for gravitational slump and acceleration set-back. These results are presented in the form of an engineering handbook (Volume III) which also includes simplified methods for determination of the viscoelastic operators.

(6) Application of the above methods for the determination of the thermal environment capabilities of various large booster motors. These results are contained in Volume III-A, which is a classified addendum to Volume III.

(7) Determination of the existence of a generalized cyclic thermal input over a fixed temperature range which will produce a greater tendency to failure than a step function input over the same range. This problem was not resolved analytically. However, a series of calculations for a wide range of motor sizes and input variations was carried out. Within the limits of accuracy of the computer solution, no situation was found wherein the cyclic input caused stresses or strains exceeding those produced by a step input. The worst failure condition still was found to be that of a motor subjected to rapid cooling to a low temperature, followed -- after thermal equilibrium was established -- by rapid external heating. In one sense this is a cyclic input, but not in the sense of the originally posed question regarding stress accumulation beyond the step input condition. Questions of cyclic fatigue are not considered the same as stress build-up.

(8) Determination of a method of stress analysis using dynamic birefringence on viscoelasticity -- or photoviscoelasticity, as it is frequently called. The experimental work was carried out by New York University and fully reported in previously published quarterly reports to this program. Unfortunately, the plasticized Hysol material used was tested over a temperature range which included the transition point temperature of the material. Further, the experimental results did not superpose, indicating that:

(a) the material was not linearly viscoelastic or that

(b) the experimental determinations of creep and temperature were not carried out with sufficient precision.

Basically, however, it was determined during the course of this program that a proper theory for the interpretation of stresses using photoviscoelasticity did not factually exist. This problem was then defined and a theoretical treatment is given in Appendix B of Volume I. Experimental confirmation is now in progress under other programs at the California Institute of Technology, the University of Washington, and at Lockheed Propulsion Company.

Thus, to accomplish the subject purpose of the program, and to present the results in a readily usable form, the main body of this report has been divided into five main sections.

Section 2, Thermal Field Determination, presents all of the necessary analytical and experimental techniques for the determination of the time-dependent temperature distribution in a circular port grain subjected to an arbitrary external temperature variation. The results predicted by theory are shown to be accurately confirmed in experimental grains.

One aspect of the above analysis which has not been treated is that concerning the determination of the heat transfer boundary conductance. Effectively, the boundary conductance has been considered herein as infinite; the motor case thermal conductivity also was considered as infinite. For the purpose, these assumptions give answers on the safe side. In actual fact, these assumptions affect the answer but slightly for an insulating or semi-insulating material such as rocket grains, and experimental results confirm this fact. Thus, using the methods delineated herein, the problems of high speed aerodynamic induced heat transfer are readily computed.

The computational demands upon the user are reduced by the inclusion of a series of dimensionless graphs which enable ready scaling of results for various sizes of rocket motors.

Section 3, Propellant Viscoelastic Characterization, presents a brief review of reduced variable relationships for viscoelastic materials. In addition, it presents that the utilization of approximate power law relationships leads to greatly reduced effort in the utilization of the previously mentioned scaling laws.

Section 4, Grain Thermal Stress Analysis, presents the actual purpose of this work. The summary of results is presented in this volume and the complete details of the analysis are given in Volume II. The simplified limit analysis is given whereby the maximum stress or strain for a given temperature difference may be calculated. For temperature cycling, the full solution is required. Some of the examples show that the maximum stress under a cycled condition may be considerably less than the limit solution -- a result that may be extremely useful for marginal grain designs. Section 4 includes a discussion of the theoretical aspects of photothermoviscoelasticity.

Section 5, Grain Failure Analysis, concerns the experimental verification of the pertinent failure criteria associated with the thermal problems treated.

The two appendices to this volume treat more fully the subjects of Thermal Field Solutions (Appendix A), and the Theory of Photoviscoelasticity (Appendix B).

Section 2

THERMAL FIELD DETERMINATION

2.1 GENERAL

Thermal stress determination in elastic solids requires knowledge only of the instantaneous spatial distribution of temperature. Furthermore, there are many thermo-elastic problems requiring only knowledge of the average temperature for approximate solutions to the stress-strain problem.

As might be expected, however, viscoelastic solids require not only the instantaneous spatial temperature field determination, they also require the determination of the entire time history of the spatial temperature field.

Thus, this section is devoted to the following:

- Analytical determination of time varying spatial temperature distributions (Section 2.2.1 and 2.2.2)
- Numerical solution of the resulting thermal field problem for arbitrary temperature inputs (Section 2.2.2)
- Experimental determination of the pertinent propellant and motor thermal properties (Section 2.3)
- Experimental verification of the temperature distribution with the above thermal properties in cylindrical motor grains, and in circular port motors. (Section 2.4)

The laboratory determination of the pertinent propellant thermal properties (density, ρ; conductivity, c ; and specific heat,k) indicated a rather trivial variation of these properties with temperature over the temperature range of interest, -100^0F to $+160^0$F. Thus, to make the problem more tractable to analysis, the assumption is made throughout that the above thermal properties do not vary with temperature.

Again, with the intent of producing a tractable analytical formulation of the problem, Biot's approximate solution to the Fourier heat conduction equation is used rather than attempting a rigorous solution. (Boley and Weiner, 1960, p-224f)

The excellent correlation between the predicted temperature fields in both time and space and the resulting measurement in test motors justifies the use of all the aforementioned simplifying assumptions.

2.2 TEMPERATURE FIELDS IN CIRCULAR PORT GRAINS

2.2.1 Biot's Approximation Method

The solution of the Fourier heat conduction equation usually leads to forms of solutions which are computationally cumbersome. As an engineering alternative, therefore, Biot's approximation method (Boley and Weiner, 1960, p.226) will be used. A brief description is given below for the case of axisymmetrical temperature input to the outside of an infinitely long cylindrical propellant grain with temperature independent thermal properties and an insulated circular port.

The temperature, T, must satisfy the heat conduction equation (one-dimensional because of axial symmetry)

$$k \frac{\partial^2 T}{\partial n^2} = \rho c \frac{\partial T}{\partial t} \tag{2-1}$$

where

T = temperature

n = direction of heat flux

t = time

k = specific heat

ρ = density

c = thermal conductivity

and defining a heat flow vector H by

$$k \frac{\partial^2 T}{\partial n^2} = \rho c \frac{\partial T}{\partial t} = - \frac{\partial^2 H}{\partial n \partial t} \tag{2-2}$$

so that it follows

$$\rho c T = - \frac{\partial H}{\partial n} \qquad \text{or} \qquad H = - \int_{q_1}^{n} \rho c T dn \tag{2-3}$$

and

$$k \frac{\partial T}{\partial n} = - \frac{\partial H}{\partial t} \quad . \tag{2-3a}$$

where q_1 is the depth to which heat has penetrated at time, t.

Employing variational techniques, one can derive functions

$$V = \frac{1}{2} \rho c \int_0^r T^2 \, dn, \text{ the thermal potential}$$

$$D = \frac{1}{2k} \int_0^{q_1} \left(\frac{\partial H}{\partial t}\right)^2 dn, \text{ the dissipation function} \qquad (2\text{-}4)$$

and

$$Q = T(t) \frac{\partial H}{\partial q_1} \Bigg|_{n=o}, \text{ the thermal force}$$

which must satisfy the Lagrangian

$$\frac{\partial V}{\partial q_1} + \frac{\partial D}{\partial \dot{q}_1} = Q \qquad (2\text{-}5)$$

Solution of the above equation then requires

- specifying the heat input at the surface, thus determining the thermal force, Q, and
- specifying the spatial temperature, T, so that the function H and hence the functions V and D may be determined.

The solution of Equation (2-5) will yield the penetration depth, q_1, as a function of time and hence the spatial distribution as a function of time.

Because of the Lagrangian Equation (2-5), the form of the temperature distribution specified through the body must be that of a potential function.

2.2.2 External Step Function Temperature Input

Applying the results of the previous section to a circular port grain with an insulated port and a step function temperature input on the outside requires specifying the spatial distribution of T, temperature.

Referring to Figure 2-1, the geometrical coordinates are

b = outer radius of grain

a = inner radius

r = radius at any point.

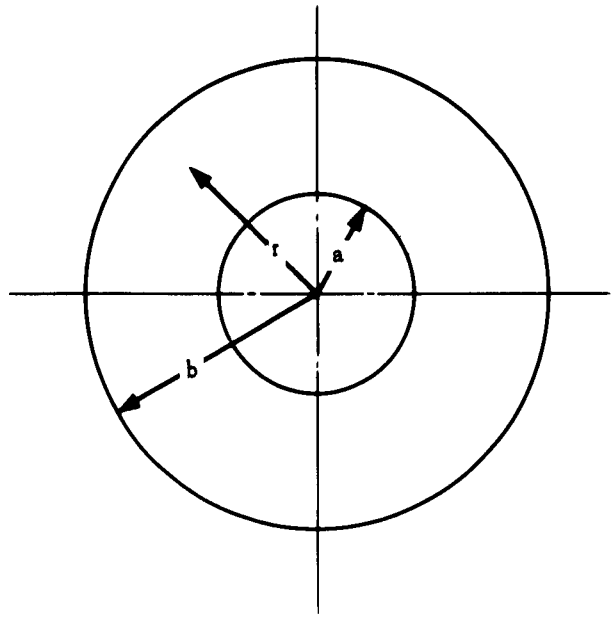

234

Figure 2-1 Geometry and Related Coordinates

Two time regimes are defined:

- The time, t, range $o < t < t_a$, where t_a is the time necessary for the heat front (defined as the distance q_1 from the outside to reach the inner port
- The time range $t_a \leq t \leq \infty$ after the heat front has reached the inner port

The input function for the step temperature is

$$T(t)\Big|_{r=b} = T_o\, U(t) \tag{2-6}$$

where U(t) is the unit step function.

The spatial temperature is assumed in the quadratic form for the time range until the heat front reaches the inner port as

$$T(r) = \begin{cases} T_o\left[1 - \dfrac{b-r}{q_1}\right]^2 ; & b - r \leq q_1 \text{ and } o \leq t \leq t_a \\ \\ O \qquad\qquad ; & b - r \geq q_1 \text{ and } t_a \leq t \leq o \end{cases} \tag{2-7}$$

Rewriting Equations (2-1) through (2-5) in polar coordinates, defining Equation (2-3) for H in terms of Equation (2-6) for T_o at r = b, defining V and D in terms of T(r) and H, and solving Equation (2-5) yields the relation

$$q_1^2\, \dot{q}_1 - 2bq_1\, \dot{q}_1 = -10\, \kappa\, b \tag{2-8}$$

where

$$\kappa = \frac{k}{\rho c}\text{, thermal diffusivity, } ft^2/sec$$

for the penetration depth, q_1, in terms of k, b, and t (Figure 2-2).

Solving the differential Equation (2-8) for q_1 then yields the cubic

$$\frac{q_1^3}{3} - bq_1^2 = -10\, \kappa\, b\, t \tag{2-9}$$

whose one real root of significance is

$$q_1 = b\left[2\cos\left(\frac{\theta + 4\pi}{3}\right) + 1\right] \tilde{=} b\sqrt{11.03\,\eta^2} \tilde{=} \frac{10}{3}\,\eta b \tag{2-10}$$

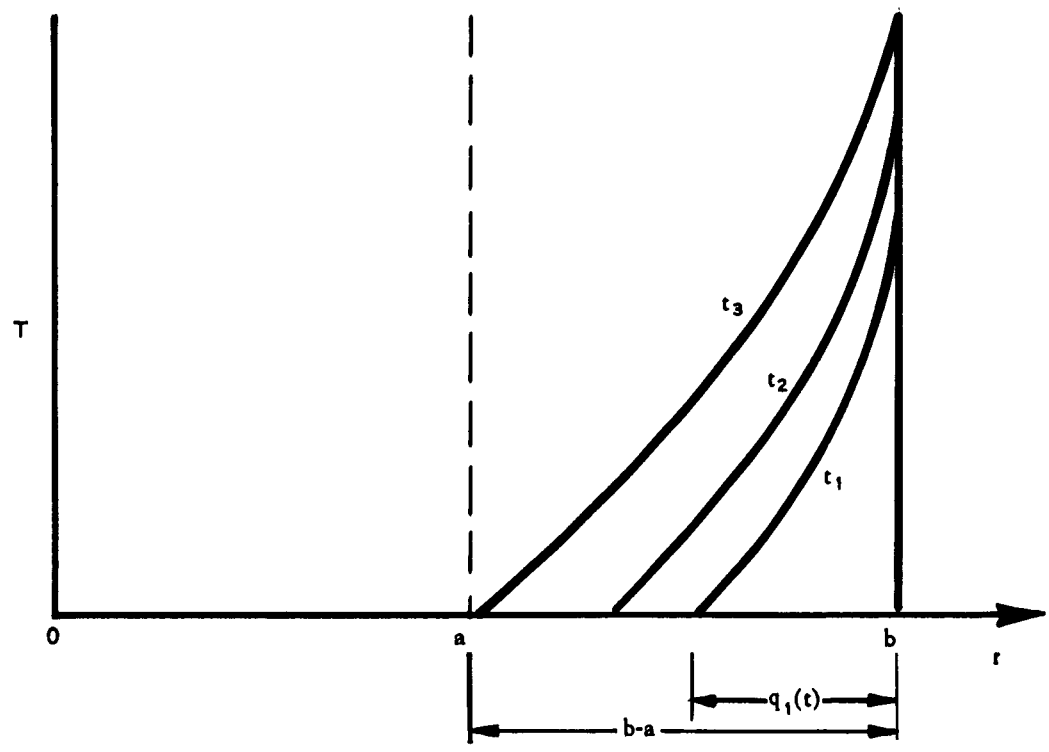

Figure 2-2 Transient Temperature Distribution for a Hollow Cylinder

where

$$\cos\theta = 1 - 15\eta^2 \tag{2-11}$$

and

$$\eta^2 = \frac{\kappa t}{b^2}\text{, thermal diffusion parameter} \tag{2-12}$$

Rewriting Equation (2-10) and Equation (2-12) as

$$q_1 = \frac{10}{3}\sqrt{\kappa t}$$

it can be seen that the time, t_a, for the heat to reach the inner port, $q_1 = b-a$ is, letting $\lambda = b/a$

$$t_a = \frac{0.09\,b^2}{k}\left(\frac{\lambda - 1}{\lambda}\right)^2 \tag{2-13a}$$

or somewhat more accurately

$$t_a = \frac{b^2}{30\kappa}\left(\frac{2\lambda^3 - 3\lambda^2 + 1}{\lambda^3}\right) \tag{2-13b}$$

In the limit as $a \to o$ and $\lambda \to \infty$ for a solid cylinder

$$t_a \to \frac{2b^2}{30\kappa}$$

and for a thin cylinder as $a \to b$ and $\lambda \to 1$

$$t_a \to O\ .$$

It is more convenient to work with the thermal diffusion parameters instead of the time, since the solution is then nondimensionalized to facilitate its extension to different cylinder sizes and materials. From Equation (2-13b) then

$$\eta_a^2 = \frac{1 - 3\lambda^2 + 2\lambda^3}{30\lambda^3}\ . \tag{2-14}$$

As λ approaches 1.0, η_a^2 approaches zero. That is, the heat front traverses an infinitely thin cylinder instantaneously.

Once the temperature field reaches the inner port a new function must be selected in lieu of Equation (2-7).The new function must meet the following requirements:

- At r=a the temperature must gradually increase until the temperature of the entire cylinder approaches a constant value (Figure 2-3).
- Since the inner port was assumed insulated, the derivative of the temperature with respect to r must be zero at r=a.

For all $t \geq t_a$ or $\eta^2 \geq \eta_a$ the following thermal field was assumed:

$$T = T_o \left[1 - \frac{T_a}{T_o}\right] \left[1 - \frac{(b-r)^2}{(b-a)}\right] + T_a \qquad (2\text{-}15)$$

where T_a is defined in Figure 2-3.

Setting r=a, it is clear that T_a represents the temperature at the inner port, and, hence, is a function of time. The procedure for finding this functional relationship is similar to that used for q_1, yielding

$$T_a = T_o \left[1 - e^{-\gamma(\overline{\eta}^2 - 1)}\right] \qquad (2\text{-}16)$$

where

$$\gamma = \frac{10\lambda^3[3\lambda+1]\eta_a^2}{(\lambda-1)^2[5\lambda+1]} = \frac{[3\lambda+1][2\lambda+1]}{3\lambda[5\lambda+11]} \qquad (2\text{-}17)$$

and where

$$\overline{\eta}^2 = \frac{t\kappa}{\eta_a^2 b} = \frac{\eta^2}{\eta_a^2}$$

An inspection of Equation (2-16) reveals that when

$$\eta^2 = \eta_a^2 \; ; \; \overline{\eta}^2 = 1$$

then

$$T_a = 0$$

when

$$\overline{\eta}^2 \rightarrow \infty \; ; \; T_a \rightarrow T_o$$

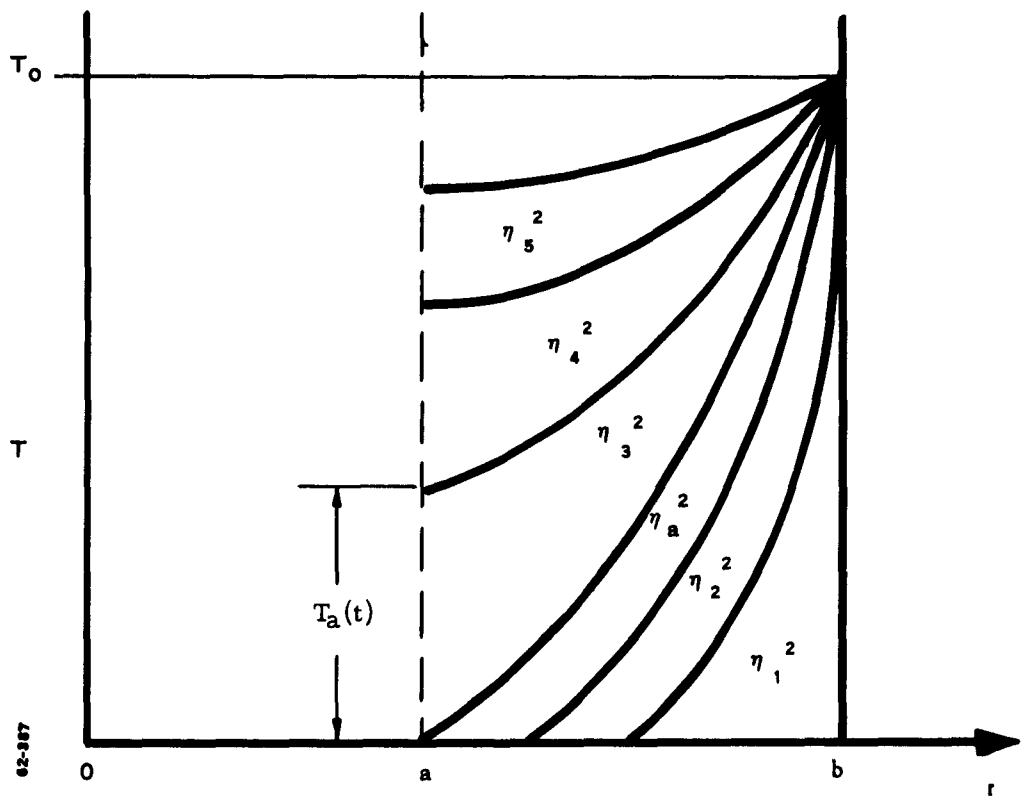

Figure 2-3 Change of Inner Port Temperature with Time

Since, as stated above, T_a represents the temperature of the inner port, the relation for T_a is physically reasonable. The results for a cylinder with b/a equal to 2 are shown in Figure 2-4. Equations (2-7) and (2-15) completely describe the temperature distributions in a hollow cylinder with an insulated inner port and a case-temperature variation consisting of a step change T . The values of t_a, q_1 T_a, and γ can be determined from Equations (2-5), (2-13), (2-16), and (2-17) for given values of λ and κ. The parameter λ depends, of course, on the geometry and the thermal diffusivity κ on the type of propellant. Plots of η_a^2, γ, κ, and T_o are the only required input parameters necessary for the thermal field determination in any hollow cylinder with the aforementioned boundary conditions.

2.2.3 Arbitrary External Temperature Variation

In determining thermal fields for more general types of case-temperature variations, the following approach was used:

- Representation of an arbitrary surface temperature variation by a series of step changes. This allows the direct use of the step solution described in Section 2.2.2. The solution for a step surface temperature is known; hence, if a varying surface temperature is degenerated into discrete steps, the resulting thermal field can be accurately approximated by correctly adding the appropriate step solutions.

The use of this method is illustrated in the following example. Consider as before a hollow cylinder, initially at thermal equilibrium, subject to a step exterior surface temperature change at time zero. At the time when the resulting heat front arrives at the inside of the cylinder, a step exterior temperature change opposite in sign to the first condition is imposed. The temperature input and resulting thermal fields in the cylinder, obtained by superposition of the two-step input, are shown in Figure 2-5. Figure 2-5 indicates the complexity of interaction of the two heat inputs leading to a transient condition where heating and cooling proceed simultaneously in different parts of the cylinder. It is this interaction which makes cyclic inputs an interesting problem for viscoelastic materials. The analysis for this problem is given in Appendix A.

The method illustrated by the hollow cylinder example discussed above can be systematically extended to a sequence of step inputs without introducing any restrictive complexity, and was used for the initial evaluation of the viscoelastic thermal stress accumulation problem.

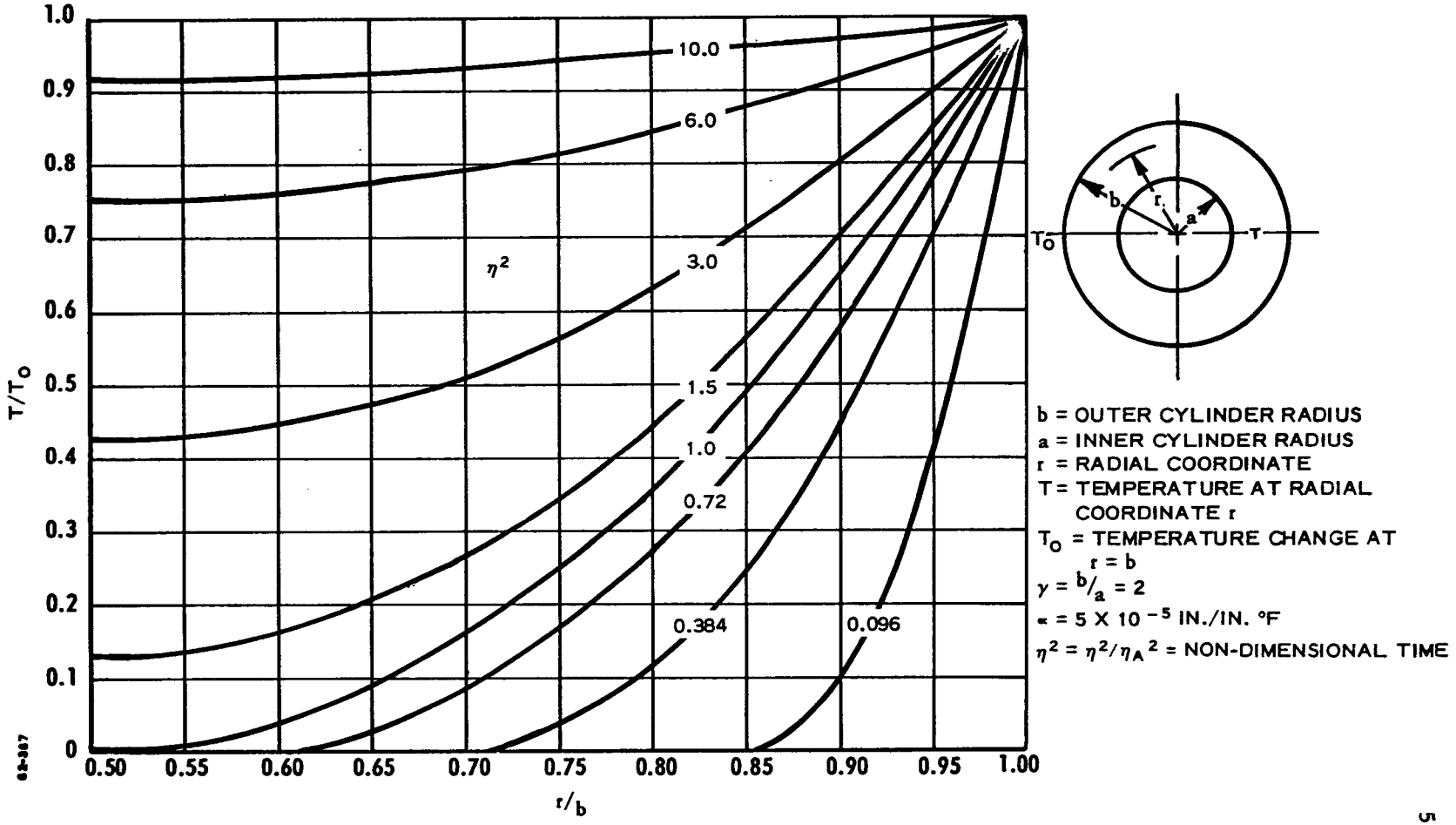

Figure 2-4 Time-Temperature Distribution in a Hollow Cylinder (port insulated) with Zero Initial Temperature and a Suddenly Applied Surface Temperature, T_o

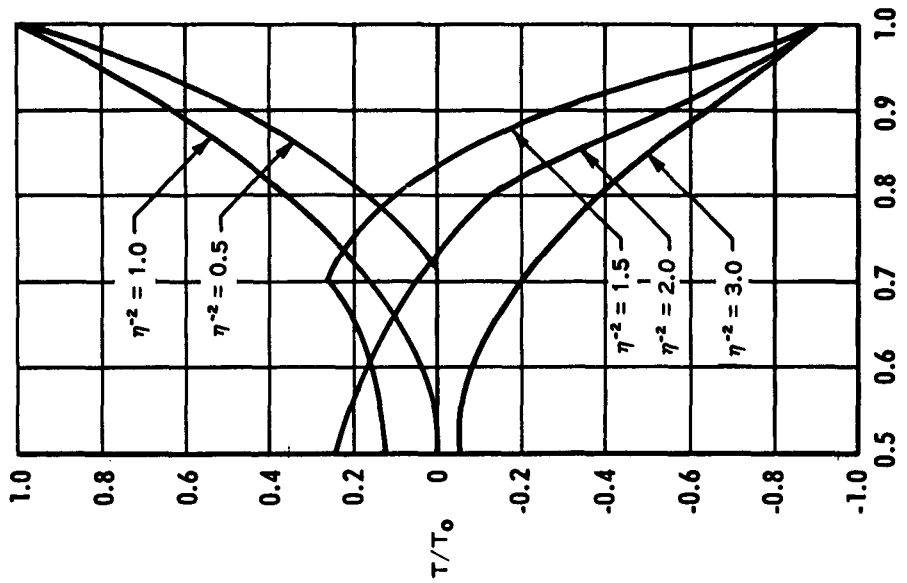

(b) TEMPERATURE DISTRIBUTION

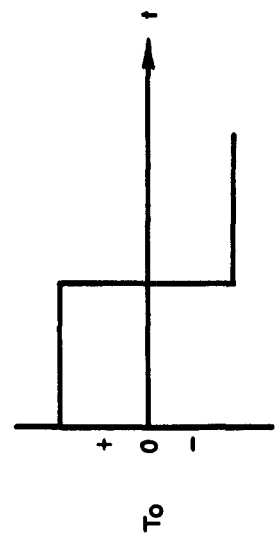

(a) THERMAL INPUT

Figure 2-5 Temperature-Time Distribution for a Double Step Input

2.3 PROPELLANT THERMAL PROPERTIES

2.3.1 Conductivity, Specific Heat and Diffusivity

Before numbers can be extracted from the thermal field solutions, the thermal properties must be obtained. The pertinent properties are:

c = thermal conductivity

κ = thermal diffusivity

k = specific heat

where

$\kappa = k/\rho c$, ρ = density

κ, k, and c are dependent on temperature. However, the inclusion of such a dependence in the heat conduction equation would result in a nonlinear equation whose solution would be too complicated to be of value for the present study. The experimental effort at LPC was directed at obtaining engineering values rather than scientific values for the thermal properties. It was felt that this approach would expedite the extraction of sufficiently accurate values for the properties for use in the thermal field calculations. The experimental values obtained for these constants, when used in the theoretical thermal field solutions, did in fact result in thermal field predictions which agreed accurately with the thermal field tests in the temperature range of interest (70^0 to -100^0F).

The experimental values for c, the thermal conductivity, were obtained using a standard Cenco-Fitch thermal conductivity apparatus (Figure 2-6). Tests of Polycarbutene R propellant gave an average value for c of

$$c = 9.34 \times 10^{-4} \frac{\text{Cal-Cm}}{\text{Sec-C}^2_{\text{in}}\text{-}^0\text{C}}$$

Measurements of the specific heat were performed using a standard laboratory calorimeter. The specimens were coated with silicone-base paint to prevent absorption of the conducting medium by the propellant sample. An average value for the specific heat as obtained from replicate tests was

$$k = 0.26 \text{ BTU/lb/}^0\text{F}$$

The resulting thermal diffusivity was calculated to be:

$$\kappa = 134.1 \times 10^{-6} \text{ ft}^2\text{/min.}$$

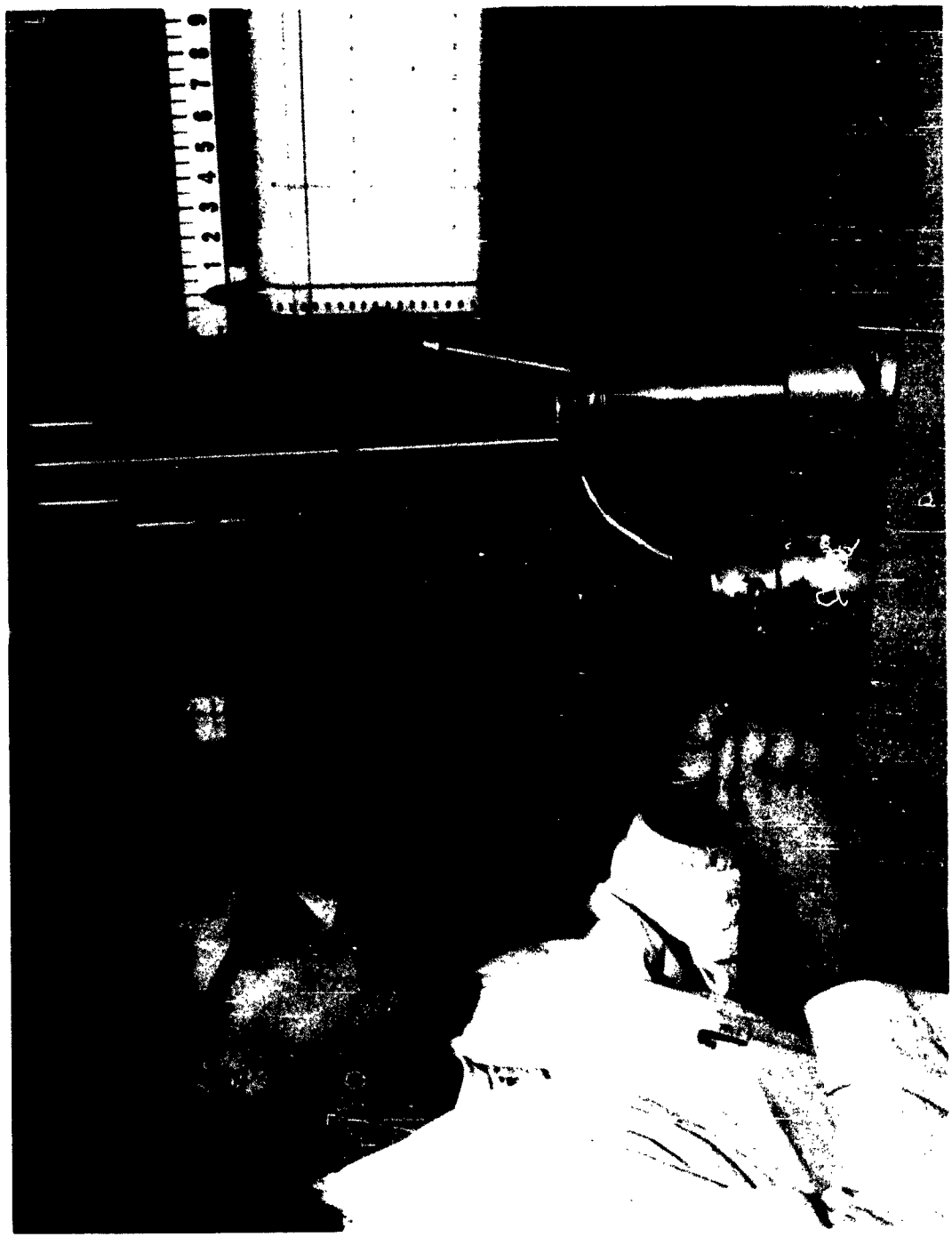

Figure 2-6 Cenco-Fitch Thermal Conductivity Apparatus

2.3.2 Linear Expansion

Experimental apparatus for measuring the coefficient of thermal expansion consisted of a simple quartz-tube linear dilatometer employing electronic means for length measurement (Figure 2-7).

The linear expansion thermal coefficient of Polycarbutene propellant in the 70^0 to -100^0F range was 5.6 ± 0.2 in./in./^{0}F.

2.3.3 Heat Transfer Coefficients

The determination of thermal fields for a motor placed suddenly into a conditioning box involves heat transfer through an air boundary layer and heat conduction through a composite cylinder composed of steel, rubber insulation, and a hollow grain. The heat transfer coefficient is a function of geometry, air temperature and air circulation. Each motor would have a different heat transfer coefficient; however, for practical considerations, a reasonable average value for the heat transfer coefficient could be used for different motors.

Two tests were performed at LPC to determine a suitable value for the heat transfer coefficient for a 4 by 10-inch, $\frac{1}{4}$-inch thick, steel case. The interior of the case was stuffed with insulating material and a thermocouple was embedded in the case. The resulting case temperature versus time was plotted. An approximate value for the heat transfer coefficient was then calculated based on the following assumptions:

- The temperature gradient through the case is small so that the case has a uniform but time-dependent temperature and no heat is lost through conduction into the interior.
- The heat input to the case is directly proportional to the difference in the ambient and case temperature.

These assumptions lead to the following relations:

$$q = h(T_o - T_c) \qquad (2\text{-}18)$$

where

q = heat input in BTU/hr

h = heat transfer coefficient in BTU/hr - ^{0}F

T_o = temperature of ambient air ^{0}F

T_c = temperature of case ^{0}F

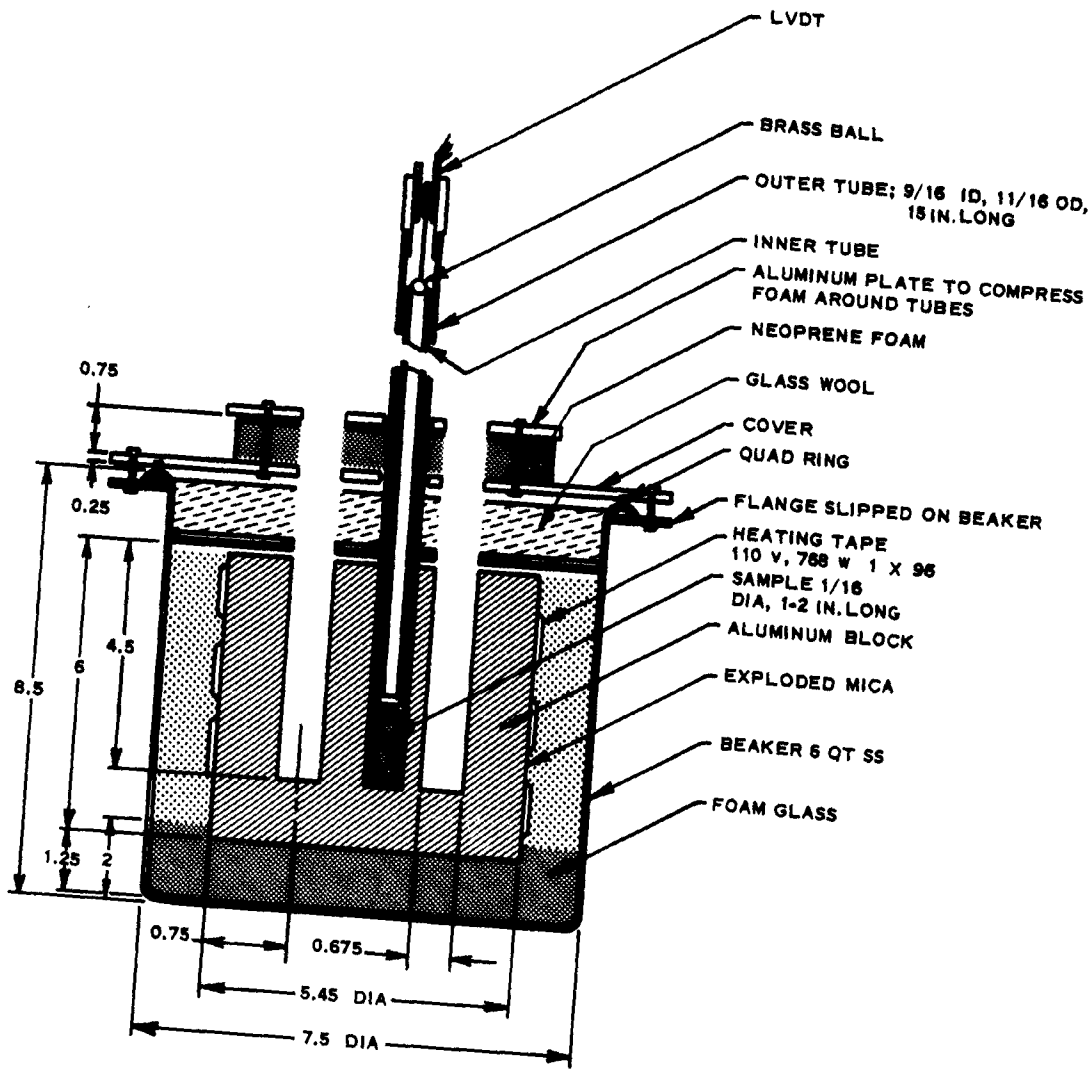

Figure 2-7 Quartz Tube Dilatometer

and

$$q = -MC_p \frac{d(T_o - T_c)}{dt} \tag{2-19}$$

where

M = total mass

C_p = specific heat of case

Substituting Equation (2-18) into Equation (2-19) results in

$$h(T_o - T_c) = MC_p \frac{d}{dt}(T_o - T_c) \tag{2-20}$$

hence

$$\overline{T} = \frac{T_o - T_c}{T_o} = e^{-ht/MC_p} \tag{2-21}$$

The relations indicate that a plot of $\overline{T}$ should be a straight line on semi-log paper and the value of h can be determined from the slope of this line. The plot of the experimental data obtained from tests on the steel case mentioned above did in fact prove to be a straight line on semi-log paper (Figure 2-8). The value for h as obtained from these tests was

$$h = 5.55 \text{ BTU}/^0\text{F-hr}$$

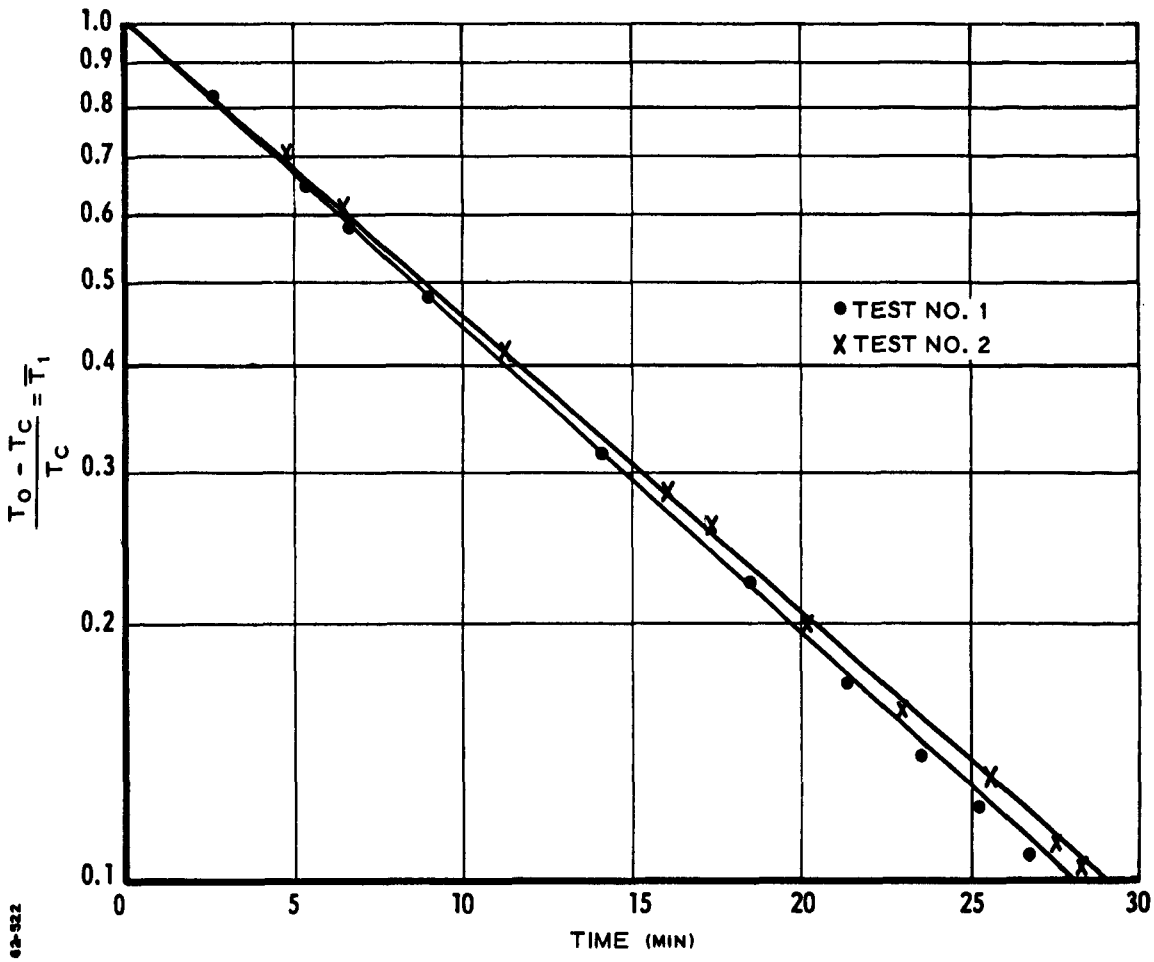

Figure 2-8 Heat Transfer Coefficient Test

2.4 EXPERIMENTAL TEMPERATURE DISTRIBUTIONS IN CIRCULAR PROPELLANT GRAINS

Experimental tests were performed at LPC to verify the approximate variational step solutions and other theoretical solutions based on them, as well as the accuracy of the thermal properties.

Thermocouples were cast in situ in 6-inch diameter cylindrical grains of Polycarbutene R propellant (Figures 2-9 and 2-10). The grains were solid cylinders with heavily insulated ends. During the tests the thermocouples were monitored to obtain the time-temperature variation at various radii in the grains.

2.4.1 External Step Temperature Variation

The step surface temperature variation test was performed by immersion of a laquer coated grain, initially at thermal equilibrium at 70^0F, in a liquid bath at 20^0F. The resulting temperature versus dimensionless time as measured at three radial positions in the grain are compared with the exact and approximate solutions in Figures 2-11, 2-12, and 2-13. The experimental values agree within 5 or 6 percent with those predicted by the approximate technique.

2.4.2 Arbitrary External Temperature Variation

Experiments in which sequential step and continuously varying thermal inputs were imposed on a solid cylinder were performed for evaluation of the superposition method of specifying thermal fields for time varying thermal inputs. In the sequential or double step experiment, a coated solid cylinder was subjected to a step surface temperature variation from equilibrium at 70^0F to 20^0F by immersion in fluid at the latter temperature. After conditioning at 20^0F for 45 minutes, the cylinder was immersed in a second liquid bath at 120^0F. The temperature variation with time was measured at different radial positions in the cylinder. In Figures 2-14, 2-15 and 2-16, data for the test are compared to predictions based on the step solution superposition approach previously described. The agreement between the predicted and measured temperature time variation was within 5 percent.

Evaluation was made of the effects of a continuously varying surface temperature on a solid grain by a test in which a grain was first subjected to a step decrease in surface temperature to 33^0F by liquid immersion. Subsequently, the surface temperature of the grain was warmed to 120^0F in the liquid bath

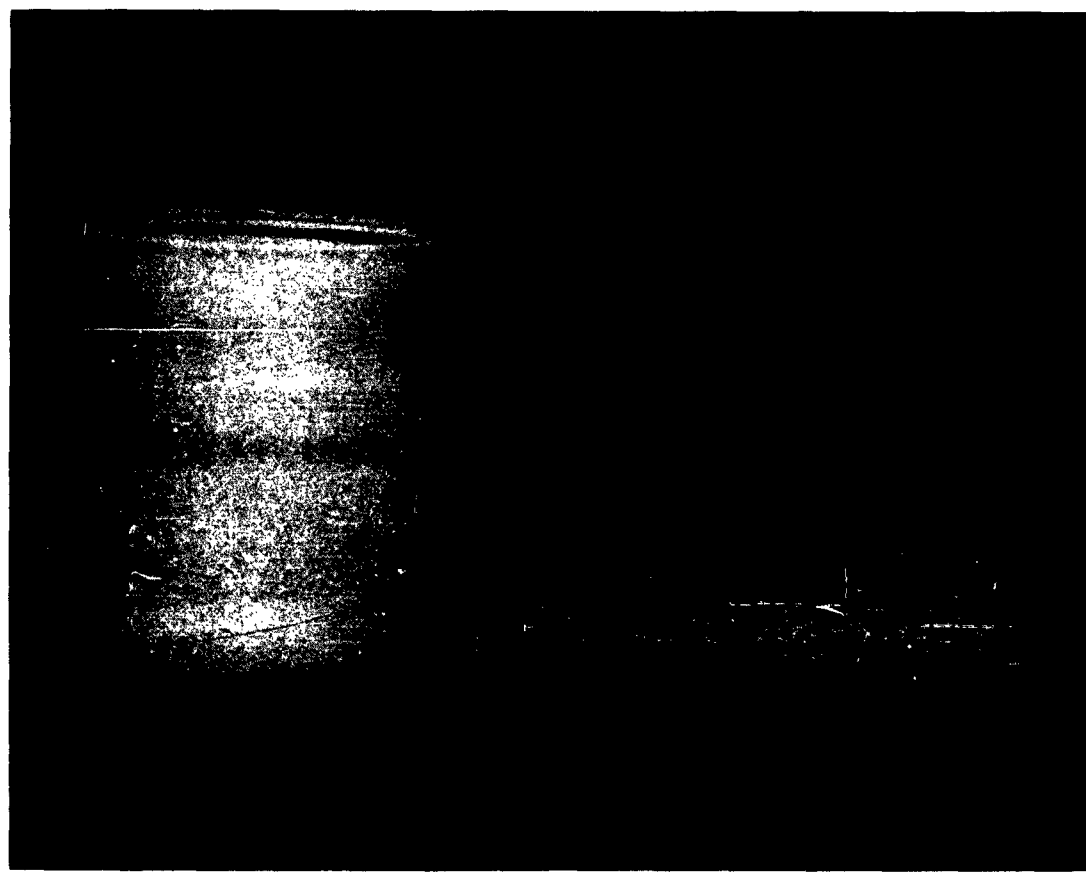

246

Figure 2-9 Sealrite Casting Assembly (side view)

245

Figure 2-10 Sealrite Casting Assembly (top view)

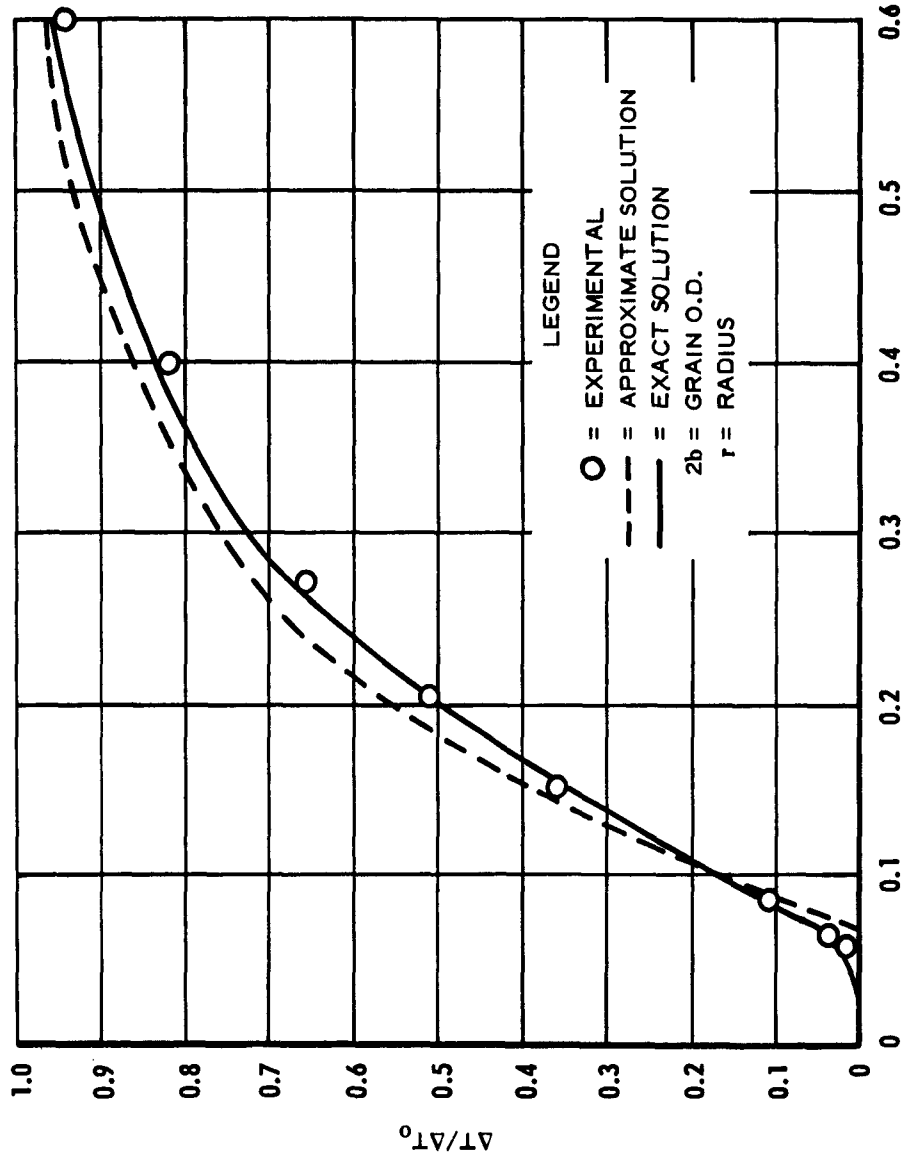

Figure 2-11 Temperature versus Time in a Solid Cylinder Subjected to a Sudden Temperature Change at r = 0.45 b

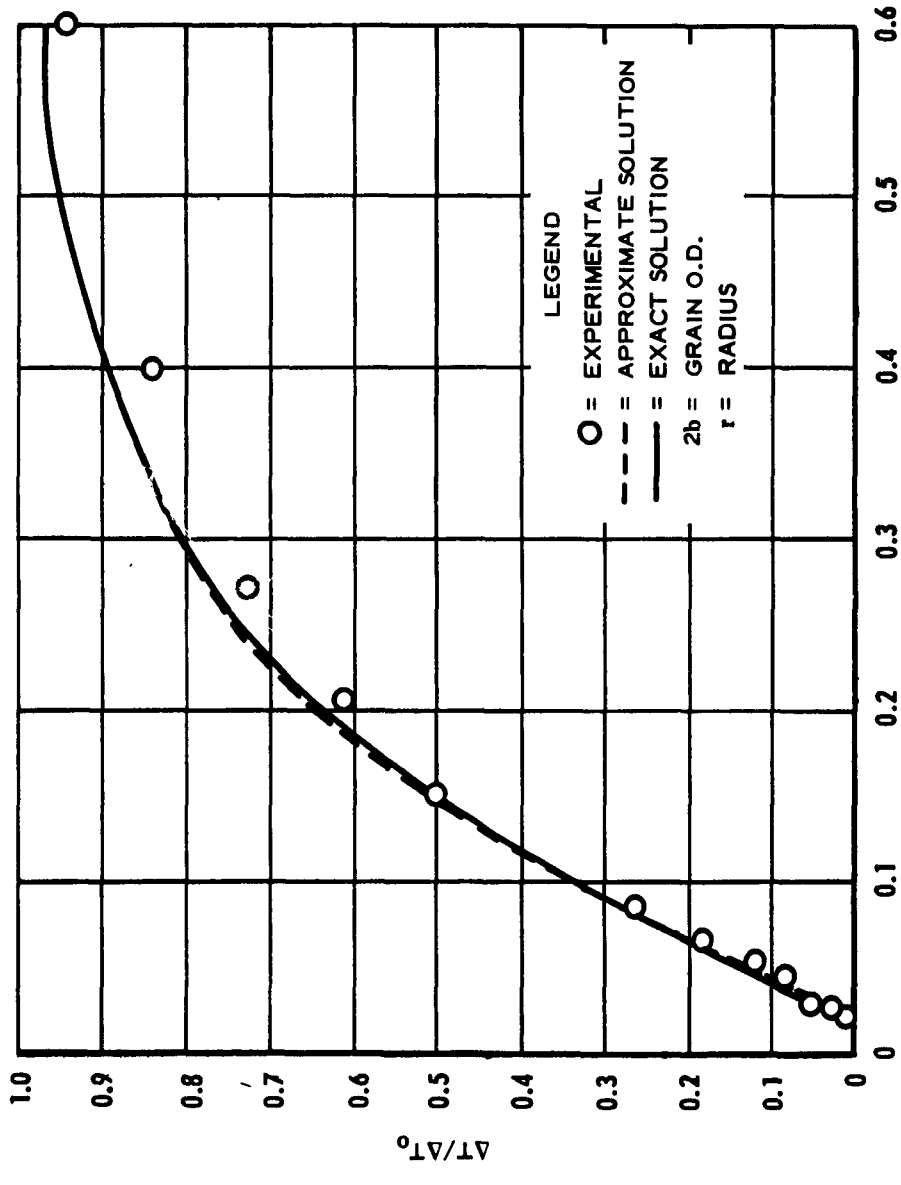

Figure 2-12 Temperature versus Time in a Solid Cylinder Subjected to a Sudden Temperature Change at r = 0.45 b

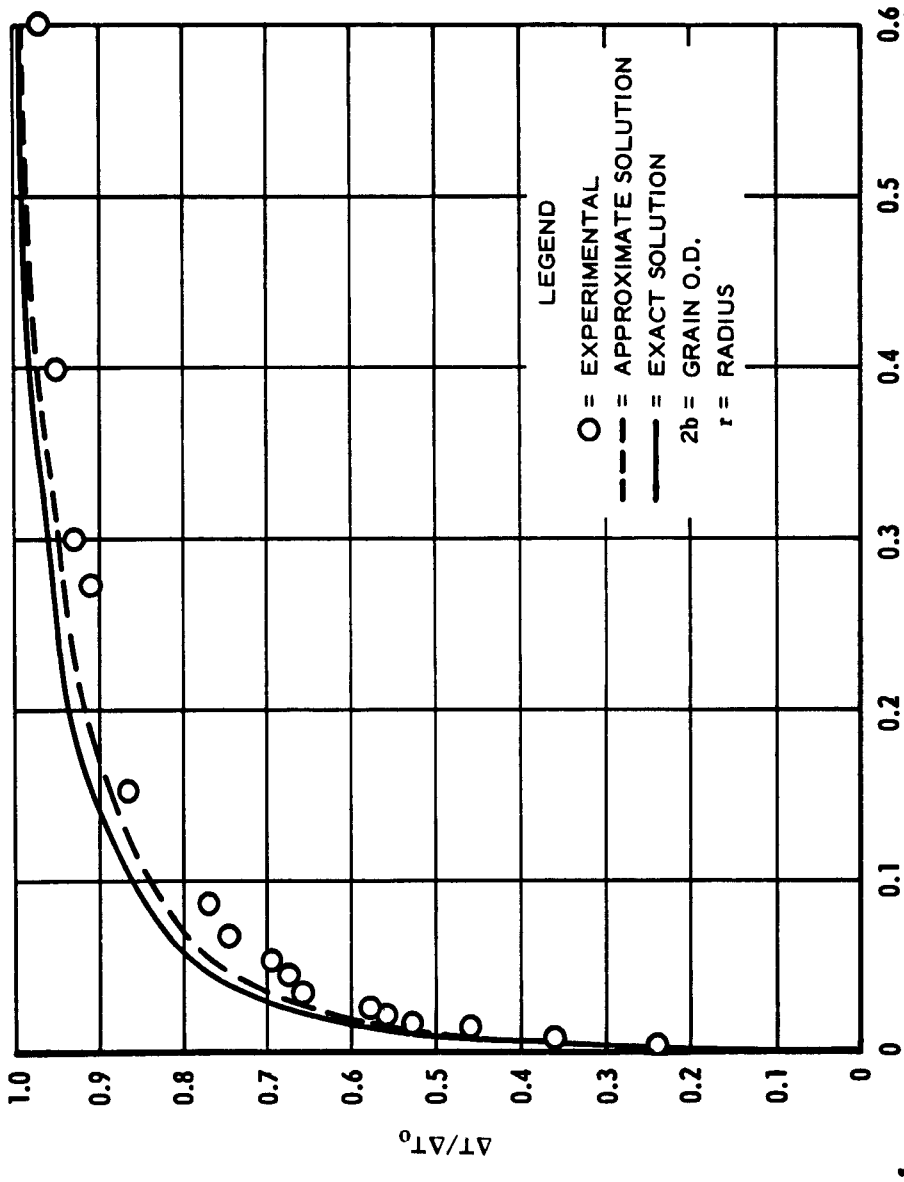

Figure 2-13 Temperature versus Time in a Solid Cylinder Subjected to a Sudden Temperature Change at r = 0.896

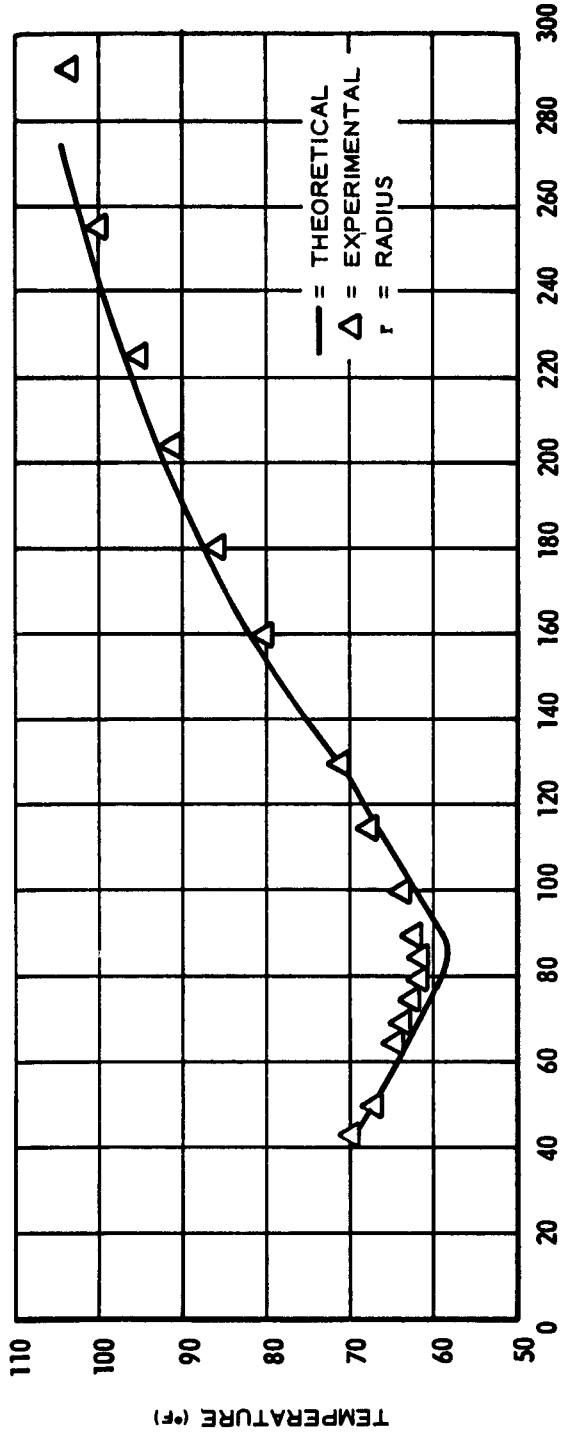

Figure 2-14 Temperature versus Time, r = o, Sequential Step Surface Temperature Variation

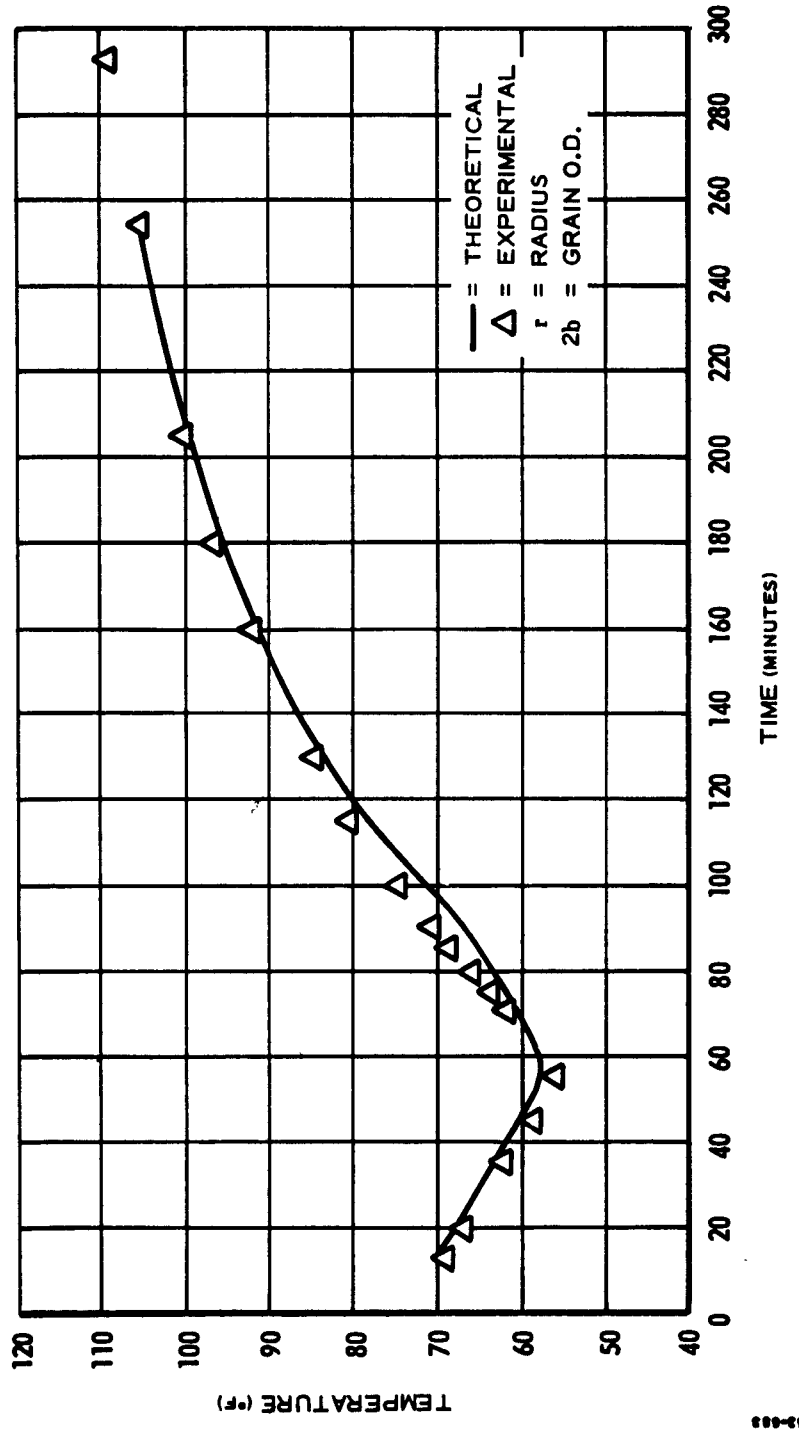

Figure 2-15 Temperature versus Time, r = 0.466, Sequential Step Surface Temperature Variation

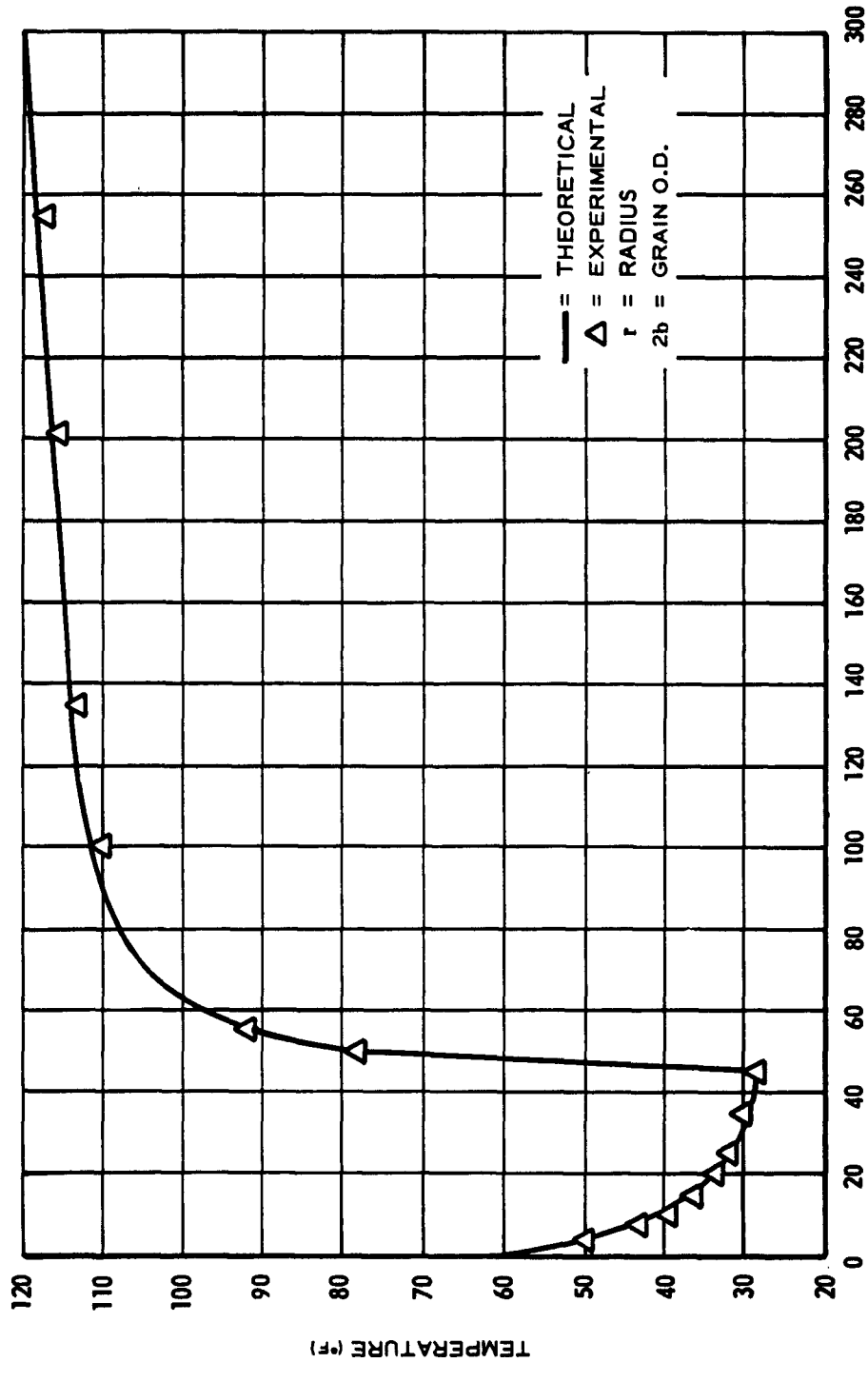

Figure 2-16 Temperature versus Time at r = 0.896, Sequential Step Surface Temperature Variation

over a period of 155 minutes and held constant at 120^{0}F (Figure 2-17). The temperature-time variation at two radii in the grain is compared with that predicted by the superposition integral approach previously delineated in Figures 2-18 and 2-19. The observed agreement was again within 5 percent.

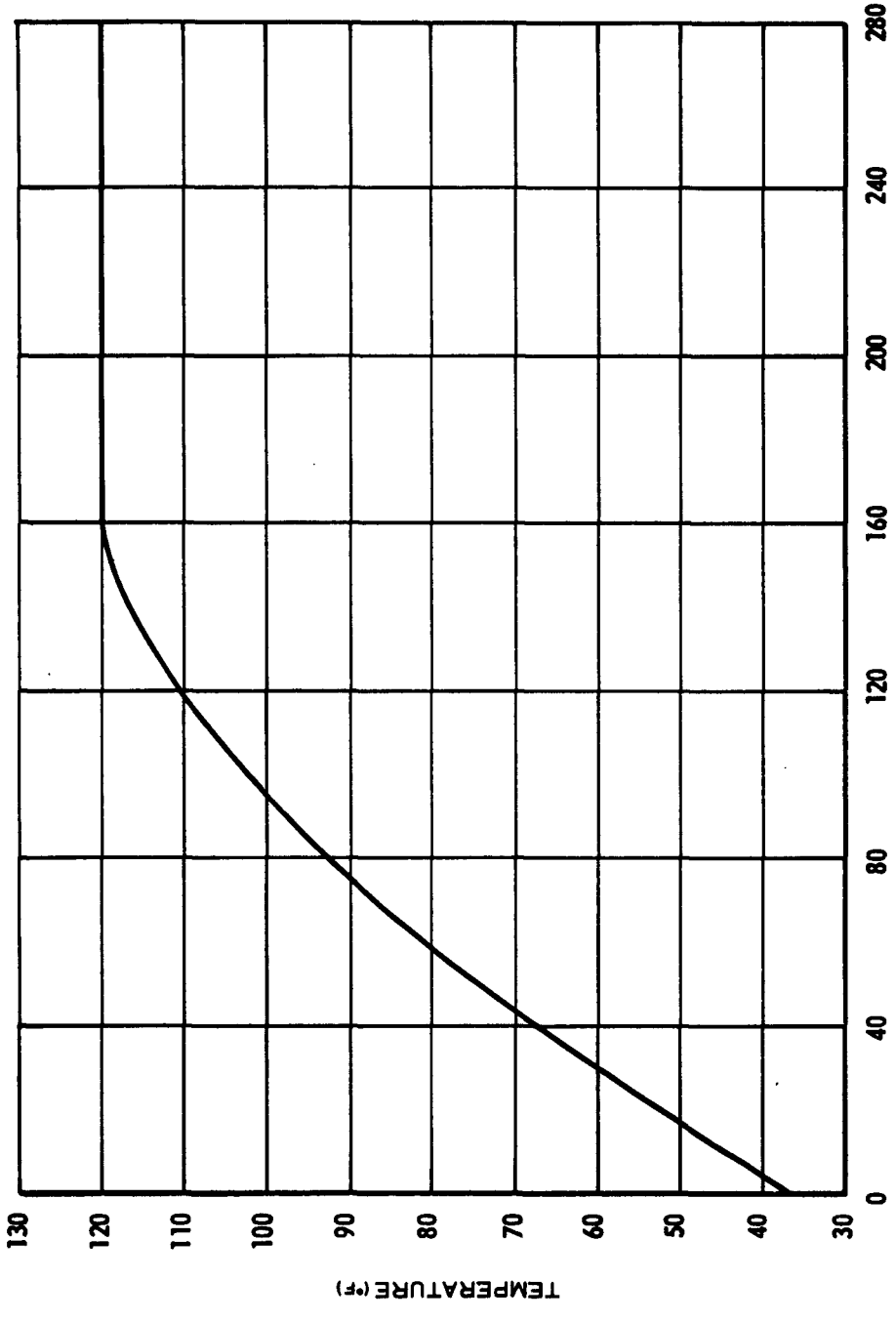

Figure 2-17 Liquid Bath Temperature versus Time

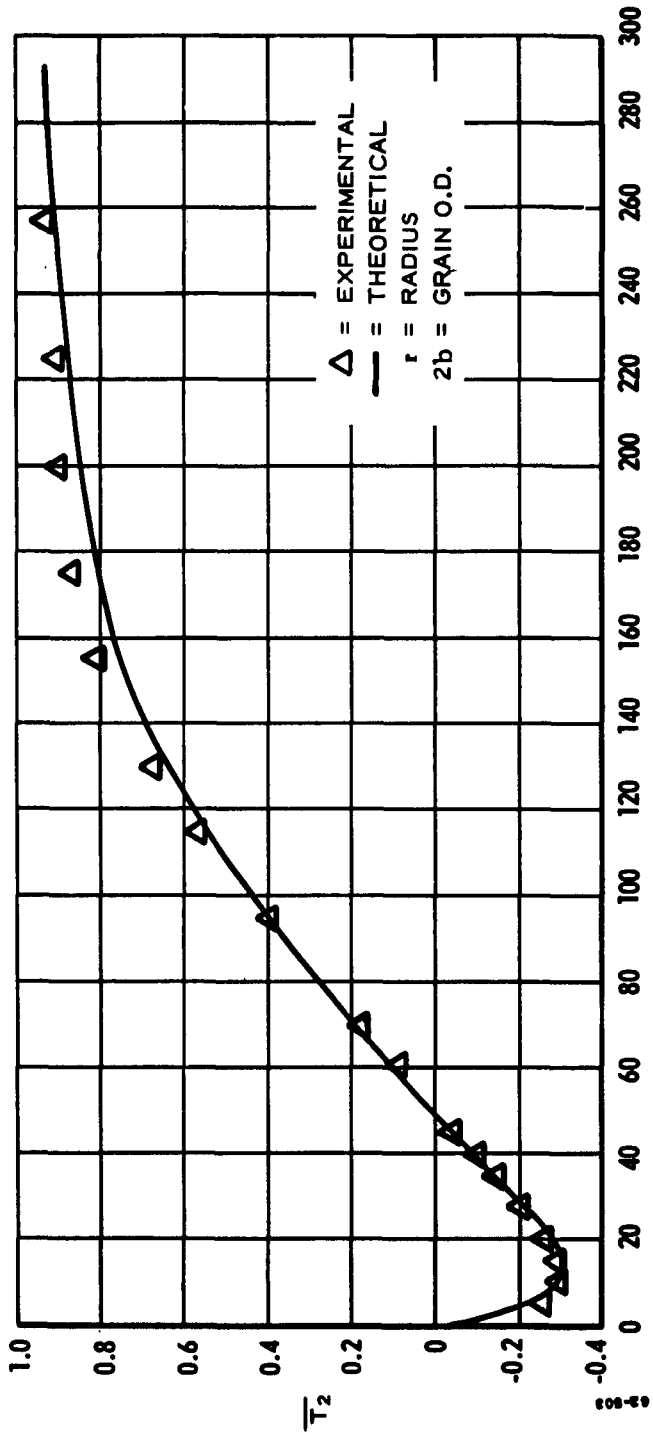

Figure 2-18 Temperature versus Time, r = 0.890b, Continuous Surface Temperature Variation

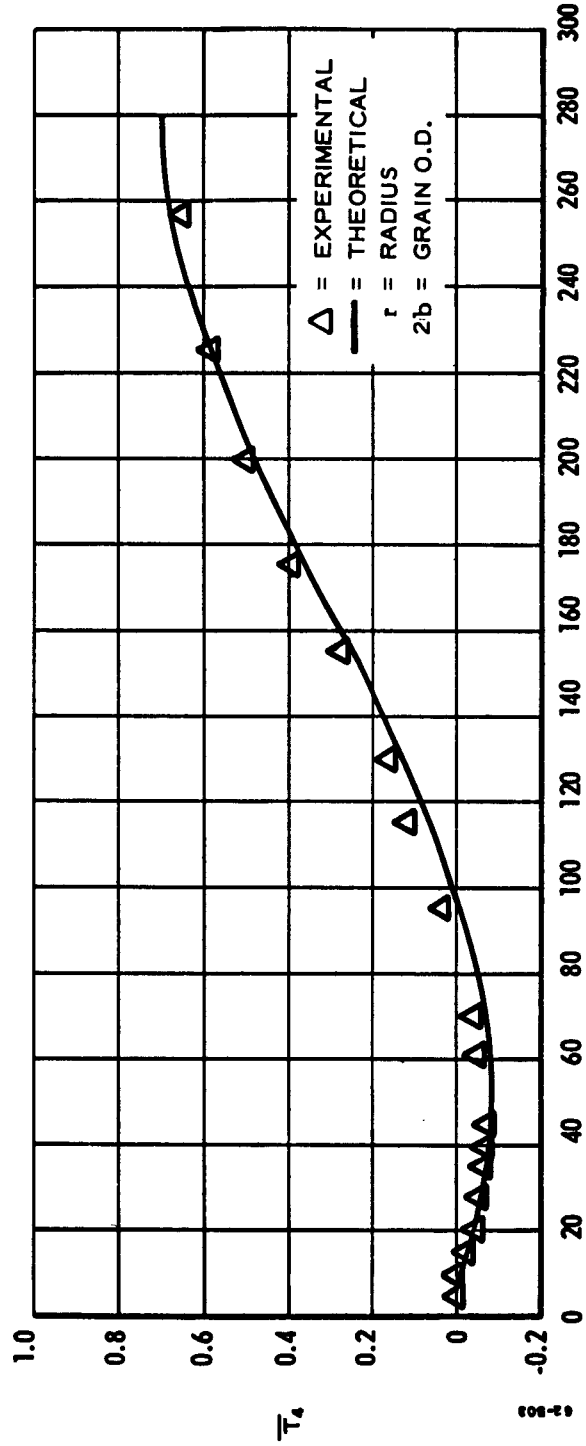

Figure 2-19 Temperature versus Time, r = 0.45 b, Continuous Surface Temperature Variation

2.5 DISCUSSION

While the experimental thermal field data for propellant grains examined in this program are not sufficient for a realistic error analysis, the results show that good engineering accuracy can be obtained by using the approximate energy techniques. The problems considered, theoretically and experimentally, treated only the condition where a uniform surface temperature of an axisymmetric body was specified. The prediction of thermal fields in a rocket grain heated or cooled with heat transfer through a gaseous external boundary layer is subject to considerably larger error because of the uncertainty of the heat transfer coefficients. A second source of error in calculation of thermal fields in rocket grains in heat transfer through the motor case, liner and insulation. It is expedient and, indeed, sufficiently accurate for engineering purposes to ignore thin liners and insulation and to assume no thermal gradient through the case. A comparison of predicted and observed thermal fields for this situation are shown in Section 5.2.

The problem of axisymmetric thermal fields in star perforated propellant grains is accessible to solution by using generalized thermal field analysis techniques based on digital computer methods. The associated transient viscoelastic stresses for the star grain cannot, however, be rigorously specified except by approximation of the grain as a circularly perforated one with stress concentrations. The generalized problem of arbitrary non-axisymmetric thermal inputs to a rocket grain is as yet an unresolved problem -- as is the associated viscoelastic stress analysis problem.

The present problem of axisymmetric thermal fields in an infinite length circularly perforated grain has been resolved to an acceptable degree to engineering practice in a theoretical framework uncomplicated enough to permit introduction of the thermal field data into the transient viscoelastic stress analysis framework.

Section 3

PROPELLANT VISCOELASTIC CHARACTERIZATION

3.1 BACKGROUND

Solution of the transient thermal stress problem requires the assumption of thermorheologically simple behavior for the propellant, which is treated as a linear viscoelastic material. Thermorheological simplicity stipulates a relationship between the effects of time and temperature whereby a change in temperature produces a change in a given stress-strain relationship identical to that obtained if the time scale of observation were to be expanded or contracted without alteration of the temperature. In view of the importance of the thermorheological viscoelastic relationships in the transient thermal stress problem, the temperature-time reduced variable approach was examined in considerable detail. The development of reduced variable mathematical treatments for operational and hereditary forms of the stress-strain law in uniaxial tension is presented in detail in Section 3.2. Experimental data for the Polycarbutene R Propellant studied in this program are included in Section 3.3.

3.2 REDUCED VARIABLE CONCEPTS

The concept of reduced variables or viscoelastic corresponding states provides a valuable simplification in the mathematical description of the mechanical behavior of linear viscoelastic materials by separating the principle variables time and temperature. In reduced variable representation the properties of a polymer are represented in terms of single functions of time and temperature whose forms can be determined experimentally even when the function representing temperature effects is not conveniently represented in analytic form (Ferry, 1961).

In its least restrictive sense, the concept of viscoelastic corresponding states can be defined as follows. Mechanical behavior of a linear viscoelastic material at different equilibrium temperatures can be related through treatment of behavior at the various temperatures in terms of a reduction parameter which stipulates a numerical relationship between the relaxation and retardation spectra for the material as a function of temperature. The reduction parameter specifies, for example, the ratio of relaxation times at one temperature to the corresponding relaxation times at another temperature.

Through time-temperature superposition, hence, data for various temperatures can be translated in stress, strain, time space to superimpose and form a single or reduced representation of stress-time or strain-time behavior at an arbitrary reference temperature. Reduced or master physical property plots will in general display the viscoelastic behavior of the material over a wider span of time than can be obtained in experiments possible at a single temperature. In tests of a viscoelastic material at one temperature, observation of effects associated with a very short relaxation time is hampered by the experimental necessity for causing finite stress or strain variations in a time interval of the same order as that of the relaxation or retardation time itself. The accurate elucidation of relaxation times of below 10^{-3} seconds at a given temperature is an experimental problem of considerable difficulty. However, a reduction in the test temperature of a practical amount will in effect slow the short relaxation times so as to bring them into the easily observable experimental range. Hence, the reduction in temperature causes a "magnification" of the effects of the short relaxation times both in terms of their time duration and their contribution to stress or strain variation on the reduced time scale. The converse effects brought about by increasing temperature are observed also; relaxation or retardation times too slow to be observed at one temperature can be speeded by increases in temperature.

For materials that are thermorheologically simple (i. e., those that can be treated accurately in reduced variable form) the concept of viscoelastic corresponding states is an empirical adjunct of vital importance. Experimental data that can be resolved accurately in a moderate time span only can be obtained at various temperatures and reduced to provide data for a broad spectrum determination of the viscoelastic properties of a material. Broad spectrum viscoelastic material property data are essential for stress analysis of rocket grains, both for consideration of dynamic loading and for the transient thermal stress problem.

The following presents an approach to the mathematical treatment of the reduced variable concept. The mathematical treatment is simplified for consideration of the reduced variable method in power law and linear differential operator viscoelastic material specifications, and for development of methods to accurately determine the temperature-time reduction variable through experimentation.

3. 2. 1 Basic Reduced Variable Relationships

The reduced variable treatment of time-temperature viscoelastic properties takes into account the variation of the viscous and elastic aspects of polymer behavior with absolute temperature. The terms viscous and elastic are used herein in a descriptive sense rather than in an explicitly interpretative sense with respect to polymer molecular mechanics. The temperature-time viscous behavior is related through the shift parameter a_T by noting that the reciprocal relaxation times $\alpha_i(T)$ for a material at absolute temperature T are related to the relaxation times $\alpha_i(T_s)$ at an arbitrary reference temperature T_s by

$$\alpha_i(T) = a_T/\alpha_i(T_s) \tag{3-1}$$

where a_T by definition equals unity at the reference temperature. The elastic component of behavior is related to temperature through noting that the elastic component $E_i(T)$ at temperature T is related to the elastic component $E_i(T_s)$ at the reference temperature T_s by

$$E_i(T) = \frac{T}{T_s}\ E_i(T_s) \tag{3-2}$$

This latter observation (Equation 3-2) arises theoretically from consideration of an equilibrium molecular rubber network as a network of entropy springs (Treloar, 1958). The validity of the relationship expressed by Equation 3-2 has been demonstrated experimentally in tests on fully relaxed rubbers. The validity of the shift parameter a_T has been demonstrated

empirically. Theoretical rationales for interpretation of the molecular origin and significance of a_T have been advanced, but their consideration is not germane to this discussion. Theoretical rationale has also predicted the existence of second order time-temperature reduction parameters, such as a density ratio for various temperatures. The second order reduction parameters will be neglected in the subsequent discussion since they are clearly below the level of numerical significance in engineering treatments of problems pertinent to this contract.

Separation of that portion of the elastic response associated with glassy behavior as a temperature independent phenomenon, as has been suggested (Ferry, 1961), will be ignored also. While there are theoretical approaches that suggest this is advisable, in practice the separation of the effect is complicated and the associated effects are trivial in engineering calculations.

3.2.2 Reduced Variable Treatment for Linear Viscoelastic Materials

A viscoelastic material, linear or not, cannot be considered to be a structure of springs and dashpots in the literal sense. However, the mathematics describing linear viscoelastic physical behavior also describe the mechanical behavior of a network of Hookean springs interconnected with Newtonian dashpots. Hence, because of the inherent analogy between linear viscoelastic behavior in the real sense and the behavior of a linear network composed of elastic springs and viscous dashpots, it is both expedient and, with some restrictions, mathematically valid to rationalize linear viscoelastic behavior in terms of a spring and dashpot assemblage.

Consider, for example, the model analog illustrated in Figure 3-1,

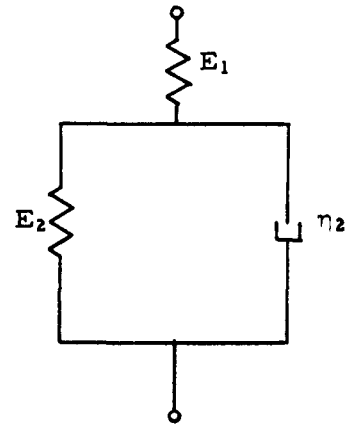

Figure 3-1 Spring and Dashpot Analog

where E_1, E_2 are the stress-strain constants of Hookean springs and η_2 is a Newtonian viscosity. For convenience, force-deflection relationships will be considered in terms of the normalized quantities stress and strain. In general operational form, the stress strain law for the analog is

$$\left[\frac{\partial}{\partial t} + \frac{E_1 + E_2}{\eta_2}\right] \sigma(t) = E_1 \left[\frac{\partial}{\partial t} + \frac{E_2}{\eta_2}\right] \epsilon(t) \qquad (3\text{-}3)$$

where $\sigma(t)$ and $\epsilon(t)$ are the time dependent stress and strain, respectively. The terms

$$\frac{\eta_2}{E_1 + E_2} = \frac{1}{\alpha} \qquad (3\text{-}4)$$

and

$$\frac{\eta_2}{E_2} = \frac{1}{\beta} \qquad (3\text{-}5)$$

are the relaxation and retardation times for the analog. Consistent with the empirical reduced variable approach, it is appropriate to write Equation (3-3) as

$$\left[\frac{\partial}{\partial \tau} + \frac{T_r(E_1+E_2)}{\eta_2 A_T}\right] \sigma(\tau) = T_r E_1 \left[\frac{\partial}{\partial \tau} + \frac{T_r E_2}{\eta_2 A_T}\right] \epsilon(\tau) \qquad (3\text{-}6)$$

where τ is reduced time, T_r is the ratio of absolute temperature T to the reference temperature T_s and A_T is defined as

$$\frac{A_T}{T_r} = a_T \qquad (3\text{-}7)$$

The differentiation between A_T as used here, and a_T, as developed historically, is made primarily to indicate a separation between absolute temperature effects on the "springs" and "viscosity" changes with temperature in the "dashpots". Solution of Equation (3-6) for a step function strain input condition at an equilibrium temperature T yields, for reduced time:

$$\sigma(\tau) = T_r E_1 \left[\frac{\beta - (\beta - \alpha)e^{-\alpha t \cdot \frac{T_r}{AT}}}{\alpha}\right] \epsilon_o \; . \qquad (3\text{-}8)$$

In proceeding to consideration of the generalized solution of more pertinent engineering interest, it is convenient to consider the model made up in Figure 3-2 below, of parallel assemblages of the model shown in Figure 3-1.

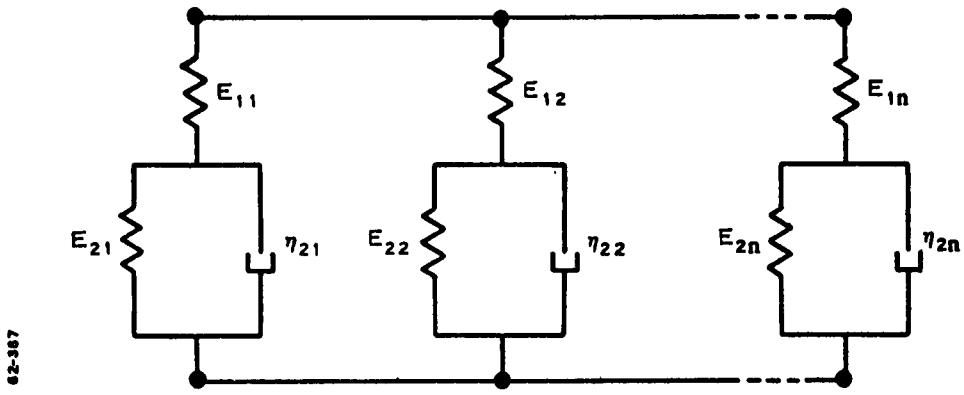

Figure 3-2 Parallel Assemblages of Model Analog

The generalized operator equation for this model is

$$\left[\frac{\partial^n}{\partial t^n} + a_{n-1}\frac{\partial^{n-1}}{\partial t^{n-1}} + \ldots + a_o\right]\sigma(t)$$

$$= \left[b_n\frac{\partial^n}{\partial t^n} + b_{n-1}\frac{\partial^{n-1}}{\partial t^{n-1}} + \ldots + b_o\right]\epsilon(t) \qquad (3\text{-}9)$$

where the coefficients of the operator a_i, b_i describe the specific behavior of the generalized model. In terms of the model, the coefficient b_n is identified as

$$b_n = \sum_{i=1}^{n} E_{1,i} \qquad (3\text{-}10)$$

Equation (3-9) can be solved for either analytic stress or strain input functions. The input functions of general interest are:

Stress Relaxation: $\epsilon(t) = \epsilon_o U(t)$

where $U(t)$ is the Heaviside unit step at $t = o$ and ϵ_o is the constant strain level;

Creep: $\sigma_o U(t)$

where σ_o is the constant stress level;

Constant Strain Rate: $\epsilon(t) = Rt\, U(t)$

where R is the strain rate;

Ramp Strain Relaxation: $\epsilon(t) = Rt\, U(t) - R(t - t_1)\, U(t - t_1)$

where $U(t - t_1)$ is the Heaviside unit step at $t = t_1$. Physically, the ramp stress relaxation input is a constant strain rate ramp to $t = t_1$ and a constant strain level $\epsilon(t_1) = Rt_1$ for $t > t_1$. The solutions for these input conditions are given below for the reduced variable interpretation:

Stress Relaxation

$$\sigma(\tau) = \epsilon_o T_r \sum_{i=1}^{n} E_{1,i} \left\{ \frac{\beta_i - (\beta_i - \alpha_i)}{\alpha_i} \right\} e^{-\alpha_i T_r / A_T t} \tag{3-13}$$

Creep

$$\epsilon(\tau) = \frac{\sigma_o}{T_r} \left[\frac{\prod_{i=1}^{n} \alpha_i}{b_n \prod_{i=1}^{n} \beta_i} + \sum_{i=1}^{n} B_i\, e^{-\beta_i T_r / A_T t} \right] \tag{3-14}$$

$$B_i = \frac{\prod_{k=1}^{n} (S + \alpha_k)}{b_n S \prod_{k=1}^{n} (S + \beta_k)} (S + \beta_i) \Bigg|_{\substack{S = -\beta_i \\ \beta_i \neq o}} \tag{3-15}$$

Constant Strain Rate

$$\sigma(\tau) = R\,T_r \sum_{i=1}^{n} E_{1,i} \left[\frac{\beta_i}{\alpha_i} t + \frac{A_T}{t_r \alpha_i} \left(1 - \frac{\beta_i}{\alpha_i}\right) \left(1 - e^{-\alpha_i \frac{T_r}{A_t} t}\right) \right] \tag{3-16}$$

Ramp Stress Relaxation

$$\sigma(\tau)\Big|_{t > t_1} = R\,T_r \sum_{i=1}^{n} E_{1,i} \left[\frac{\beta_i}{\alpha_i} t_1 - \frac{A_T}{T_r \alpha_i} \left(1 - \frac{\beta_i}{\alpha_i}\right) e^{-\alpha_i \frac{T_r}{A_T} t} \left(1 - e^{\alpha_i \frac{T_r}{A_T} t_i}\right) \right] \tag{3-17}$$

Interpreting these relationships physically, it is seen that stress relaxation data for various temperatures plotted as

$$\frac{\sigma(t)}{\epsilon_0 T_r}\Bigg|_T \quad \text{vs.} \quad t \tag{3-18}$$

and creep data plotted as

$$\frac{\epsilon(t)\,T_r}{\sigma_0}\Bigg|_T \quad \text{vs.} \quad t \tag{3-19}$$

Can be shifted along the time scale to determine the shift factor a_T

$$a_T = \frac{A_T}{T_r} \tag{3-20}$$

with reference to an arbitrary reference temperature T_s at which a_T is defined as unity. Constant strain rate data plotted as

$$\left.\frac{\sigma(t)}{RT_r} - A_0 t\right|_T \quad \text{vs.} \quad t, \tag{3-21}$$

where A_0 is the rubbery equilibrium modulus, can be shifted at 45^0 (a_T vertically and a_T horizontally) to obtain the shift variable.

In reduction of the ramp stress relaxation data, a three component shift is necessary to superpose data for $t > t_1$ because of the term

$$\left(1 - e^{\alpha_i \frac{T_r}{A_T} t_1}\right) \tag{3-22}$$

in Equation (3-17). Rigorously, the shift factor cannot be found from graphical plots of the ramp stress relaxation data. On a practical basis, however, the solution for Equation (3-17) degenerates to that for Equation (3-13) for $t > 11\, t_1$, to within a fraction of a percent accuracy, the approximation becoming more accurate as t increases beyond $11\, t_1$. Thus, accurate values for the shift factor from ramp stress relaxation data may be obtained by simple graphical interpretation of the data for $t > 11\, t$, in terms of the step function stress relaxation solution.

The reduced variable plots for stress relaxation and creep,

$$\frac{\sigma(t)}{\epsilon_0 T_r} \quad \text{vs.} \quad t/a_T \tag{3-23}$$

and

$$\frac{\epsilon(t)\, T_r}{\sigma_0} \quad \text{vs.} \quad t/a_T \tag{3-24}$$

yield the master relaxation modulus and creep compliance curves for the material at the reference temperature T_s.

The reduced variable plot for constant strain rate data

$$a_T \frac{\sigma(t)}{R T_r} - A_0 t \quad \text{vs.} \quad t/a_T \tag{3-25}$$

yields the master stress-strain curve for unit strain rate for the material at the reference temperature T_s. The time derivative of this curve is equal to the relaxation modulus at T_s. In each of the above cases, the master curves for the moduli or compliance together with the time-temperature shift factor a_T fully specify the material properties for the temperature and reduced time domain considered.

Master curve data at the reference temperature are converted to master curve data at another temperature T_x by "unreducing" the data in accord with the ratio T_x/T_s and the value of a_T for the temperature T_x.

3.2.3 Power Law Approximations to the Viscoelastic Stress-Strain Law

The heriditary integral form of the stress-strain law

$$\sigma(t) = \left[E_e + \int_0^\infty \frac{H(1/\alpha)}{\left(\frac{d}{dt} + \alpha\right)} \alpha \, d(1/\alpha) \frac{d}{dt} \right] \epsilon(t) \tag{3-26}$$

where

E_e = equilibrium modulus

$H(1/\alpha)$ = relaxation distribution

is an alternate form equally acceptable mathematically to the operational stress-strain law (Equation 3-9). Indeed, the limit consideration of the hereditary form by a power law approximation is of particular interest and was used as the material properties statement in the solution of the transient thermal stress analysis problems.

For purposes of discussion, letting the term E_e of Equation (3-26) be zero and the expression under the integral be infinity for t = o, then the power law form for the relaxation modulus $E_r(t)$ becomes

$$E_r(t) = \Sigma K_i \left(\frac{1}{t}\right)^{n_i} . \tag{3-27}$$

For the class of propellants studied in this investigation it was found that the above summation was given accurately by

$$E_r(t) = K t^{(n-1)} \tag{3-28}$$

for the time and temperature range of interest in the transient thermal stress problem. As implied by Equation (3-28), the stress relaxation modulus was a straight line on a plot of log $E_r(t)$ versus log time.

In reduced variable form, the power law approximation (Equation 3-28) is, for the various test conditions of interest

Stress relaxation

$$\frac{\sigma(\tau)}{\epsilon_0} = T_r K \left(\frac{t}{a_T}\right)^{n-1} \tag{3-29}$$

Creep

$$\frac{\epsilon(\tau)}{\sigma_0} = \left(\frac{1}{K T_r}\right)\left(\frac{1}{\Gamma n \Gamma(2-n)}\right)\left(\frac{t}{a_T}\right)^{1-n} \tag{3-30}$$

Constant strain rate

$$\frac{\sigma(\tau)}{R} = a_T T_r (1-n) K \left(\frac{t}{a_T}\right)^{n} \tag{3-31}$$

Interconversion of the expressions (3-29), (3-30), and (3-31) with the expressions (3-13), (3-14), and (3-15) over the range where the power law approximation is valid can be done for known or assumed values of α_i or β_i in Equations (3-29), (3-30) and (3-31). As a more direct alternative perhaps, a single set of data can be fit by either the operational solutions or by the power law form and, in the range of applicability, are by definition equivalent statements. Choice of the method for properties specification is a matter of convenience in application of the mathematical properties statement to solution of the problems of interest.

3.3 PROPELLANT VISCOELASTIC DATA

The uniaxial viscoelastic stress-strain law for Polycarbutene R propellant was obtained from interpretation of constant strain rate data for the propellant. Tab-end tensile (specimens of the propellant were tested in replicate at temperatures between -100^0 and $+142^0$F. The data were superposed for a reference temperature of 70^0F according to Equation (3-21) to obtain the master stress-strain curve for a strain rate of 0.005 minute $^{-1}$ (Figure 3-3) and the associated shift factor variation with temperature (Figure 3-4). The strain levels in all tests were confined to values below 10 percent.

The power law approximation for the stress relaxation modulus, in reduced time, was

$$E_r(\tau) = T_r 330 \left(\frac{t}{a_T}\right)^{-0.215} \qquad (3\text{-}32)$$

$$10^4 > t/a_T > 10^{-13}$$

and the operational form, as expressed by the form,

$$E_r(\tau) = T_r \sum_{i=o}^{n} A_i \; e^{-\alpha_i t/a_T} \qquad (3\text{-}33)$$

was

i	Ai	α_i
0	63	0
1	40	10^{-3}
2	66	10^{-2}
3	108	10^{-1}
4	177	1
5	290	10
6	476	10^2
7	780	10^3
8	1,280	10^4
9	2,100	10^5
10	3,500	10^6
11	5,700	10^7
12	9,300	10^8
13	15,300	10^9
14	25,000	10^{10}
15	41,000	10^{11}
16	67,000	10^{12}

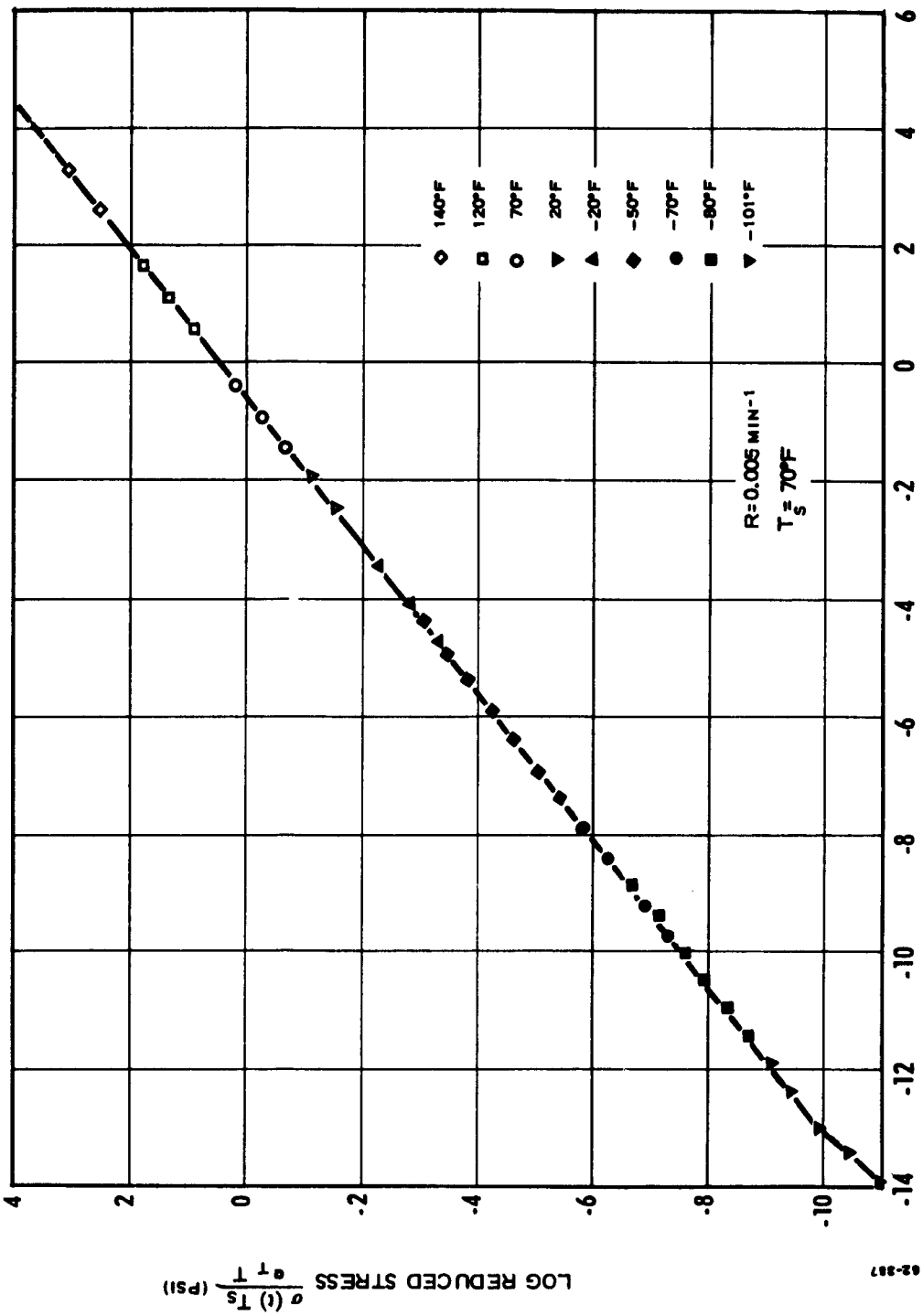

Figure 3-3 Constant Rate Master Curve, Polycarbutene R Propellant

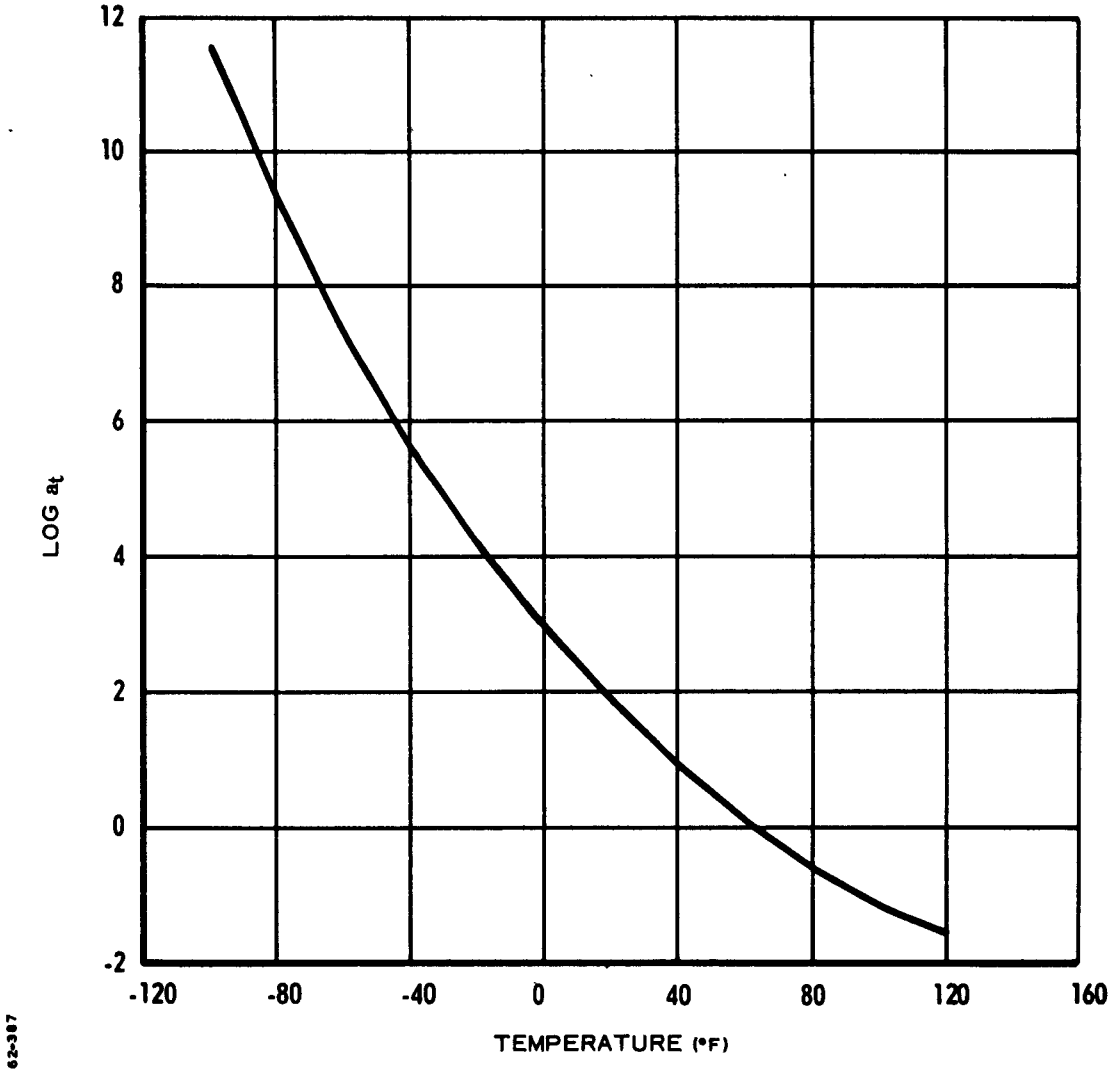

Figure 3-4 Log a_T versus Temperature, Polycarbutene Propellant, Constant Strain Rate Data

In consideration of the nature of the transient thermal stress problem, the introduction of the absolute temperature ratio T_r in the properties statement was considered to be of trivial importance in engineering calculations. Hence, the material properties statement as entered in the thermal stress calculations was

$$E_r(\tau) = 330 \left(\frac{t}{a'_T} \right)^{-0.215} \qquad (3\text{-}34)$$

$$10^4 > t > 10^{-12}$$

and the associated shift factor values a'_T measured for the data considering the value T_r to be unity for all temperatures. Comparative values for the shift factors as derived by the two techniques are listed in Table 3-1.

Table 3-1

TEMPERATURE - TIME REDUCTION PARAMETERS

$T\ (^0F)$	a_T	a_T'
115	2.95×10^{-2}	4.31×10^{-2}
70	1	1
20	8.93×10^{1}	7.04×10^{1}
-16	1.04×10^{4}	4.51×10^{3}
-20	2.70×10^{4}	1.14×10^{4}
-50	3.33×10^{6}	1.01×10^{6}
-70	2.03×10^{8}	4.85×10^{7}
-80	3.54×10^{9}	7.59×10^{8}
-100	3.35×10^{11}	5.54×10^{10}

3.5 DISCUSSION

The preceding discussions have not lead to the conclusion that reduced variable treatment of propellant properties for stress analysis problems is a completely resolved problem. However, in view of the successful reduced variable treatment of the Polycarbutene R propellant studied, it seems clear that within engineering accuracy the reduced variable treatment is valid. Additional evidence for this observation is discussed in Section 5. In stress relaxation tests (sponsored by LPC) of the propellant formulation identical to that discussed in Section 3.3, but made approximately one year later from different lots of raw materials, the viscoelastic spectral properties and shift factor variation with temperature were observed to be in good engineering agreement with the data presented in this report. This type of agreement, while not as yet supported statistically, argues effectively for the basic validity of the viscoelastic, reduced variable approach in engineering analysis of propellant grains.

Section 4

GRAIN THERMAL STRESS ANALYSIS

4.1 BACKGROUND

Methods are well established for analysis of the quasi-static boundary value problem for homogeneous, isotropic, linear viscoelastic materials under surface tractions, body forces and isothermal temperature conditions. Within the scope of small deformations and time-independent boundaries, the solutions can be obtained by application of the Laplace transform, which eliminates time dependence and reduces the viscoelastic problem to an associated elastic one (Lee, 1955).

Introduction of either a transient or steady-state thermal field produces difficulties in the solutions that are not easily surmounted. The material behavior is sensitive to temperature, resulting in a problem where the stresses associated with the thermally induced strains are sensitive functions of the spatial variables and time. The specific nature of this problem was considered in subcontract research carried out by Purdue University and methods were developed for obtaining transient thermal stresses in hollow case-constrained viscoelastic cylinders. The details of the work are reported in Volume II, Chapter 1 of this report.

Two methods of solution developed, and the one best suited for computer calculation was selected for numerical solution and programed for the IBM 7090 computer. This solution (description begins on p. 35, Volume II) considers a case-constrained, circular port grain under plane strain end constraint. The propellant was assumed to be incompressible and the case elastically rigid. The thermal fields were assumed to be axisymmetric and externally imposed. Thermal field specification and propellant viscoelastic properties were introduced as indicated in Sections 2 and 3 of this volume.

Various types of thermal inputs specified at the grain-case interface were examined numerically. The possibility of stress accumulation was investigated for various step-cycle thermal inputs and parametric data were computed showing the variation of peak stress with grain web fraction, grain diameter and temperature for step surface temperature input.

The above work is discussed in Section 4.2 and numerical data are presented. Section 4.3 discusses the possibility of estimation of peak thermal stresses using simplified limit engineering techniques. Subcontract effort in experimental photothermoviscoelasticity is reviewed in Section 1.4. Discussion of the thermal stress problem and the engineering significance of the data is presented in Section 4.5.

4.2 TRANSIENT THERMAL STRESS CALCULATIONS

The transient thermal stress calculations were based on the following set of equations, which are summarized here from Sections 2 and 3 of this volume, and from Chapter I of Volume II. The symbols used are defined in Table 4-1.

Thermal Field Equations

The following expressions are defined (Ref. Section 2.2, Vol. I)

$$A_1 = \begin{cases} [1 - \frac{(1-\bar{r})}{q_1(\bar{t})}]^2 & ; \quad (1-\bar{r}) \leq q_1(t) \\ 0 & ; \quad (1-\bar{r}) \geq q_1(t) \end{cases} \tag{4-1}$$

$$A_2 = [1 - q_2(\bar{t})] \; [1 - \frac{(1-\bar{r})\lambda}{(\lambda-1)}]^2 + T_a(\bar{t}) \tag{4-2}$$

where

$$q_1(\bar{t}) = \sqrt{11.0299\ \bar{t}} \tag{4-3}$$

$$T_a(\bar{t}) = 1 - e^{-0.2778(\bar{t}/\bar{t}_a - 1)} \tag{4-4}$$

$\bar{t}$ = nondimensional time = η^2

$\bar{t}_a$ = nondimensional penetration time = η_a^2

Hence, the complete step solution for the thermal field is

$$A(\bar{r},\bar{t}) = T_1 \quad A_1(\bar{r},t)\, 1(\bar{t}_a - \bar{t}) + A_2(\bar{r},\bar{t})\, 1(\bar{t} - \bar{t}_a) \tag{4-5}$$

where

$$1(\bar{t}_a - \bar{t}) = \begin{cases} 1.0 & ; \quad \bar{t} \leq \bar{t}_a \\ 0 & ; \quad \bar{t} \geq \bar{t}_a \end{cases}$$

$$1(\bar{t} - \bar{t}_a) = \begin{cases} 0 & ; \quad \bar{t} \leq t_a \\ 1.0 & ; \quad \bar{t} \geq \bar{t}_a \end{cases}$$

T_1 = step change on outer case
λ = b/a
$\bar{r}$ = r/b
$\bar{t}$ = $\kappa t/b^2$

Table 4-1

LIST OF SYMBOLS

$A(r,t)$	=	Temperature distribution for a unit step change on the grain outer surface
$A_1(r,t)$	=	Function defined by Equation (4-1)
$A_2(r,t)$	=	Function defined by Equation (4-2)
$F(r,t)$	=	Function defined by Equation (4-10)
$G(t) = E_r(t)$	=	Relaxation modulus of propellant
$T(r,t)$	=	Temperature change
T_o	=	Temperature change on outer surface
a	=	Inner radius of grain
a_T'	=	Shift factor
Φ	=	$1/a_T'$
b	=	Outer radius of grain
κ	=	Thermal diffusivity
q_1	=	Penetration depth of heat front, Equation (2-3)
T_a	=	Function defined by Equation (2-16)
r	=	Radial coordinate
$\overline{r}$	=	Nondimensional radial coordinate = r/b
t	=	Time
η^2	=	Nondimensional time = $\kappa t/b^2$
t_a	=	Penetration time of heat front to $r = a$
Ψ	=	Function defined by Equation (4-8)
α_o	=	Linear coefficient of thermal expansion
γ	=	Parameter defined by Equation (2-17)
ϵ_θ	=	Hoop strain
ϵ_r	=	Radial strain
λ	=	b/a
ζ	=	Function defined by Equation (4-11)
σ_θ	=	Hoop stress
σ_r	=	Radial stress
k	=	Specific heat
c	=	Thermal conductivity

The temperature field for a series of step changes on the exterior surface is given by

$$T(\bar{r}, \bar{t}) = \Sigma T_{1n} A(\bar{r}, t - t_n)\, 1\,(\bar{t} - t_n) \tag{4-6}$$

where

t_n = 1, 2, 3, 4 . . . n = time at which the step change is applied.

T_{1n} = step change in the surface temperature at $t = t_n$.

Viscoelastic Analysis

The equations for the viscoelastic analysis are (Ref. Chap. 1, Vol. II, Section 3.3, Vol. I)

$$\epsilon_\theta(\bar{r}, \bar{t}) = 3\alpha_0 \Psi(\bar{r}, \bar{t}) \tag{4-7}$$

$$\Psi(\bar{r}, \bar{t}) = \frac{1}{\bar{r}^2} \int_1^{\bar{r}} \rho\, T(\rho, \bar{t})\, d\rho \tag{4-8}$$

$$\sigma_r(\bar{r}, \bar{t}) = \int_{\frac{1}{\lambda}}^{\bar{r}} F(\rho, \bar{t})\, d\rho \tag{4-9}$$

where

$$F(\bar{r}, \bar{t}) = \frac{3\alpha_0}{\bar{r}} \int_0^{\bar{t}} G[\zeta(\bar{t}, \bar{r}) - \zeta(\tau, \bar{r})] \frac{\partial}{\partial \tau} [2\Psi(\bar{r}, \tau) - T(\bar{r}, \tau)]\, d\tau \tag{4-10}$$

$$\zeta = \frac{b^2}{k} \int_0^{\bar{t}} \Phi[T(\bar{r}, \bar{\tau})]\, d\tau \tag{4-11}$$

$$G(t) = E_r(t) = 330\, t^{-0.215} \tag{4-12}$$

The function $\Phi(T)$ is the reciprocal of a'_T (Section 3.3). The hoop stress is given by

$$\frac{\partial \sigma_r}{\partial \bar{r}} = F(\bar{r}, \bar{t}) \tag{4-13}$$

$$\bar{r} \frac{\partial \sigma_r}{\partial \bar{r}} + \sigma_r = \sigma_\theta(\bar{r}, \bar{t}) \tag{4-14}$$

and the radial strain specified by

$$\epsilon_r = \bar{r} \frac{\partial \epsilon_\theta}{\partial \bar{r}} + \epsilon_\theta \,. \tag{4-15}$$

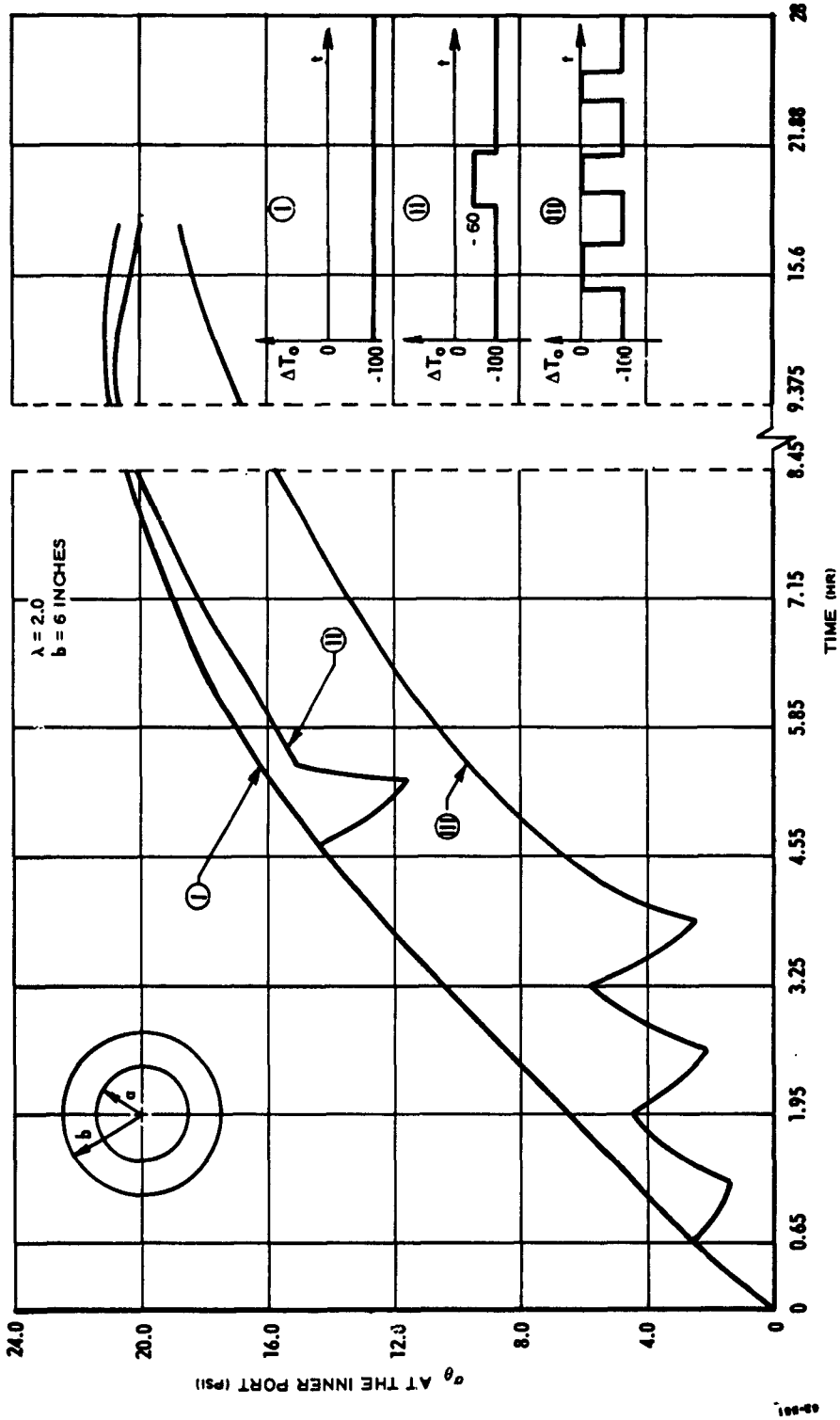

Figure 4-1 Hoop Stress at Port versus Time for Step, Step with a Jog, and Cyclic Thermal Inputs

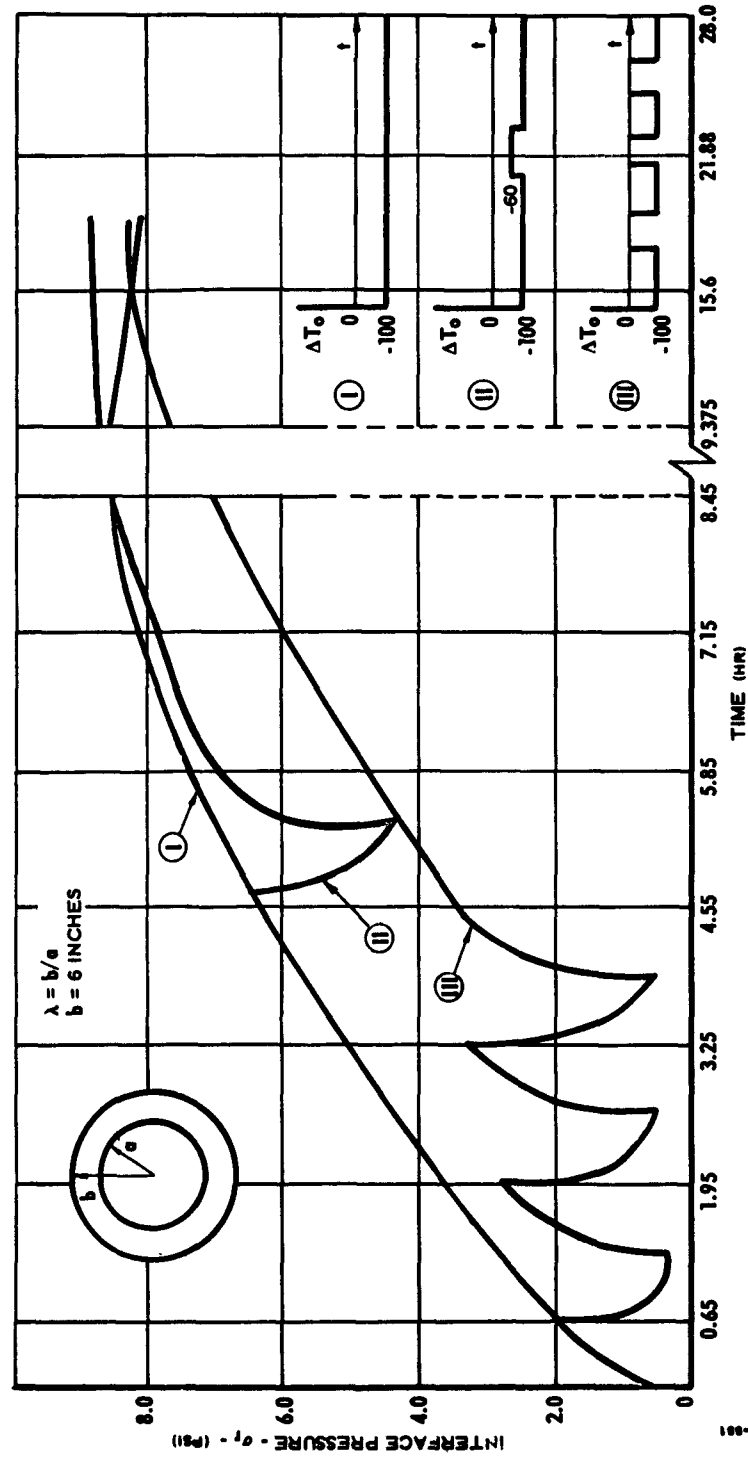

Figure 4-2 Case-Grain Interface Pressure versus Time for Step, Step with a Jog, and Cyclic Thermal Inputs

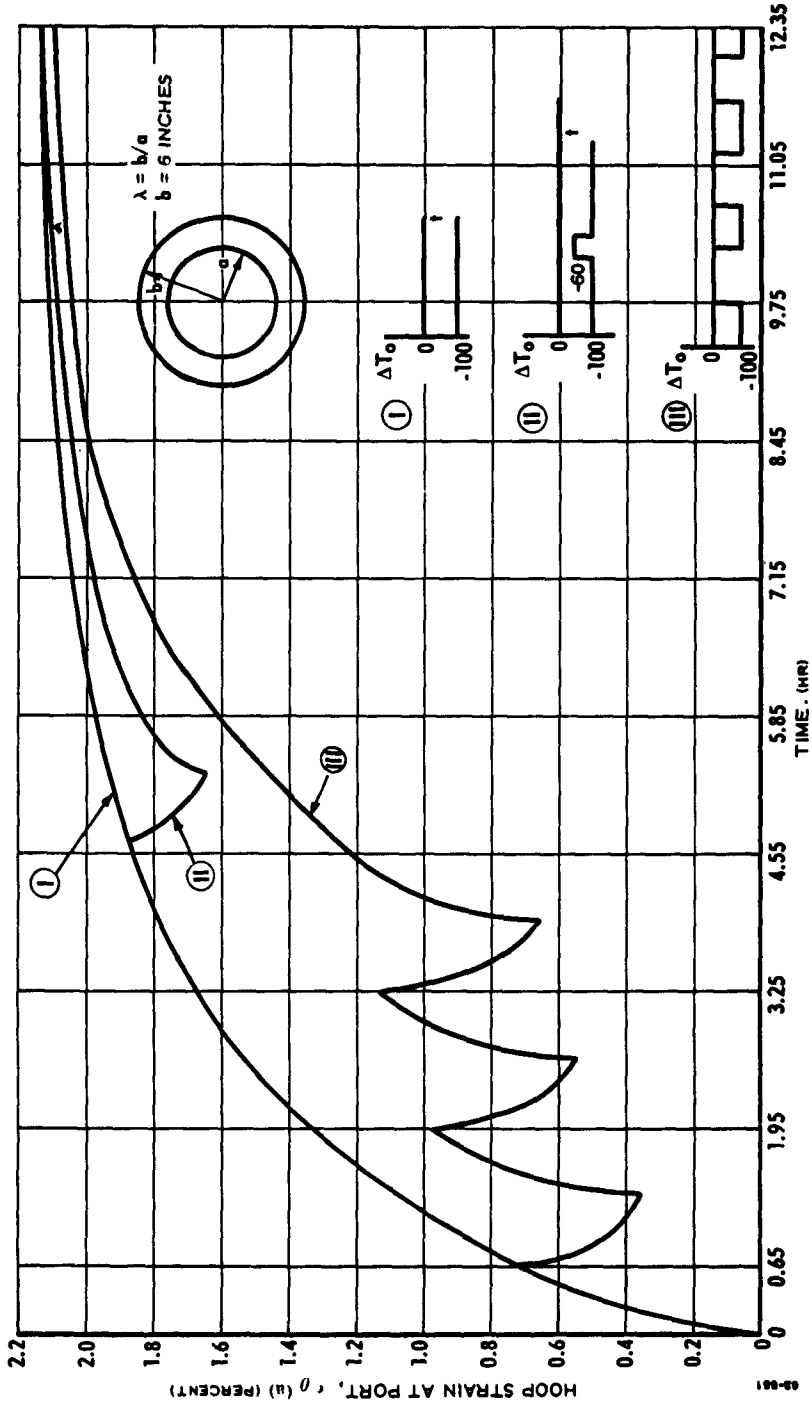

Figure 4-3 Hoop Strain at Port versus Time for Step, Step with a Jog, and Cyclic Thermal Inputs

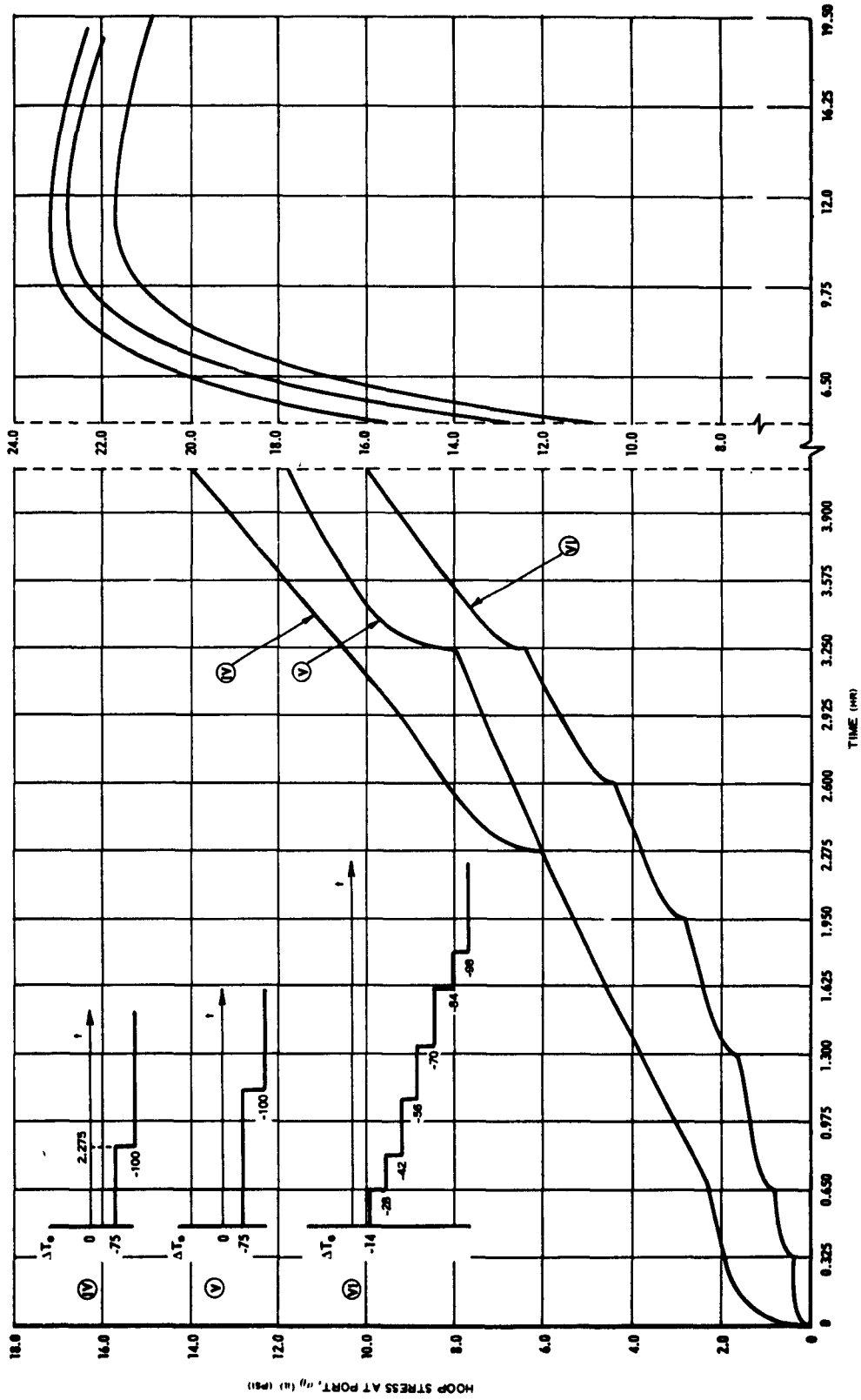

Figure 4-4 Hoop Stress at Port versus Temperature for Stairstep Thermal Inputs

on the peak stresses obtained as a result of step environment changes in a one-foot diameter motor. The calculations considered the following parametric variations:

- Thermal step inputs of -40°F, -100°F, -130°F, and -160°F from a reference temperature of 70°F.
- Web fractions of 9, 50, 66.7, 75 and 80 percent.

The resulting peak stresses are shown in Figures 4-5 through 4-8.

Peak stresses for various motor diameters can be determined from the data in Figures 4-5 through 4-8 by the following scaling law:

- Obtain the stresses σ_0 for a given λ (grain outer diameter to inner diameter ratio) and a particular grain outer diameter, $2b_0$.
- For a new grain outer diameter = $2b_1$, the new stress value σ_1 is obtained as

$$\sigma_1 = \left(\frac{b_0}{b_1}\right)^{0.43} \sigma_0$$

This scaling law is applicable only for the particular viscoelastic properties of the Polycarbutene R propellant studied in this program. In general, for any power law approximation to the relaxation modulus of the form

$$E_r(t) \cong \kappa\, t^{-m}$$

the exponent of the approximation, m, can be used to obtain the scaling law as

$$\sigma_1 = \left(\frac{b_0}{b_1}\right)^{2m} \sigma_0.$$

The ratio σ_1/σ_0 for various motor diameter ratios is shown in Figure 4-9.

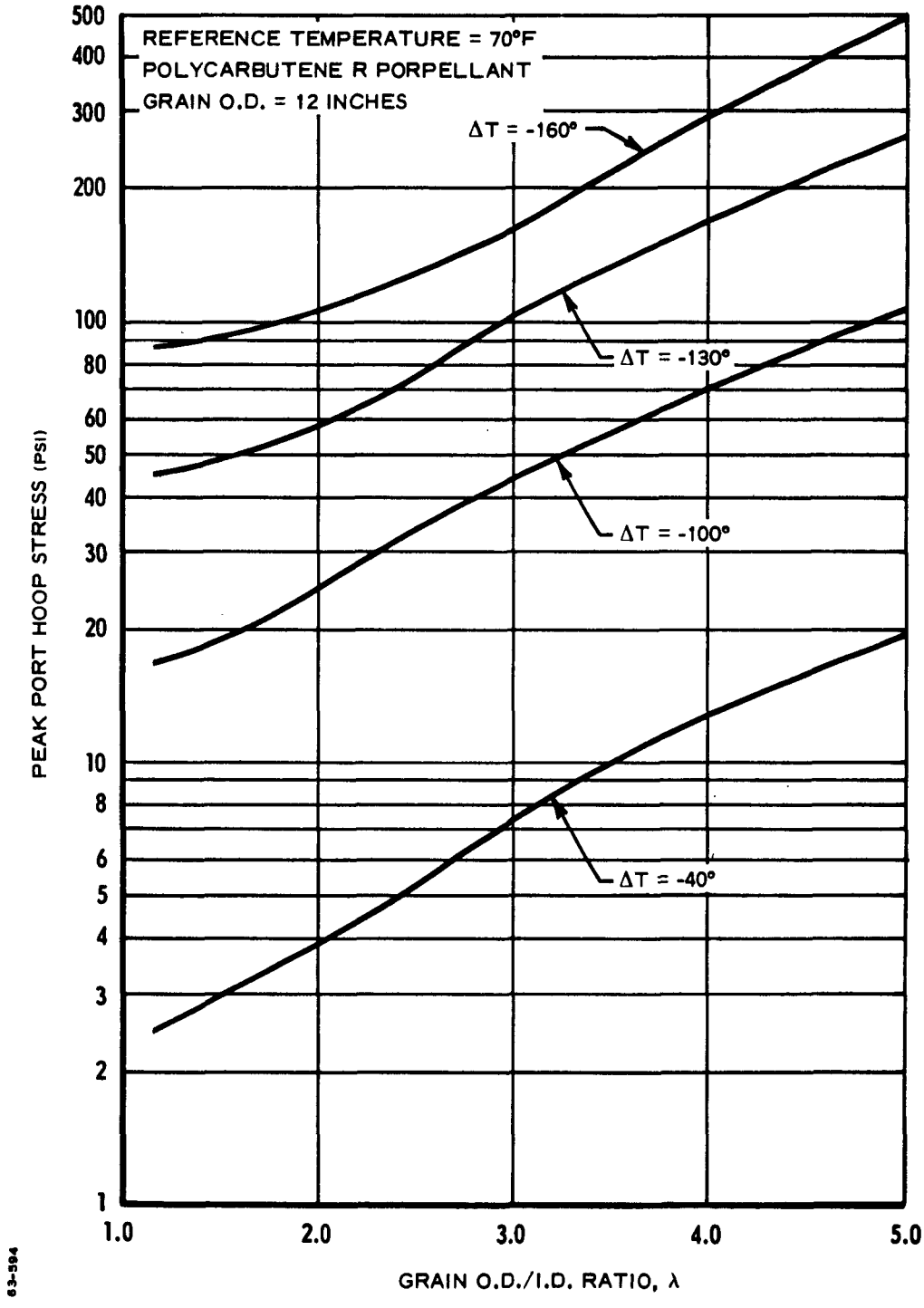

Figure 4-5 Peak Port Hoop Stress versus Temperature Step and Grain O. D. to I. D. Ratio

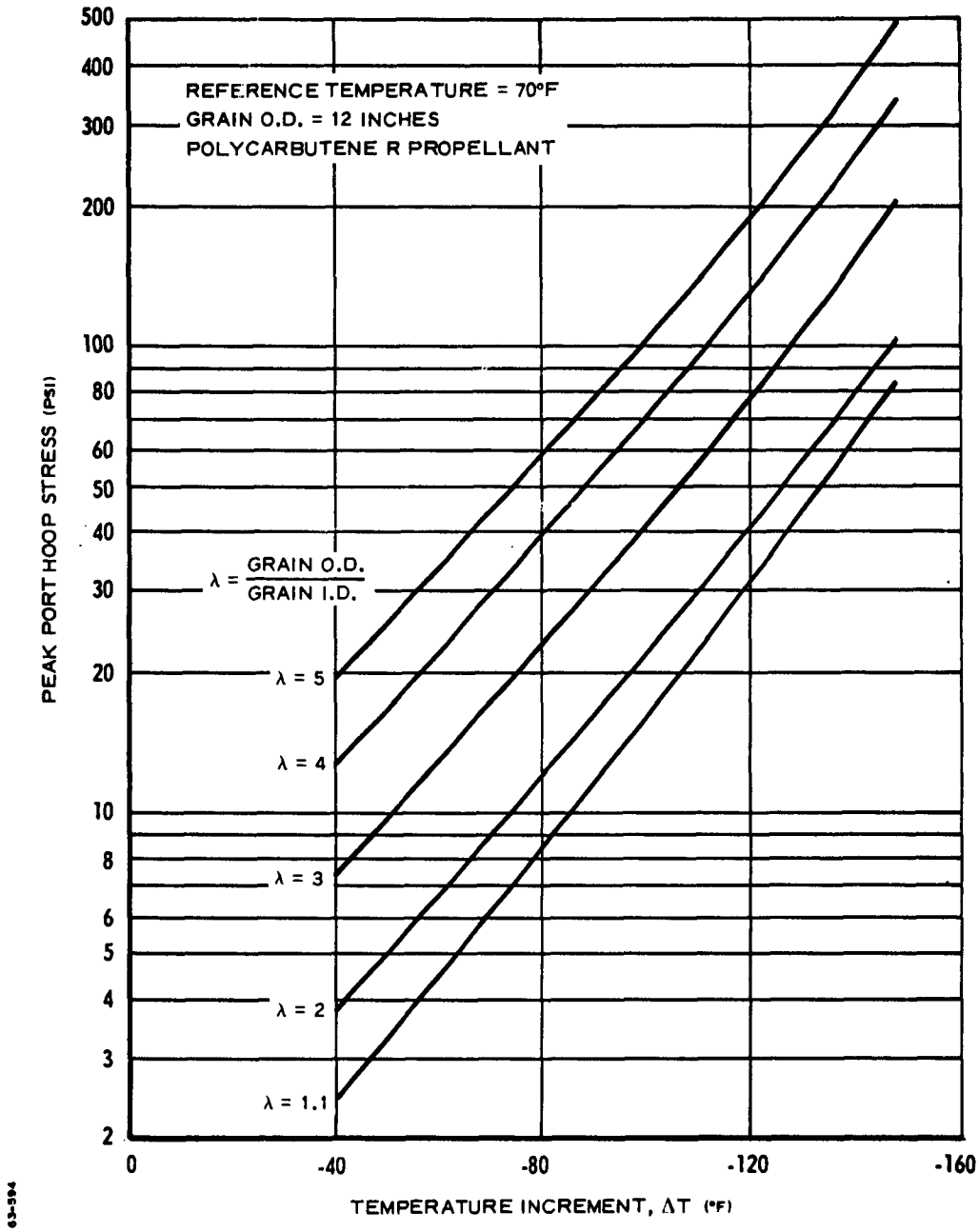

Figure 4-6 Peak Port Hoop Stress versus Temperature Step and Grain O. D. to I. D. Ratio

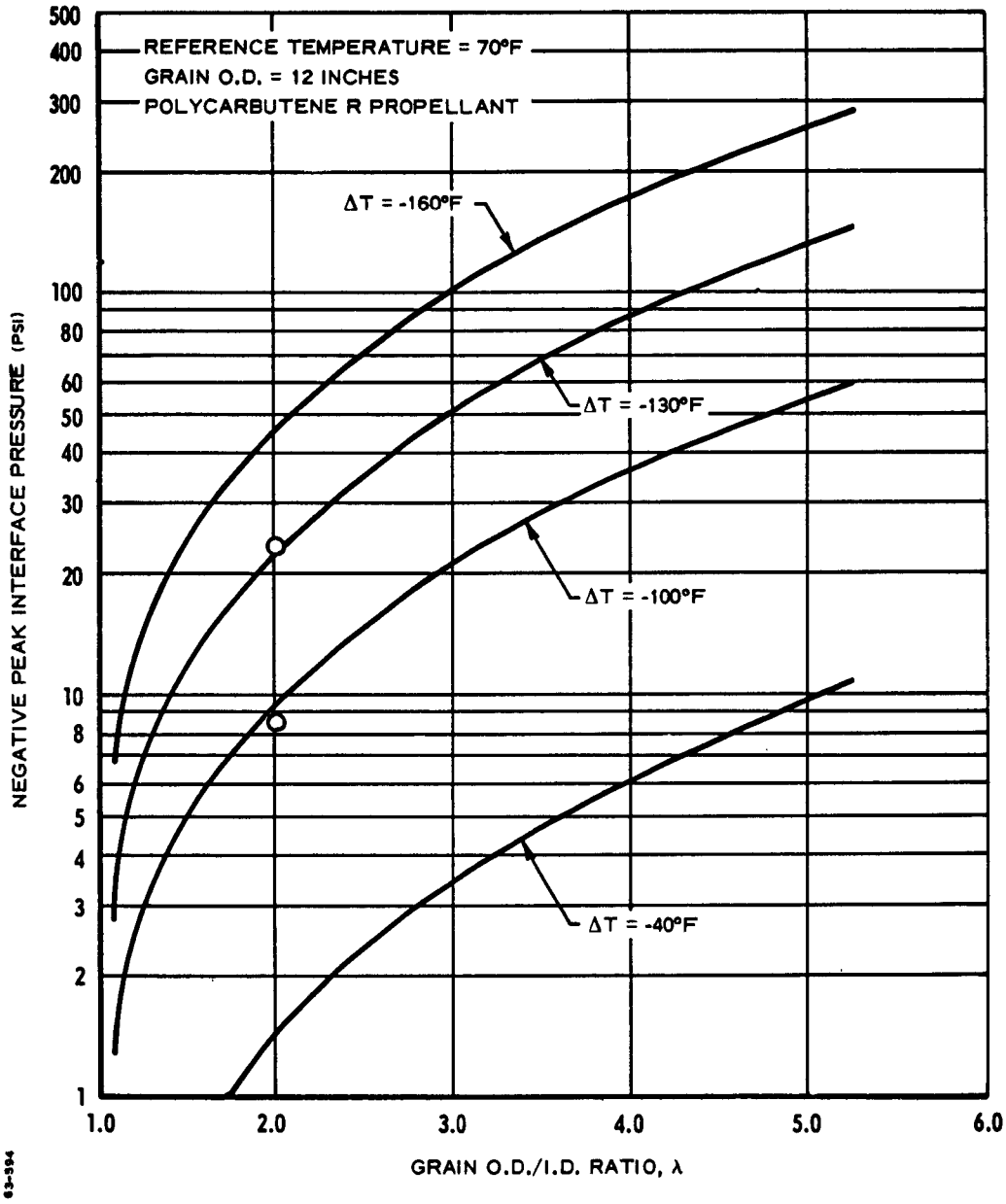

Figure 4-7 Case-Grain Interface Pressure versus Temperature Step and Grain O. D. to I. D. Ratio

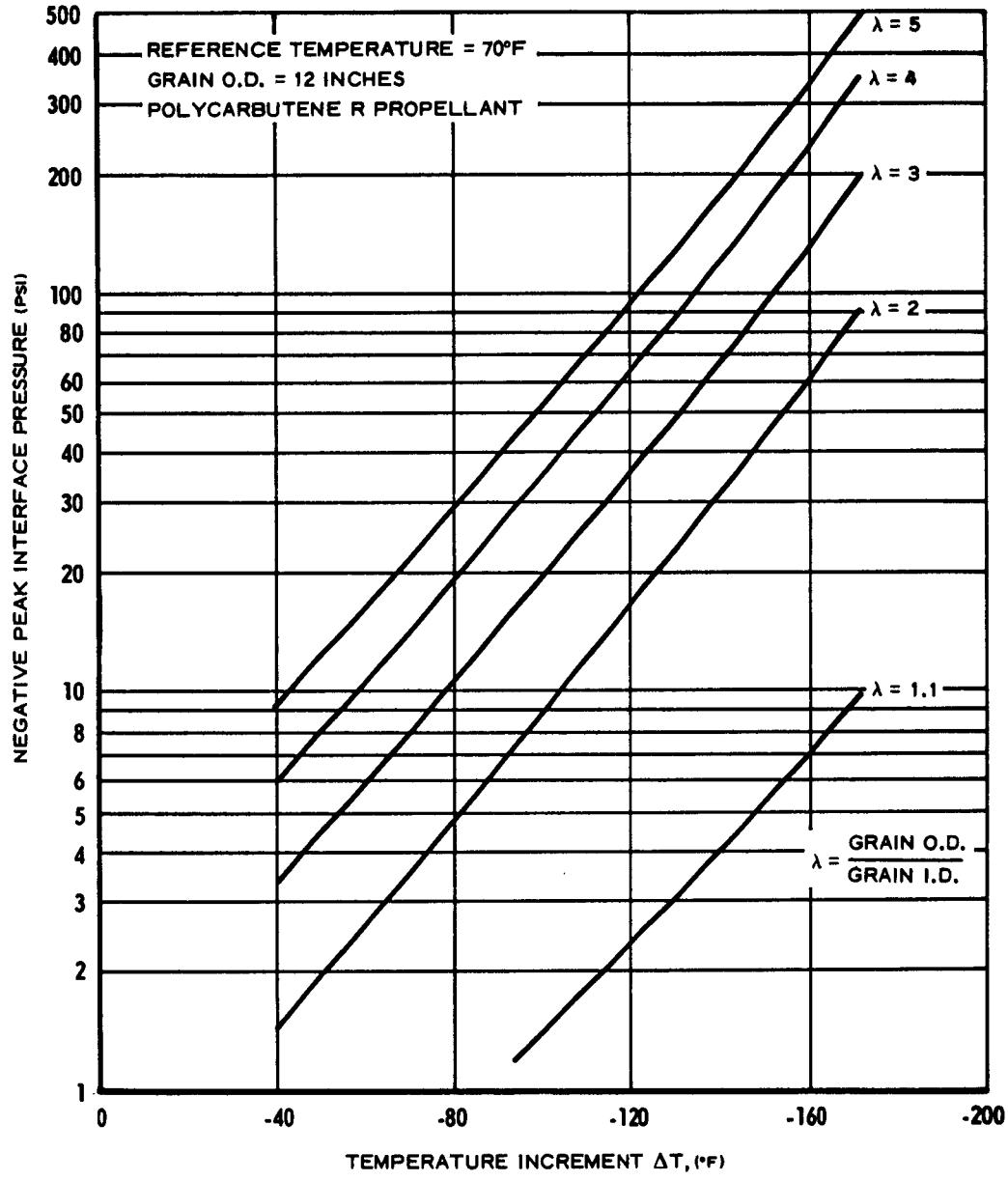

Figure 4-8 Case-Grain Interface Pressure versus Temperature Step and Grain O. D. to I. D. Ratio

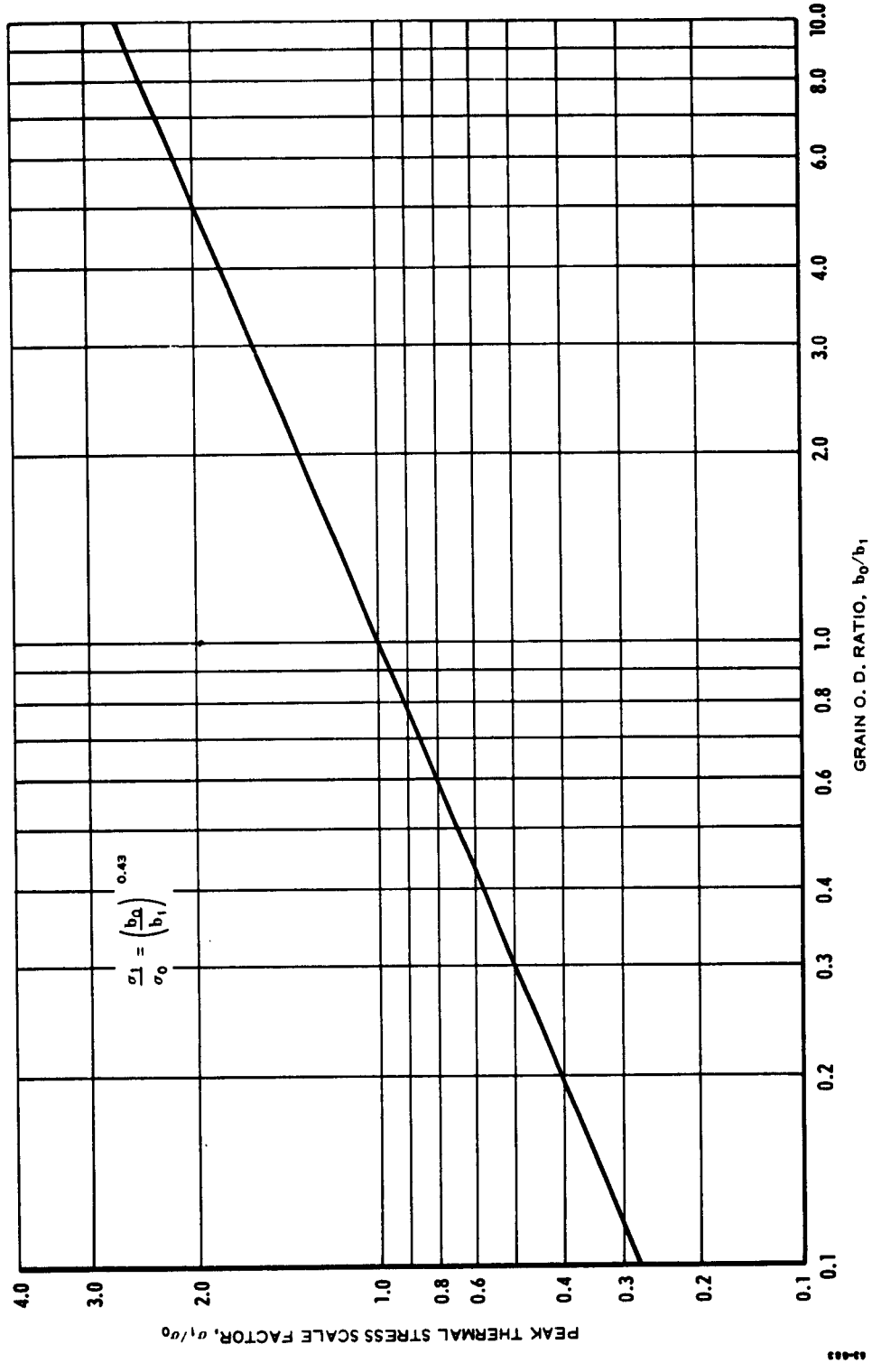

Figure 4-9 Peak Thermal Stress Scale Factor versus Grain Outer Diameter Ratio

4.3 ELASTIC AND VISCOELASTIC LIMIT ANALYSIS

In many instances it is useful to calculate limits for stresses in a body on the basis of assumptions that enable simplification in computation, but which lead to reliable values for limits within which the rigorously derived answer must lie. In the thermal transient problem the following two approaches are obvious.

- Calculation of the limit stresses associated with the glassy and rubbery propellant moduli.
- Calculation of the stress assuming a step function body change in the grain temperature, using the propellant properties at the new temperature and solving for the time at which thermal equilibrium is attained.

Noting that the glassy and rubbery equilibrium stresses will be different by approximately three orders of magnitude, the first approach can be ruled out without detailed consideration. Equilibrium stresses for the rubbery condition are obtained only after long times at moderate temperatures and at high temperatures after short times. The thermal stress calculations indicate values for these stresses of the order of 1 psi for temperatures above 70^0F for Polycarbutene R propellant for the more severe cases (small motor diameter, high web fraction). Equilibrium stresses associated with glass-like behavior are physically unattainable even by shock cooling of a real grain because of finite thermal equilibrium times and the virtual impossibility of cooling a practical grain below its glass transition temperature without failure by web cracking.

The second approach is more promising, but is arbitrary in that a thermal equilibrium time must be assumed. The thermal equilibrium time is mathematically infinite and therefore does not permit selection of a non-arbitrary time for solution. Taking the time to be that at which the grain reaches 98 percent of thermal equilibrium (about the time that the peak stresses are obtained in the transient step temperature solution) leads to a calculated core-grain interface stress of 15 psi for a 1-foot diameter, 50 percent web fraction grain. This compares to the computer value of about 9 psi (Figure 4-2).

While in this instance the limit calculation yields an estimation for the stress that is in the "ballpark", the size of the ballpark can be expected to change an analytically unpredictable amount with temperature, grain diameter, and web fraction. The calculation yields stress values that are probably better than an uninformed guess, but of little real engineering use.

4.4 PHOTOTHERMOVISCOELASTICITY

The use of photothermoviscoelastic techniques as an experimental adjunct to transient thermal stress analysis was studied in this program, largely in subcontract activities at the University of Washington and at New York University. The purpose of the New York University program was to obtain, variously, photoviscoelastic data for transient thermal fields. The University of Washington effort, much smaller in scope, was directed at theoretical inquiry in this area of interest.

The New York University effort, under the personal direction of H. Becker, proceeded in a photoviscoelastic calibration of a Hysol material at temperatures near the glass transition temperature of the material. Photographs of fringe patterns in simulated plane stress rocket grain configurations made from the Hysol were also obtained. However, the work did not yield information of specific technical worth to the program, largely because of insufficient development of the theoretical aspects of the problem[1].

Redirection of the photothermoviscoelastic research was made to permit concentration on the theoretical problems, with the redirected work being carried out at the University of Washington under the direction of Prof. R.J.H. Bollard and with the assistance of Dr. Ellis Dill. A report of this investigation is presented in Section 4.4.1

[1]The final report of N.Y.U. effort was submitted on 12 Nov 1962 with LPC Monthly Progress Report No. 11.

4.4.1 University of Washington Subcontract Work[1]

Introduction. A theoretical basis was developed for the experimental determination of the stress state of a viscoelastic material in transient plane stress due to temperature changes and external loads.

The following summarizes the theoretical and experimental results of this work.

Basic Theory. Experiments on the birefringence of high polymers indicate that the birefringence depends on the time history of the mechanical state in the same way as constitutive relations for linear viscoelastic materials. This suggests the hypothesis that the dielectric tensor to the one-half power depends on the strain tensor by a Duhamel type or hereditary integral, of the same form as for the dependence of the stress tensor on strain history, but with a different kernel which may be called the optical-relaxation function. For isothermal deformations this leads to a relation between stress and fringe order n of the form

$$\sigma_x - \sigma_y = \frac{1}{h} \int_o^t \kappa(t-\xi) \frac{d}{d\xi} \left\{ \eta(\xi) \cos 2\alpha(\xi) \right\} d\xi \ ,$$

$$t_{xy} = \frac{1}{h} \int_o^t K(t-\xi) \frac{d}{d\xi} \left\{ \eta(\xi) \sin 2\alpha(\xi) \right\} d\xi \ ;$$

where h is the model thickness and $\alpha(t)$ is the angle between the x-axis and the axis of polarization.

If it is found that the temperature dependence of the optical-relaxation function can be described by a temperature shift-factor which is identical

[1]This section was prepared by Professor R. J. H. Bollard and Associate Professor E. H. Dill, University of Washington.

to that for the mechanical response, then the thermal stresses depend on the birefringence in a similar way[1]:

$$\bar{\sigma}_x - \bar{\sigma}_y = \frac{1}{h} \int_0^\tau \bar{K}(\tau - \xi) \frac{d}{d\xi} \left\{ \bar{\eta}(\xi) \cos 2\bar{\alpha}(\xi) \right\} d\xi ,$$

$$\bar{\tau}_{xy} = \frac{1}{h} \int_0^\tau \bar{K}(\tau - \xi) \frac{d}{d\xi} \left\{ \bar{\eta}(\xi) \sin 2\bar{\alpha}(\xi) \right\} d\xi ;$$

where $\tau(t)$ is the reduced time,

$$\tau(t) = \int_0^t \Phi(T(\xi) d\xi ;$$

$\Phi(T)$ is the temperature shift factor;

$$\bar{\sigma}_x = \sigma_x(t(\tau)), \text{ etc. } ;$$

and

$$K(t) = \bar{K}(\Phi(\tau) t)$$

is the optical relaxation function at temperature T.

Experimental Procedure. According to the theory, it is necessary to have a complete record of fringe order n(t), the angle of polarization $\alpha(t)$, and the temperature T(t) at a point in order to determine the difference in principal stresses and the axis of principal stress at that point.

The fringe order is found by observation of the isochromatic lines. A number of photographs of the isochromatic pattern at a sequence of times $t_1, t_2, \ldots . t_n$ will allow the determination of n(t) at each point.

In order to find the axis of polarization at an arbitrary point it is necessary to make simultaneous observations of the isoclinic pattern for various angles of polarization of the incident light. In an ordinary photoelastic polariscope this is accomplished by manually rotating the polarizing and analysing element. However, in the transient viscoelastic problems which may be of interest the isoclinic field may vary rapidly, and it will be necessary to make perhaps ten photographs of the isoclinic field for ten different orientations of the polarizer and analyser. The need for this "instantaneous" sweep of the isoclinic field precludes the use of manually rotated elements in the bench. Mr. Michael Fourney has suggested that the rapid rotation of the angle of polarization of the incident light can be accomplished by means of

[1]Appendix B

the Faraday effect. This electronic means will allow the recording of ten photographs of the isoclinics for each photograph of the isochromatic pattern at practically the same time instant t_1.

The photographic record can then be analyzed to determine n(t) and α(t) for any point.

The complete experimental apparatus is diagramed in Figure 4-10. The details of operation for a bench of this type were described in the earlier report.

Program for Experiment. Phase one of the experimental program should be to determine whether there exists model materials which have the desired mechanical properties and for which a linear integral relation between strain tensor and dielectric tensor exists. Some initial tests have been carried out in this program to determine whether further studies are justified.

A tension test creep specimen was placed in a standard plane polariscope. The change in length was recorded automatically as a function of time by means of an LVDT displacement gage. The fringe order variation with time was determined from continuous recording of the intensity of light transmitted by the model with a photocell. The apparatus is shown in Figure 4-11.

The most promising material found was a polyester-styrene resin with trade name Polylite 8151 supplied by Reichold Chemical Company to which 1% MEK peroxide hardener was added and the batch poured in the mold and cured at room temperature. The results of the test are purely qualitative and are shown in Figures 4-12 and 4-13.

It can be seen that the optical creep is a curve of the same form as the mechanical creep, but not exactly the same. Thus, the optical creep function can not be a simple scalar factor times the mechanical creep compliance.

A more elaborate experimental calibration apparatus has been constructed which will allow an accurate determination of the limits of applicability of the linear integral relation at various temperatures, and to investigate the existence of an optical temperature shift factor for the Polylite and other materials. This apparatus is diagramed in Figure 4-14. This bench has recently been completed and is shown in Figure 4-15.

Phase two of the experimental program will be to develop methods of practical stress analysis. In conjunction with this phase the experimental apparatus of Figure 4-10 will be assembled.[1] It is hoped to have an operating bench for quantitative investigations by midsummer of 1963.

---

[1]Partially supported by a grant from the National Aeronautics and Space Administration.

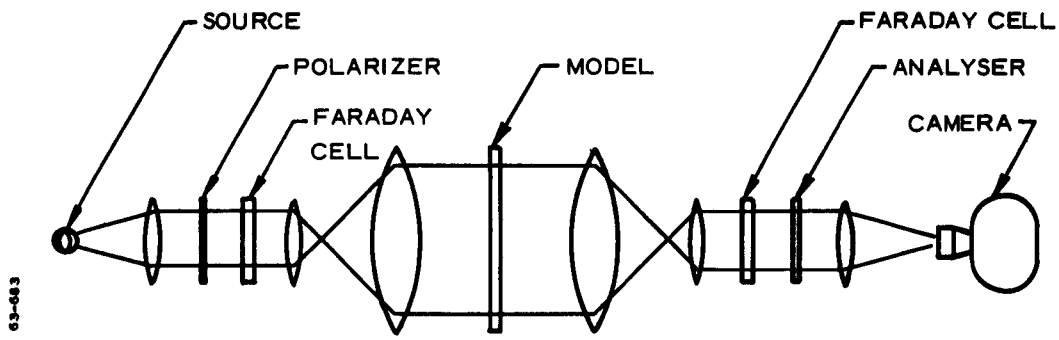

Figure 4-10 Plane Polariscope for Transient Loadings

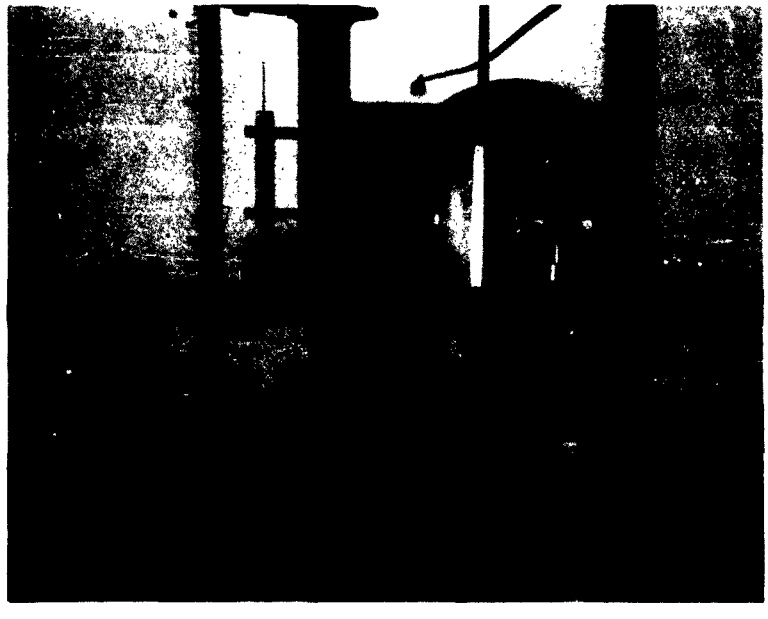

Figure 4-11 Mechanical and Optical Creep Test

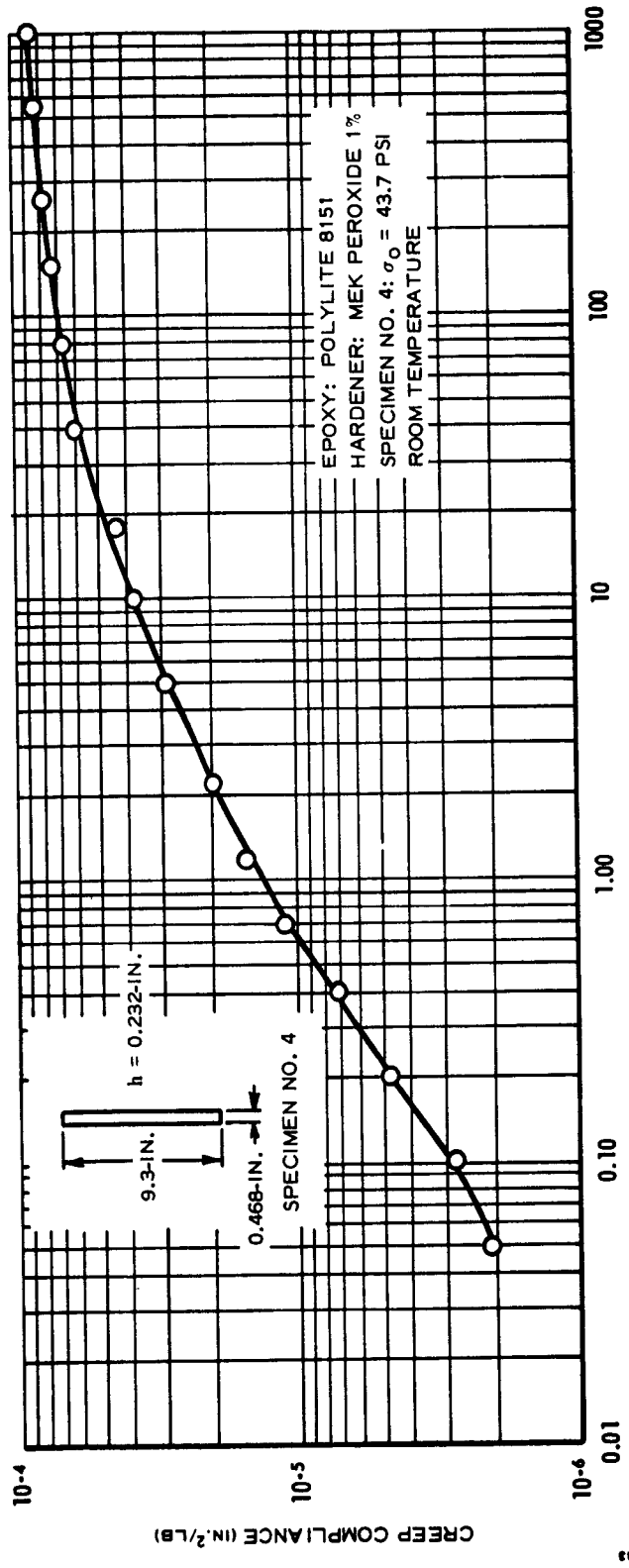

Figure 4-12 Mechanical Creep

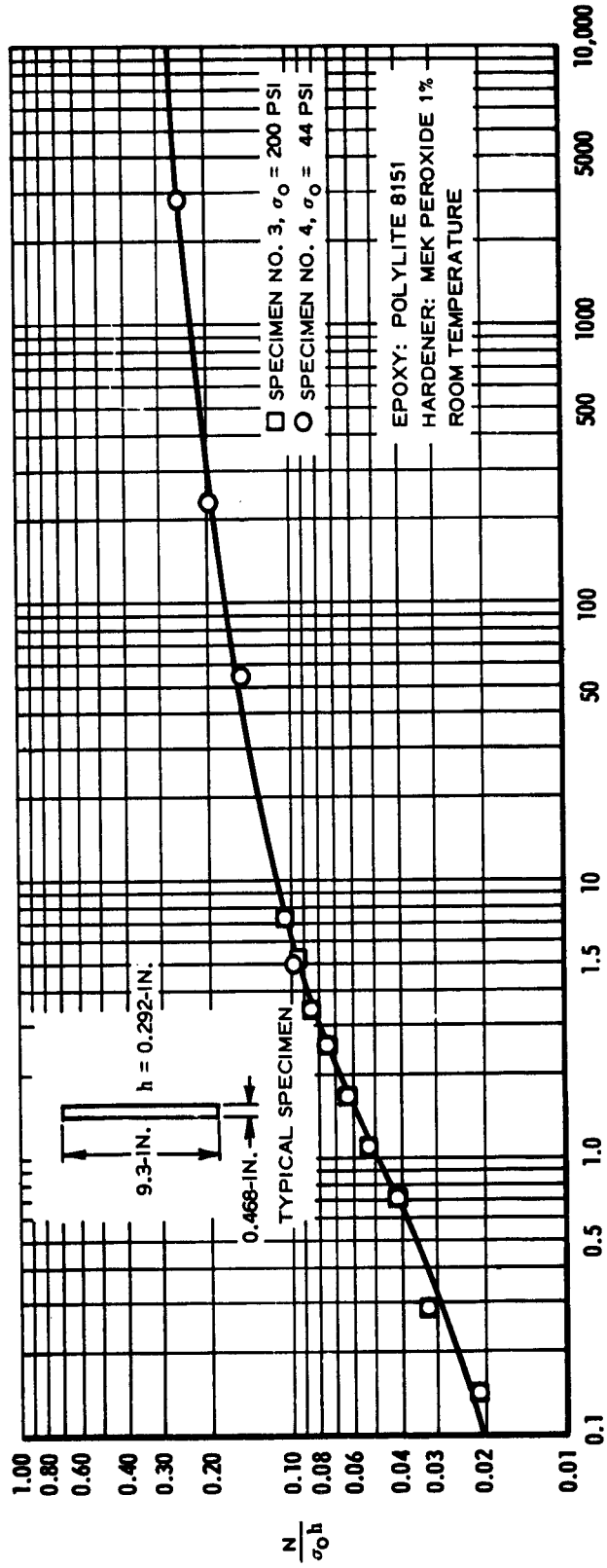

Figure 4-13 Optical Creep

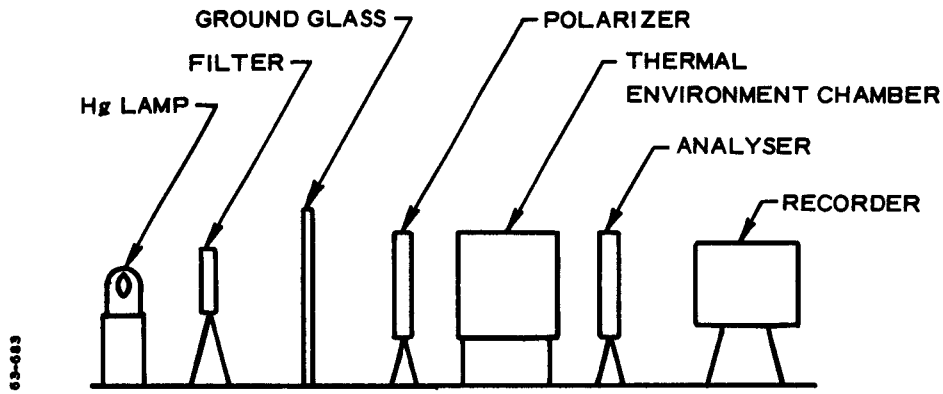

Figure 4-14 Diffused Light Polariscope for Material Characterizations

Figure 4-15 Material Calibration Apparatus

Recommendations. Steps should be taken to establish at least two different centers to undertake experimental characterization of materials which may be used to mechanically simulate solid propellant materials and which exhibit the birefringent effects. It appears that, with the numerous resins and plasticizers available, mechanical properties of nearly arbitrary nature can be achieved. It is recommended that some standard material and curing procedure be agreed upon by the various centers. The experimental program should then proceed in the indicated manner -- first, complete characterization of the standard material; second, development of a routine stress analysis technique.

Theoretical work toward establishing a basis for applying photoanalysis where nonlinear viscoelastic behavior is present should be started at this time. It is felt that photoanalysis may prove to be an effective tool for such problems.

4.5 DISCUSSION

4.5.1 Transient Thermal Stress Computation

The data presented in Section 4.2 for transient thermal stresses in a circular port, plane strain, rigid case propellant grain are the only such data known to be available as of this date. The engineering validity of the data for thermal stresses is subject to unknown but presumably small error limits. Following is an examination of the transient analysis data, considering the accuracy of the various input parameters to the problem, and a review of the engineering applicability of the analysis.

Thermal field input information as entered in the computer analysis explicitly determines the grain strains and the spatial dependence of the grain properties Hence, the associated stress field is that required by the thermal field and its interaction with the grain. As specified by the field expressions discussed in Section 2, Volume I, thermal distributions have been verified to be accurate for specified temperature boundary conditions both in motors and in uncured propellant grains. In both the particular case of a grain surface (or motor case) temperature specification and in the general case of a specification of a motor environmental temperature, the thermal field solutions for the grains converge in accuracy as thermal equilibrium is approached. The sensitivity of the stresses is highest to thermal field variation near the thermal equilibruim condition for a negative temperature change. Therefore, the thermal field predictions are estimated to be of excellent engineering accuracy for a given thermal input in which the case temperature is decreased in some time-dependent manner, arriving at a specific constant level. The above comments are predicated upon axisymmetric thermal field conditions.

The propellant viscoelastic data used in the thermal stress problem are probably the likeliest source of error. This is partially because of an inherent difficulty in obtaining broad spectrum physical data for a propellant and certain pragmatic objections to the reduced variable approached used in construction and application of the master viscoelastic representation. The master or reduced relaxation specification (Section 3.2, Volume I) is constructed from isothermal tests across discrete time intervals for various temperatures. Hence, the master relaxation spectrum, which extends across approximately 20 decades of time at a single temperature, is assembled from segments of isothermal data each of which is rigorously valid only across the 2 to 5 decades of time of actual observation. The associated time-temperature shift relation, a_T, is developed as a product relation in the reduction procedure, a technique inherently susceptible to cumulative inaccuracy. The accuracy of the shift factor, a_T, is of paramount importance in the thermal stress calculations since the sensitivity of the stresses to variation of a_T in the solution is higher than for any other single parameter

Additionally, the fundamental question arises as to the validity of equating, for example, a 160°F temperature change to a 10-decade time scale shift. Theory in this connection is not particularly well developed; however, experimental observations do lend credence to the results obtained in the reduced variable approach (Section 5.4, Volume I).

The preceding commentary on the accuracy of the propellant viscoelastic properties presents a pessimistic view of the problem, but probably an unrealistically pessimistic view. It was noted previously that a replicate viscoelastic characterization of the Polycarbutene R propellant conducted on a batch cast from different lots of raw materials gave reduced properties essentially identical to the data used in this program (Section 3.5, Volume I). The observation shows that the viscoelastic data are generally reproducible, a vital intrinsic characteristic for engineering analysis. In addition, the nature of the stress analysis problem is such that errors arising from propellant property error would tend to increase with the magnitude of the temperature excursion from the reference state. Restricting the temperature range of interest to -65°F and above, the errors appear tolerable from the point of view that the computed stress fields are consistent with observed grain failure behavior (Section 5.4, Volume I).

In summary, while determination of the absolute accuracy of propellant reduced variable data for stress analysis purposes requires additional sophisticated experimental inquiry, acceptable engineering accuracy in propellant broad spectrum properties characterization has been attained, as judged by available criteria.

The asumptions made in the transient thermal stress analysis are reasonable engineering idealizations of practical rocket motor grains. Stipulation of propellant rubberlike incompressibility has been shown to be an accurate engineering condition in independent investigations (Jones, 1963). The assumption enables certain analytic simplifications in the stress analysis solution, among which is the simplification of the basic stress-strain law for rigorous interpretation in a state of uniaxial tension, the physical state in which the propellant properties were measured. The assumption of plane strain end conditions for the grain tends in the conservative direction for most moderate length, moderate web fraction motors. In general, a plane strain analysis that predicts undesirably high stress or strain levels in a propellant grain signals a need for extreme care in the design of a finite length grain for the same diameter and web fraction. The assumption of case rigidity is consistent with the observed behavior of steel case rocket motors under low states of grain stress, such as are observed under transient thermal states.

The basic analysis as developed by Purdue University was shown to have an analytic proof of convergence. The accuracy of the calculations inherent to the mathematic framework was shown, hence, to be restricted only by the extent to which temporal iterations and calculation of series expansion

terms was done (Volume II, Appendix III). Both of these latter processes are limited by the computer storage capacity and are practical rather than theoretical problems. In practice, the observed reproducibility of the computer-determined stresses was approximately ± 2 percent, the limitation on accuracy arising from the temporal iteration flexibility of the program.

In summary, the stresses obtained in the calculation are believed to be of realistic engineering value for the imposed thermal boundary conditions.

4.5.2 Thermal Stress Accumulations

A primary objective in this program was elucidation of the possible phenomenon of thermal stress accumulation. Theoretical study of thermal stresses in a viscoelastic slab arising from step cyclic temperature boundary conditions showed, for uncomplicated constraints, that thermal stress accumulation was conceptually possible. It was not possible during the program to develop analytic proof or disproof for the phenomenon for the case-bonded circular port grain subjected to external thermal inputs. Thus, the numerical data for various types of step-cyclic external thermal inputs provide the only insight into the problem of stress accumulation in rocket grains. The data show no evidence for stress accumulation in a linear viscoelastic propellant grain, as considered in Section 4.2, Volume I, for widely varying thermal field input conditions. The conclusion reached was that stress accumulation in linearly viscoelastic propellant grains under realistic field conditions is unlikely in any significant degree, even though the conceptual possibility for accumulation represents an as yet unresolved problem

4.5.3 Peak Thermal Stresses for Shock Cooling

The parametric data for peak thermal stresses in grains subjected to various negative thermal step inputs (Figures 4-5, 6, 7, and 8) was tabulated to provide a basis for engineering limit analysis. Specifically, the stress levels shown correlate to the maximum stresses obtained following instantaneous thermal coupling of the rocket motor case to an infinite negative heat source (e.g., immersion of the motor in a fluid at the reduced temperature, for engineering purposes). Higher stress peaks are not possible for any physically realistic process by an external cooling process without stress accumulation. The peak stresses shown are conservatively high for slower rates of cooling and therefore represent useful criteria for engineering grain analysis. Considerations regarding grain failure criteria and structural integrity analysis are discussed in Section 5, Volume I, and in Volume III of this report.

4.5.4 Photothermoviscoelasticity

During this program, the state of the art in use of photoviscoelastic investigation of thermal stresses regressed from a condition of engineering applicability (as originally proposed by New York University) to a state of conceptual theoretical study. It was found upon rigorous investigation of the problem that observed fringe patterns in transiently heated viscoelastic grain models could not be interpreted for quantitative stress values because of an insufficient theoretical and experimental basis for the interpretation. However, theoretical and experimental study at the University of Washington resulted in significant progress in this area. A theoretical foundation was developed for interpretation of stresses in birefringent, viscoelastic models, and limited experimental progress was made in verification of the theory.

Continued effort in development of experimental stress analysis techniques for the transient thermal viscoelastic problem is considered important. At the present time, the possibility of analytic solution for transient thermal stresses in a star-perforated grain, or in a grain asymmetrically heated, is considered unlikely by presently known techniques. While a problem of considerable difficulty, the development of photothermoviscoelastic experimental techniques may be tractable. If so, engineering treatment of structural problems particularly pertinent to high-performance airborne missiles may prove feasible.

Section 5

GRAIN FAILURE ANALYSIS

5.1 BACKGROUND

A complete grain structural integrity analysis requires the existence of a suitably accurate method for determining grain stresses and strains and a criterion for evaluation of the possibility of failure of the grain. Grain stress analysis for isothermal grain conditions of both general and specific interest presently is in an advanced state for linear materials under small strain conditions (Fitzgerald, 1962). The state of the art in engineering analysis for transient thermal states is updated by this report. However, propellant grain failure criteria for either isothermal or transient thermal states are somewhat more tenuous on both theoretical and experimental bases.

This section presents the results of experimental grain failure investigations for transient and cyclic thermal conditions as investigated in scaled or analog rocket motors.

5.2 MOTOR ANALOG EXPERIMENTS

A set of 4-inch diameter by 14-inch long, circular port analog rocket motors (Figure 5-1) of varying web fraction were cast from a single batch of Polycarbutene-R propellant. The dimensional data for the motors are as follows:

Motor No.	Length ÷ Diameter	Grain Outer Diameter ÷ Grain Inner Diameter	Web Fraction (percent)
1, 1A, 1B	2.5	4/1.5	63.5
2, 2A, 2B	2.5	4/1.2	70
3, 3A, 3B	2.5	4/1.0	75
4	2.5	4/0.866	78

The motors were subjected to various externally imposed thermal conditions with the motors sealed, internally desiccated, and with the ends of the grain insulated. All motors were stored in a $70^0 \pm 3^0$F, desiccated environment for $3\frac{1}{2}$ months prior to initiation of the test series. The motor case and port surface temperatures were monitored with bonded, standardized thermocouples in all tests. Port diameter measurements in the motors were made at the midpoints of the grains using a Mueller gage inserted through a temporarily unsealed end of the motor (Figure 5-2). In all cases where strain measurements were made, the operation was carried out quickly enough to confine the grain thermal excursion during measurement to less than 1^0F. Grain port measurements were reproducible to within ±0.002 inch.

5.2.1 Rapid Monotonic Cooling Test

Motors No. 1, 2, 3 and 4 were subjected to rapid cooling from equilibrium at 70^0F to equilibrium at -75^0F. Figures 5-3, 5-4, 5-5, and 5-6 show the case and port temperatures, and the measured port hoop strain, calculated as the incremental change in diameter divided by the original casting mandrel diameter. Figure 5-5 shows the predicted grain port temperature versus time based on the techniques discussed in Section 2, Volume I, using the observed case temperature as the pertinent boundary condition.

Based on the cumulative strain at maximum stress technique (Jones, 1963), grain failure predictions were made taking the temperature and strain rate conditions of pertinence to be those measured at the grain ports.

Figure 5-1 5-inch Diameter by 14-inch Long Circular Port Analog Motor

Figure 5-2 Port Diameter Measurement Taken Using a Mueller Gage

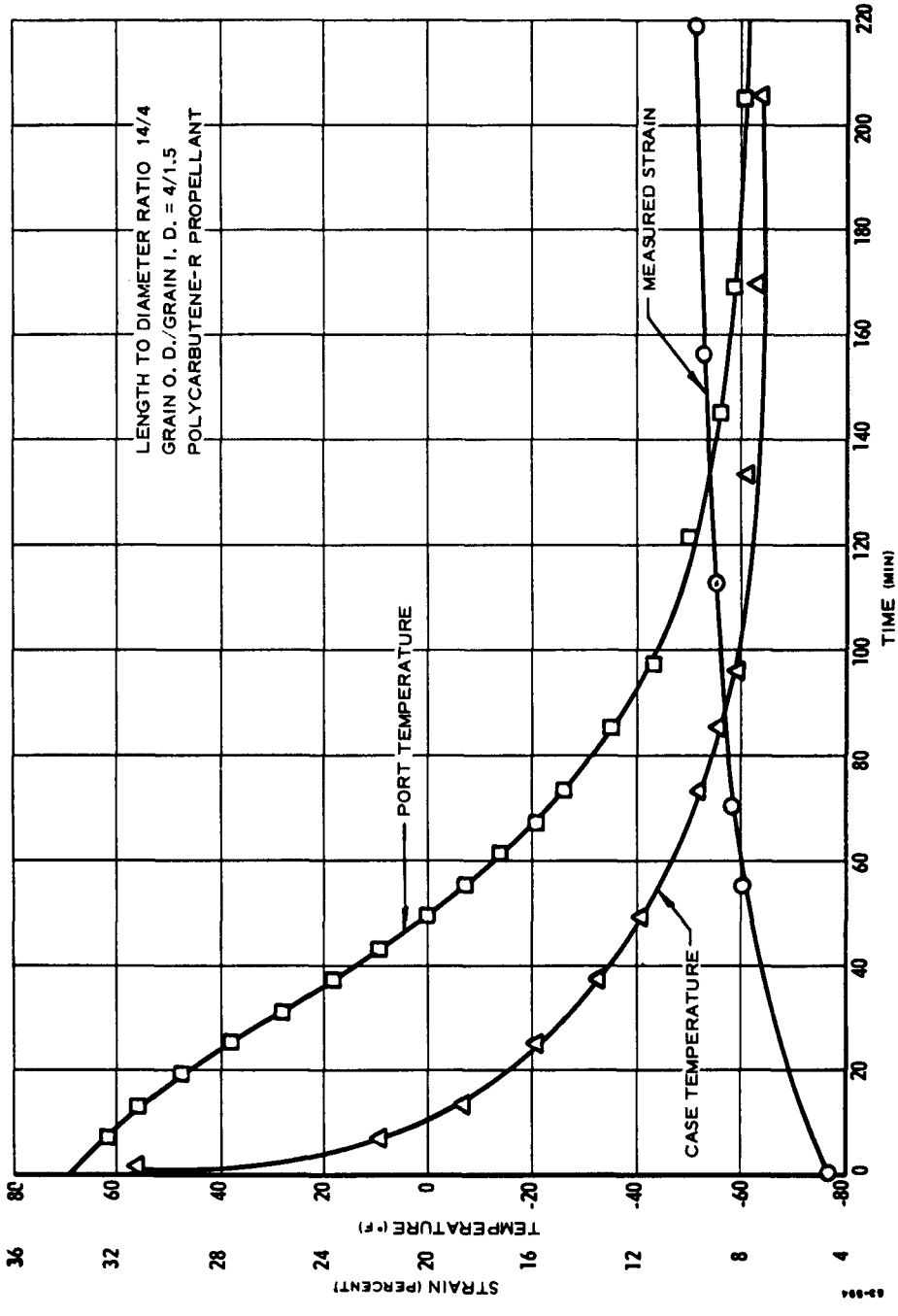

Figure 5-3 Analog Motor Test Data, Motor No. 1

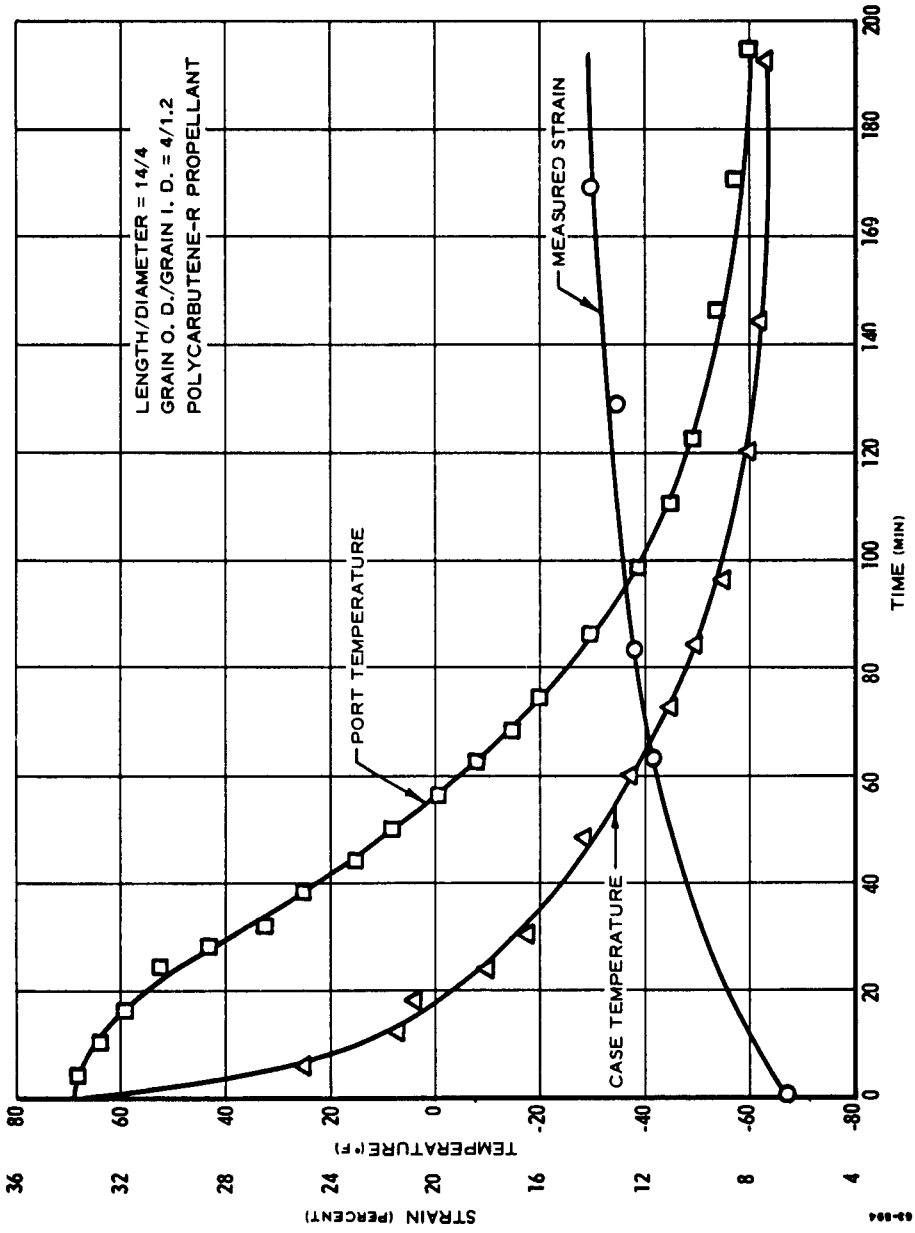

Figure 5-4 Analog Motor Test Data, Motor No. 2

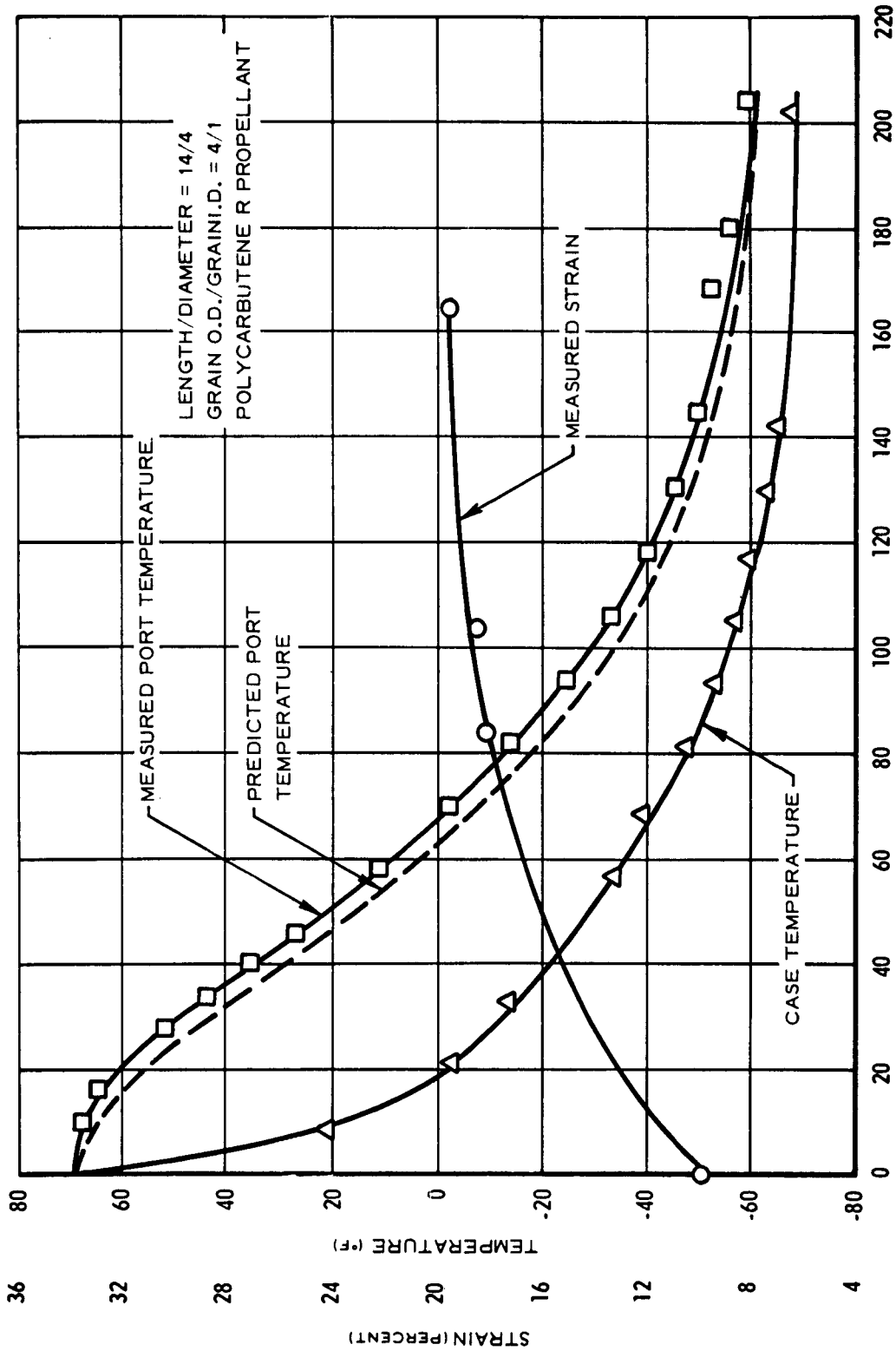

Figure 5-5 Analog Motor Test Data, Motor No. 3

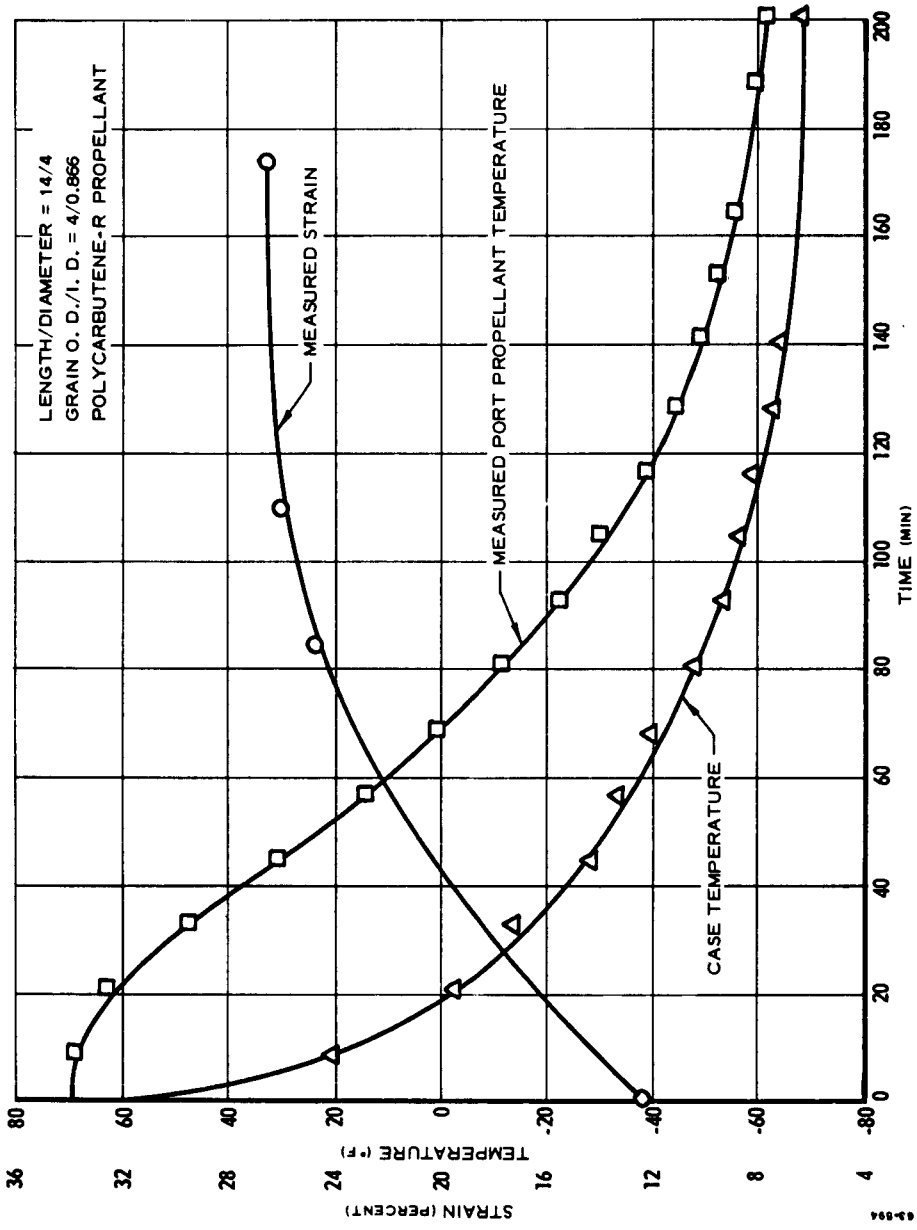

Figure 5-6 Analog Motor Test Data, Motor No. 4

The technique is as follows. For a condition of continuous slow cooling, the port hoop strain increments for small temperature increments are calculated. The strain occurring in each increment of time and temperature is related to the propellant physical data for the corresponding strain rate and temperature The fractional consumption of strain capability used in traversing each temperature increment is summed. The temperature at which the sum of the fractions equals unity is the predicted low temperature limit for the grain. A description of the analytical and interpretive methods is presented in Volume III of this report. The (isothermal) strain versus temperature profiles for the motors and the predicted failure conditions are shown in Figure 5-7. With the exception of the highest web fraction analog (No. 4), the failure temperatures were predicted quite accurately. Failure of the No. 4 motor was anticipated somewhat below the isothermally predicted temperature because of the transient conditions. The tests demonstrated excellent accuracy in prediction of failure temperatures for the motors of further interest, the replicates of motors No. 1, 2, and 3.

5.2.2 Thermal Shock Experiments

Motors No. 3A and 3B were subjected to rapid cooling to -30^0F and, after obtaining thermal equilibrium, immersed in a circulating water bath maintained at 193^0F. The pertinent thermal field data (Figure 5-8) show excellent agreement between measured and predicted port temperature versus time variation. The predicted port temperature variation was based on the energy methods described in Section 2, Volume I.

With reference to Figure 5-7, at -30^0F the motors were within 15^0F (or within 3 percent strain) of predicted failure. Limit calculations assuming a 160^0F temperature rise of the case in two minutes predicted that the additional port strain increment would accumulate the additional strain to the failure fraction required to cause grain cracking. Alternately, the grain stresses also were predicted to rise to values near those associated with either case unbonding or port cracking conditions. The motors failed by extensive port cracking.

5.2.3 Cyclic Experiments

Motors No. 1A, 1B, 2A and 2B were subjected to repetitive cycling between -50^0F and 160^0F, with each complete cycle taking place in a 24-hour period. (Figure 5-9). With reference to Figure 5-7, at -50^0F the No. 2 motors were within 10^0 to 15^0F (or $3\frac{1}{2}$ percent strain) of predicted failure and the No. 1 motors within 25^0 to 30^0F (or 9 percent strain) of failure. One of the No. 2 motors failed after one cycle, and one failed after eight cycles. The No. 1 motors survived 22 cycles without sign of failure and without change in the

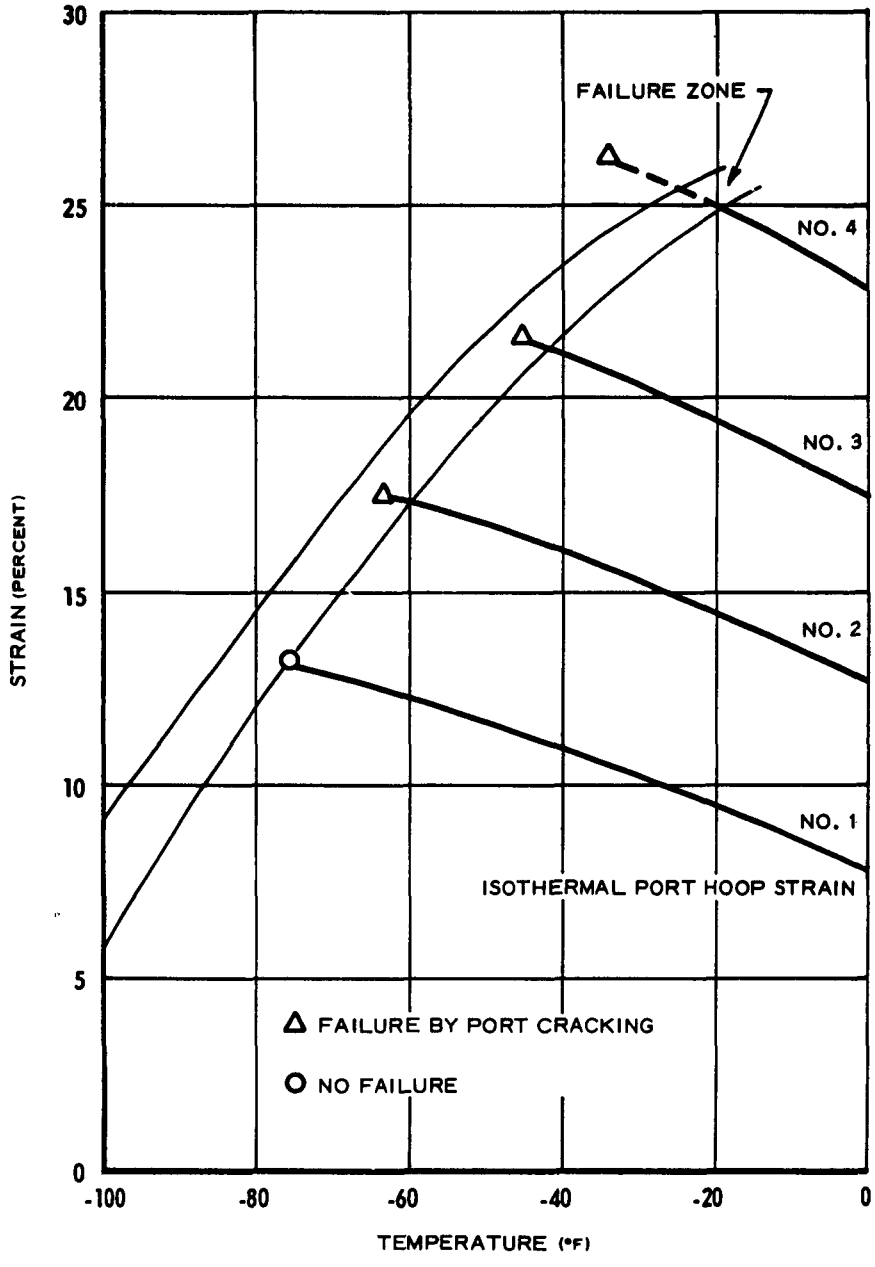

Figure 5-7 Analog Motor Experiments Shock Cooling

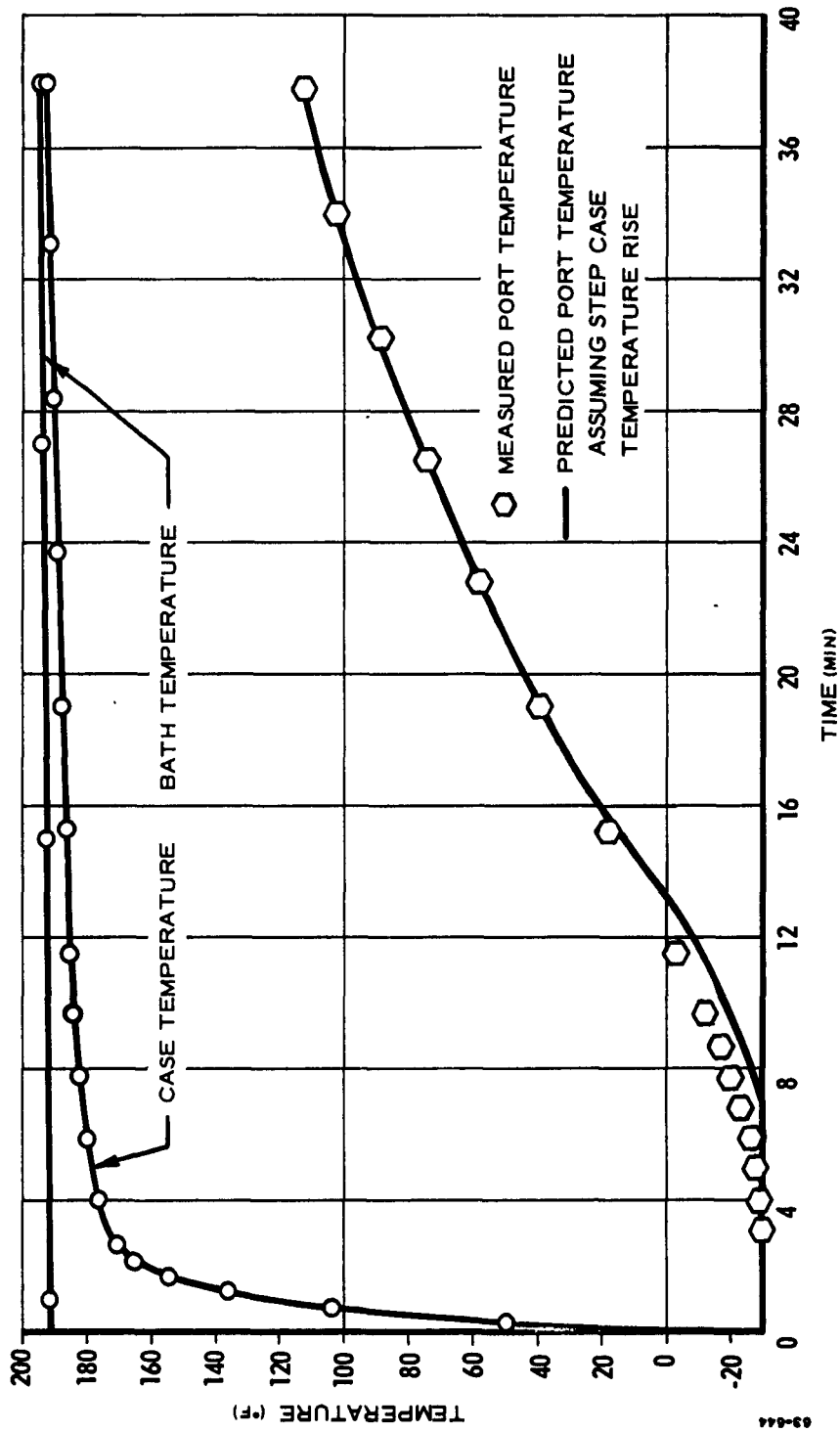

Figure 5-8 Shock Heating Experiment, 4 by 14-inch Analog Motors

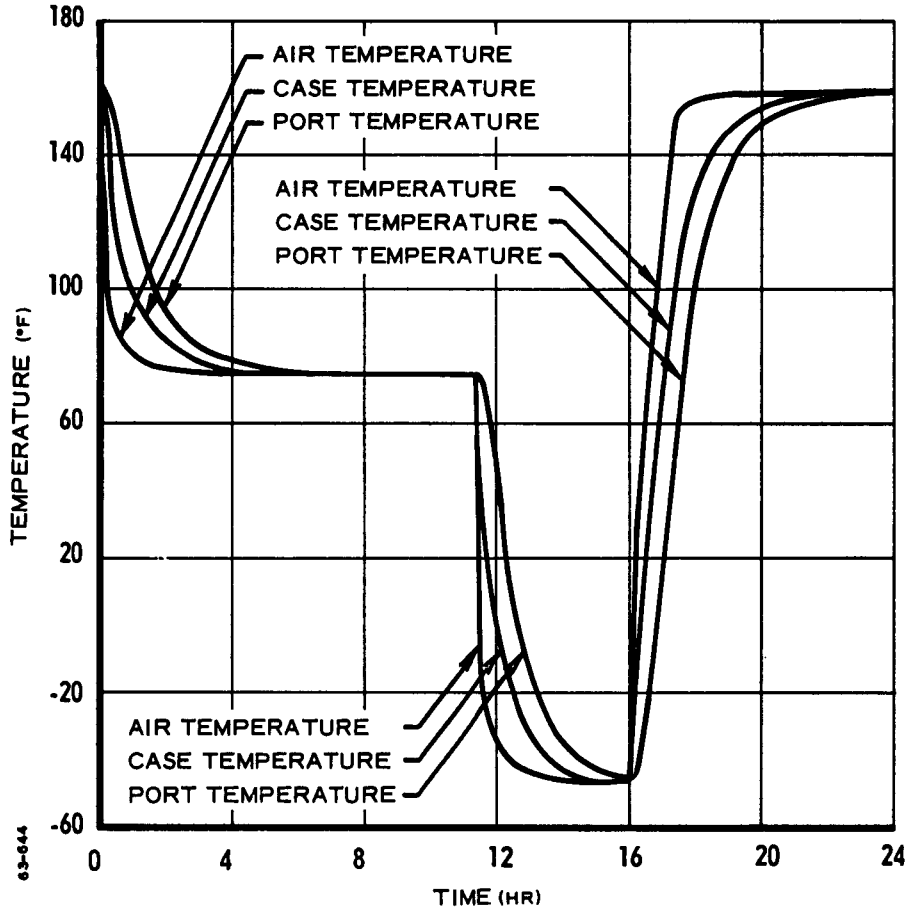

Figure 5-9 Cyclic Conditioning Test, 4 by 14-inch Analog Motor

port diameter as measured at thermal equilibrium at 70°F during each cycle. Following cycling, the No. 1 motors were cooled rapidly from 70°F to failure, which was observed at -80° to -85°F. Hence, it was observed that an accumulation process leading to failure took place in the No. 2 motors. Conversely, the No. 1 motors exhibited no accumulation of failure during cycling as demonstrated both by the dimensional stability of the grains and the final failure temperatures of the motors, which agreed with those for uncycled motors (reference Figure 5-7).

In review of the propellant constant strain rate uniaxial data, it was observed that in the temperature range 0° to -100°F, apparent nonlinearity in the viscoelastic behavior was observed at strain levels above 0.6 to 0.8 the measured strain at maximum stress value, ϵ_m, as reduced for time and temperature effects. By comparison, the No. 1 motors on each cycle were strained to approximately 0.5 ϵ_m and the No. 2 motors to approximately 0.8 ϵ_m, at -50°F.

The observations are consistent with the hypothesis that the strain limit defined by linear viscoelastic behavior of the propellant corresponds to a thermal cycling fatigue failure limit. While not statistically imposing, the data are vitally interesting and indicate an important area for further experimental effort.

5.3 DISCUSSION

The strains in a transiently cooled grain are produced only by the thermal field and not influenced to a significant degree by the stresses. Time and the temperature integration of the strains and strain criteria therefore is relatively straightforward, accepting the reduced variable treatment of the uniaxial failure strain data. The data show evidence for acceptance of the laboratory uniaxial strain at maximum stress as a grain failure criterion for monotonic cooling of a motor to failure. Additional support for this criterion has been discussed by Jones, 1963. With some trepidation, the limited experimental motor cycling data obtained in the program indicate that three-fourths the laboratory strain at maximum stress is a reasonable thermal cyclic failure criterion. The reduced variable approach to comparison of the strains is, of course, necessary.

However, evaluation of the motor analog data in terms of possible stress-determined failure criteria was not possible. Such investigation would have required theoretical and experimental effort outside the scope of the program. Complex by comparison to evaluation of the analog data by strain criteria, the nature of the problem is as follows. Transient cooling produces stresses in a grain that increase with time (and decreasing temperature) toward a maximum value. The maximum stresses are attained near the time that thermal equilibrium of the grain is reached and decay monotonically as time progresses. The strength of the propellant also increases as the temperature decreases and will be, for the stated conditions, a maximum near the thermal equilibrium time of the motor. At longer times, the comparative strength will decrease. The probability of failure, as evaluated in terms of stress, depends upon the relative rates of increase of grain stress and grain strength with decreasing temperature. The stress rates can be calculated by the methods previously discussed (Section 4, Vol. I). However, the strength increase rate with temperature cannot be interpreted accurately by presently available techniques for the condition of continuously varying temperature.

This problem area merits continued study. It is reasonable to expect that grain unbonding as a result of thermal stress will compare to a propellant stress criterion. The rationale for this instance arises from the observation that the stresses at the case-bond interface are not accompanied by significant straining, except near the ends of a finite grain.

A limit condition considered in interpretation of the shock-heated analog motor failures is of interest (Section 5.2.2 above). Viscoelastic stresses resulting from imposition of the thermal shock on the case were calculated assuming no change in the grain temperature. The increment of hoop stress at the port, introduced by the case expansion exceeded the isothermal stress capability of the propellant as measured in the laboratory at the corresponding strain rate and temperature. The case-bond interface stress increment, as compared to

the propellant strength at the case temperature, also exceeded the measured propellant strength.

However, as previously noted, the incremental port hoop strain increment also exceeded the propellant strain capacity and a separation of criteria was possible only in that port cracking, not bond failure, was observed.

REFERENCES

Boley, B.; Weiner, The Theory of Thermal Stresses, John Wiley and Sons, Inc., New York, 1960.

Carslaw, H.S.; Jaeger, Conduction of Heat in Solids, Oxford Univ. Press., 1959.

Williams, M.L.; Blatz, Schapery, 1961, Fundamental Studies Relating to Systems Analysis of Solid Propellants, Galcit Report SM-61-5.

Ferry, J.D., 1961, Viscoelastic Properties of Polymers, Wiley.

Treloar, L.R.G., 1958, The Physics of Rubber Elasticity, Oxford.

Lee, E.H., 1955; Stress Analysis in Viscoelastic Bodies, Quarterly of Appl. Math., Vol. 8, p 183.

Jones, J.W., 1963; Proceedings of 1st ICRPG Mechanical Behavior Working Group,, Facility Report, Orlando, Florida.

Fitzgerald, J.E., 1962; Bulletin of 20th JANAF Solid Propellant Group Meeting.

LPC, 1962-1963a Monthly Progress Reports No. 1-18, MPO 578, Thermal Grain Structural Analysis.

LPC, 1962-1963b Quarterly Technical Notes, No. 1, 2, and 3, MPO 578, Thermal Grain Structural Analysis.

LPC, 1963c; Final Report, MPO 556, Structural Integrity of Propellant Grains.

APPENDIX A

THERMAL FIELD SOLUTIONS

A-1. INTERNAL HEATING OR COOLING[1]

A hollow cylinder whose outer surface is insulated and whose inner port is subjected to a step change in temperature is considered. The solution assumes a temperature distribution as follows:

$$T = \begin{cases} T_o \left[1 - \dfrac{(r-a)}{q_3} \right]^2 ; & r-a \leq q_3 \\ 0 & r-a \geq q_3 \end{cases} \qquad (A.1)$$

As shown in Figure A-1, the penetration depth q_3 varies with time. The heat front in this case moves from the constant temperature inner port to the insulated outer surface. Equation A. 1 is compatible with this phenomenon and is therefore a suitable choice for the approximate techniques given by Boley and Weiner, 1960. The relation between q_3 and the time was obtained from the energy technique and is as follows:

$$\frac{q_3^3}{a^3} + \frac{3q_3^2}{a^2} = \frac{30\kappa t}{a^2} \qquad (A.2)$$

or

$$\overline{q_3}^3 + 3\overline{q_3}^2 = 30\lambda^2 \eta^2 \qquad (A.3)$$

where

$$\begin{aligned} \overline{q_3} &= q_3/a \\ \lambda &= b/a \\ \eta^2 &= \kappa t/b^2 \end{aligned} \qquad (A.4)$$

[1] Reference Section 2, Volume I for terminology.

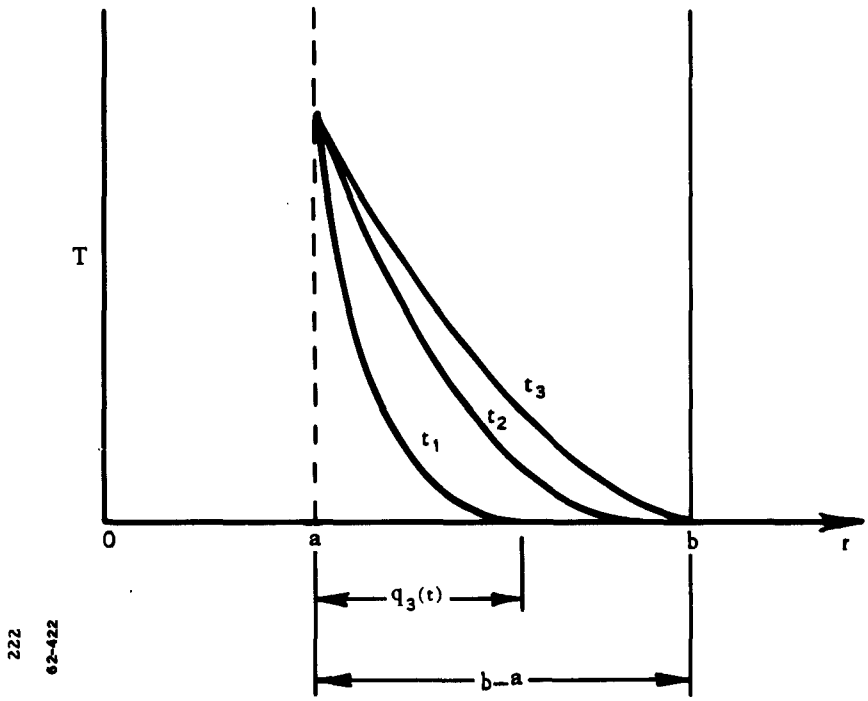

Figure A-1 Penetration Depth versus Time

Again, the equation for the penetration depth is a cubic with only one significant root. This root is obtained as follows:

$$\bar{q}_3 = y - 1 \tag{A. 5}$$

and

$$y = 2 \cos \theta / 3 \tag{A. 6}$$

where

$$\cos \theta = -1 + 15\eta^2 \lambda^2 \tag{A. 7}$$

Equation A. 7 is valid only for

$$1 \leq \frac{2}{15\lambda^2} \tag{A. 8}$$

since

$$\cos \theta \leq 1$$

For values of $\lambda \leq 2$, Equations A. 5 through A. 7 can be used to solve for $\bar{q}_3$ for each value of η^2 and hence time. However, if $\lambda > 2$, the solution of the cubic cannot be solved in this simple manner. Since $\bar{q}_3$ is the nondimensional penetration depth, physically it must lie between 1 and $\lambda - 1$. Hence the value of $\bar{q}_3$ can be computed for each value of time, for example, by an iteration technique.

As time progresses, $\bar{q}_3$ increases until it obtains the value

$$\bar{q}_3 = \frac{q_3}{a} = \frac{b-a}{a} = \lambda - 1 \tag{A. 9}$$

or the heat front reaches the outer surface. The time interval necessary for this to occur is found by setting

$$\bar{q}_3 = \lambda - 1$$

hence from Equation (A. 3) the value of the thermal diffusion parameter, η^2 is given by

$$\eta_a^2 = \frac{\lambda^3 - 3\lambda + 3}{30\lambda^2} = \frac{(\lambda - 1)^2(\lambda + 2)}{30\lambda^2} \tag{A. 10}$$

Hence the time, t_a, can be found from the definition of η^2 (Equation A. 4). It is interesting to note that as $\lambda \longrightarrow 1$, $n_a^2 \longrightarrow 0$; and as $\lambda \longrightarrow \infty$, $\eta_a^2 \longrightarrow \infty$.

That is, the heat front traverses an infinitely thin cylinder, ($\lambda = 1$), instantaneously; while for a cylinder with a "pin hole" for an inner port, ($\lambda = \infty$), it takes an infinite time. It is also interesting to note that the expression for η_a^2 (Equation A-10) for external cooling does approach a finite limit as $\lambda \longrightarrow \infty$. That is, the equations for a hollow cylinder given in the main text are also valid for a solid cylinder. This is accomplished by letting $\lambda \longrightarrow \infty$.

Once the temperature front reaches the outer port, a new function must be selected in lieu of Equation (A. 1). This new function must meet the following two requirements:

(1) At r = b, the temperature must equal T_o

(2) Since the outer surface was assumed insulated. the derivative of the temperature with respect to "r" must equal zero at r = b.

Obviously, Equation (A. 1) does not meet these requirements. Hence for all $t \geq t_a$ or $\eta^2 \geq \eta_a^2$ the following thermal field was assumed:

$$T = \frac{T_o}{(b-a)^2} \left\{ \left(1 - \frac{q_4}{T_o} \right) (b-r)^2 + \frac{T_4}{T_o} (b-a)^2 \right\} \qquad \text{(A. 11)}$$

Setting r = b, it is clear that T_4 represents the temperature at the outer insulated surface (Figure A-2) and hence is a function of time. The procedure for finding this functional relationship is similar to that used for $\overline{q}_3$. The result is as follows:

$$T_4 = T_o \left[1 - e^{-\alpha_1 (\overline{\eta}^2 - 1)} \right] \qquad \text{(A. 12)}$$

where

$$\overline{\eta}^2 = \frac{\eta^2}{\eta_a^2} \qquad \text{(A. 13)}$$

$$\alpha_1 = \frac{(\lambda + 3)(\lambda + 2)}{3(11\lambda + 5)} \qquad \text{(A. 14)}$$

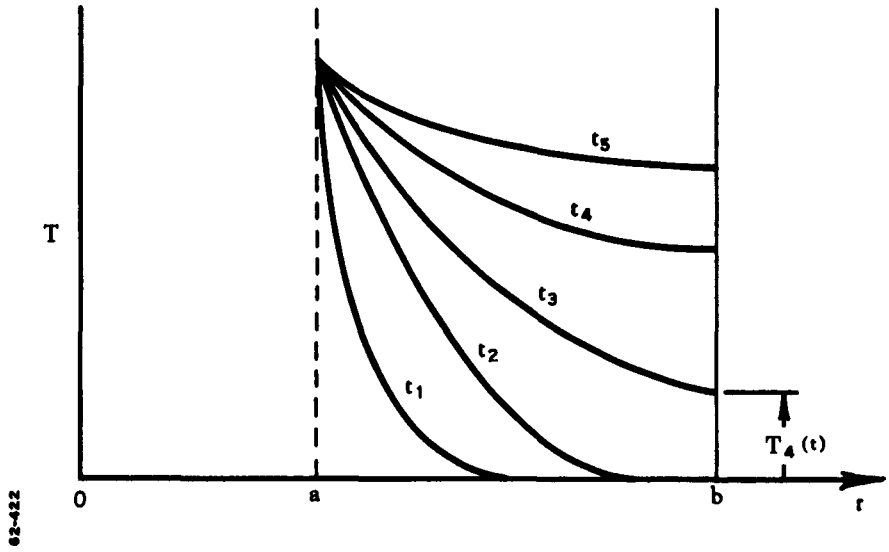

Figure A-2 Outer Surface Temperature Distribution for Various Times

An inspection of Equation (A. 12) reveals that when

$$\eta^2 = \overline{\eta}_a^2$$

or

$$\overline{\eta}^2 = 1$$

then

$$T_4 = 0$$

and when

$$\overline{\eta}^2 > \infty \; ; \; T_4 > T_o$$

since, as stated above, T_4 represents the temperature at the outer surface, the relation for T_4 is physically reasonable. Hence, an approximate solution for this case results from the use of Equations (A. 1), (A. 10) and (A. 11) once $\overline{q}_3$ and T_4 are determined from Equations (A. 3) and (A. 12). The results for a cylinder with a b/a ratio equal to 2 are shown in Figure A-3.

A-2 INTERNAL AND EXTERNAL HEATING OR COOLING

A hollow cylinder whose outer and inner surfaces are subjected to a simultaneous step temperature change is considered. This solution is more complicated than the previous two because instead of one moving heat front there are now two. Hence, it is necessary to choose two functions for the temperature.

The assumed functions are:

$$T_1(r,t) = \begin{cases} T_o \left[1 - \frac{(r-a)}{q_3}\right]^2 & r - a \le q_3 \\ 0 \quad ; & r - a \ge q_3 \end{cases} \qquad \text{(A. 15)}$$

$$T_2(r,t) = \begin{cases} T_o \left[1 - \left(\frac{b-r}{q_1}\right)\right]^2 \quad ; & b - r \le q_1 \\ 0 \quad ; & b - r \ge q_1 \end{cases} \qquad \text{(A. 16)}$$

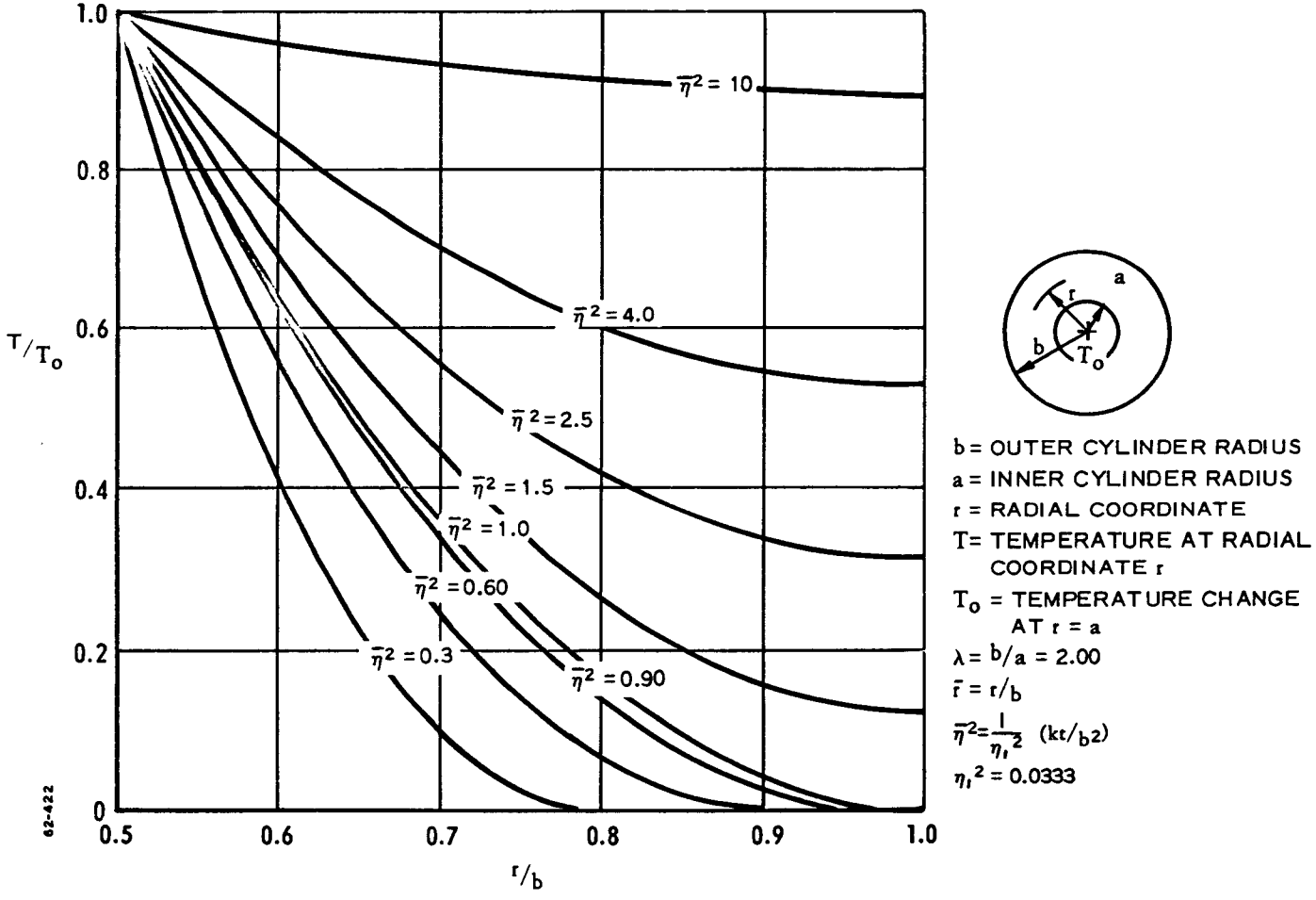

Figure A-3 Time-Temperature Variation in a Hollow Cylinder with Zero Initial Temperature and a Suddenly Applied Surface Temperature, T_o, on the Inner Port (outer surface insulated)

where (Figure A-4)

$T_1(r, t)$ = temperature distribution initiating at the inner port

$T_2(r, t)$ = temperature distribution initiating at the outer surface

q_3 = penetration depth for the heat front proceeding from the inner surface

q_1 = penetration depth for the front moving away from the outer surface

Once again, the heat fronts progress through the web. Before the two fronts meet, material points lying in the region $r - a \leq q_3$ are not "aware" of the conditions on the outer surface. Similarly, material points in the region $b - r \leq q_1$, are not "aware" of the conditions on the inner port. Thus, the variations of q_1 and q_3 with respect to time are the same as those given in Section A. 1 of this appendix and the solution in the main text.

Such is not the case when the two fronts meet. When this occurs, the two aforementioned solutions do not apply. That is, one cannot superimpose those temperature distributions to obtain the distribution for the present case. Since the boundary conditions for those cases are not equivalent conditions for this case, superposition is not valid. Thus, the values of the respective penetration depths and the time must be determined at the instant the two fronts meet. This is accomplished by using Equation (2-10) of Section 2, Volume I, and Equation (A.3) of the present section as follows:

$$\bar{q}_3^3 + 3\bar{q}_3^2 - 30\lambda^2\eta^2 = 0 \qquad \text{(A. 17)}$$

$$\bar{q}_1^3 - 3\bar{q}_1^2 + 30\eta^2 = 0, \qquad \text{(A. 18)}$$

where

$$\bar{q}_3 = q_3/a$$

$$\bar{q}_1 = q_1/b,$$

and from the geometrical fact that when the fronts meet

$$q_1 + q_3 = b-a$$

or

$$\bar{q}_1 + \frac{\bar{q}_3}{\lambda} = \frac{\lambda - 1}{\lambda} \qquad \text{(A. 19)}$$

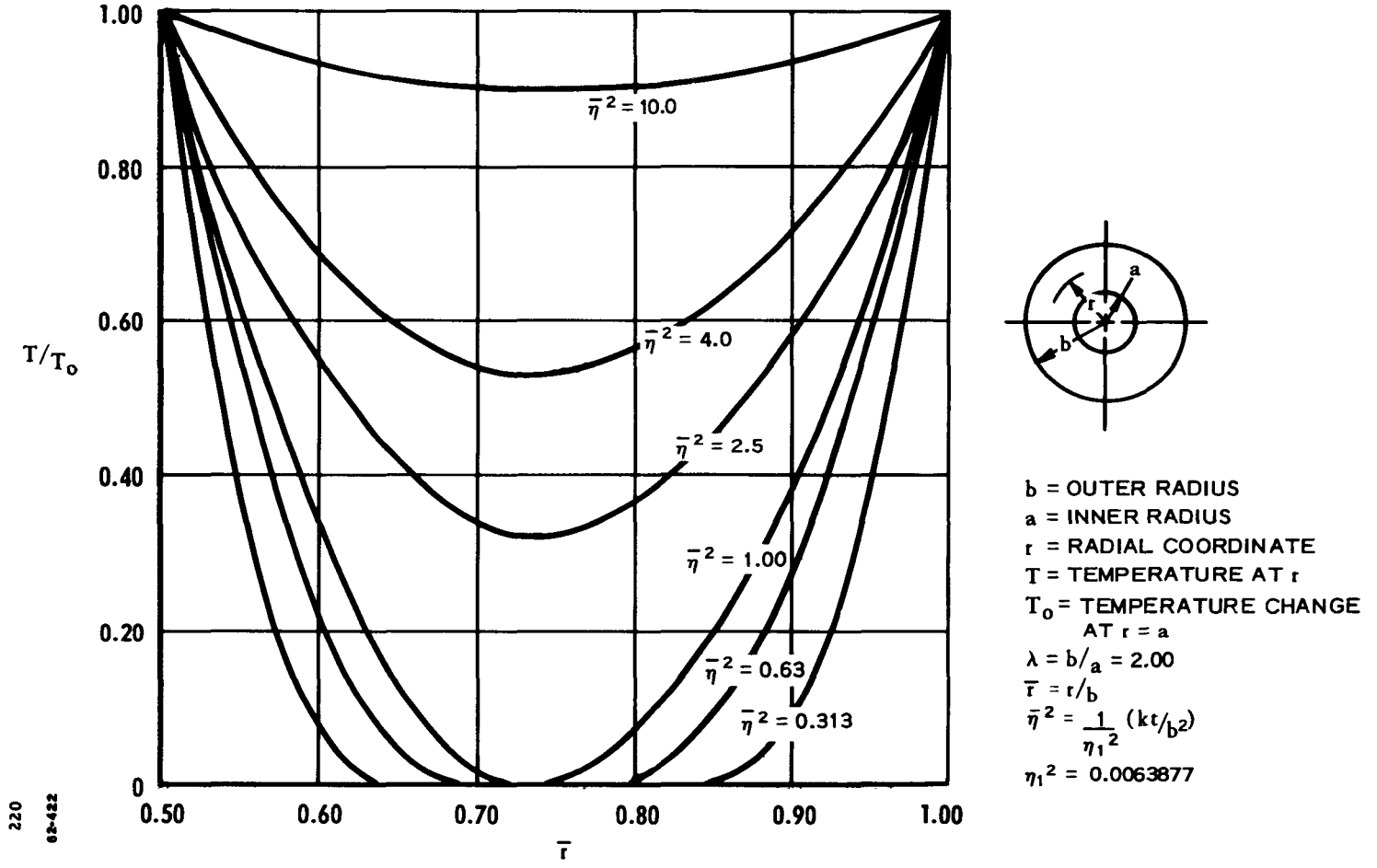

Figure A-4 Time-Temperature Distribution of a Hollow Cylinder with Zero Initial Temperature and a Suddenly Applied Surface Temperature, T_o, on the Outer and Inner Surfaces

The simultaneous solution of Equations (A. 17, 18, 19) for the unknown quantities q_{1a}, q_{3a}, and η_a^2 results in the following:

$$\bar{q}_{3a}^3 + 3\,\bar{q}_{3a}^2 + 3\,\bar{q}_{3a}\,(\lambda+1) - (2\lambda+1)\,(\lambda-1) = 0 \qquad \text{(A. 20)}$$

$$\bar{q}_{1a} = \frac{(\lambda-1) - \bar{q}_{3a}}{\lambda} \qquad \text{(A. 21)}$$

$$\eta_a^2 = \frac{\bar{q}_{3a}^3 + 3\,\bar{q}_{3a}^2}{30\lambda^2} \qquad \text{(A. 22)}$$

where $\bar{q}_{1a}$, $\bar{q}_{3a}$, and η_a^2 are the values of the quantities at the instant the two fronts meet. For example, if $\lambda = 2$, and $b = 1$, the values are:

$$\bar{q}_{3a} = 0.47$$

or

$$q_{3a} = 0.235$$

$$\bar{q}_{1a} = 0.265$$

or

$$q_{1a} = 0.265$$

and

$$\eta_a^2 = 0.00639$$

Thus, the fronts meet slightly to the left of the web midpoint ($r = 0.735$).

Once the fronts meet, two new functions are necessary to describe the temperature. They are as follows:

$$\underline{T_1} = \frac{T_o}{(r_a-a)^2}\left\{\left(1-\frac{T_5}{T_o}\right)[r_a-r]^2 + \frac{T_5}{T_o}[r_a-a]^2\right\} \quad ; \; r \le r_a \qquad \text{(A. 23)}$$

$$\underline{T_2} = \frac{T_o}{(r_a-b)^2}\left\{\left(1-\frac{T_5}{T_o}\right)[r_a-r]^2 + \frac{T_5}{T_o}[r_a-b]^2\right\} \quad ; \; r \ge r_a \qquad \text{(A. 24)}$$

where

r_a = distance from origin at which the two fronts meet

$T_5(t)$ = temperature at $r = r_a$.

The dependence of T_5 with respect to time was found by using the same technique as before. The expression for T_5 for $\lambda = 2$ is

$$T_5 = T_o \left[1 - \bar{e}^{\alpha_1 (\eta^{-2} - 1)} \right] \qquad \text{(A. 25)}$$

where

$$\bar{\eta}^2 = \frac{\eta^2}{\eta_a^2}$$

$$\alpha_1 = 0.2539$$

The thermal distribution for a cylinder with $\lambda = 2$ is given, for various times, in Figure A-4.

Appendix B

ON THE THEORY OF PHOTOVISCOELASTICITY*

Abstract

The general problem of photoviscoelasticity cannot be solved by a simple extension of the experimental and interpretive methods which are used in classical photoelasticity. For viscoelastic materials a complete time history of isochromatics and isoclinics must be recorded. The stress state is then determined by an integral operation.

* Ellis Harold Dill
Department of Aeronautical Engineering
University of Washington

1. Summary

The stress analysis of bodies with irregular boundaries is such a complicated problem that it is frequently desirable to determine the stress state by experiments upon a model. Photoelasticity has been of great value in the design with elastic materials, and it would be desirable to have this tool available in all cases. However, for some materials, including solid propellants, the material from which the prototype is constructed cannot be regarded as an elastic substance, but instead must be treated as a viscoelastic material. In general, the strain state in the viscoelastic material is different from that in an elastic material which is subjected to the same boundary conditions. In such problems the viscoelastic strains cannot be obtained directly from observations on a model made of an elastic material. This problem of correlation between model and prototype would be merely a matter of geometric scaling if the model material has the same mechanical properties as the prototype. It may be possible, for example, to manufacture a model of the desired viscoelastic properties from a high polymer by proper selection of epoxy resin, plasticizer, and hardener.

Photo-analysis is based upon the observation that certain materials exhibit polarization which depends upon the mechanical state variables. Such materials are termed birefringent. They are electromagnetically anisotropic, except perhaps in the natural state. The propagation of a plane electromagnetic wave through a slice of such material is reviewed in Section 2. It is shown that the wave is completely linearly polarized in certain planes. Thus, an incident wave is divided into two waves propagating at different velocities characterized by the principal indices of refraction. By observation on the emanating wave it is possible to determine the refractive indices and thus the dielectric constants.

The principles of linear thermoviscoelasticity are reviewed in Section 3. For linear viscoelastic materials, stress and strain are uniquely related to each other by integral or differential operators.

A viscoelastic material may be expected to exhibit optical as well as mechanical time effects, such as creep at constant stress. The dielectric constants which determine the refractive indices will depend not only on the instantaneous values of the state variables, but also on the history of mechanical states. In the case of linearly viscoelastic materials, the mechanical state variables may be either stress or strain. The one being related to the other uniquely, they are interchangeable. For the small changes in the mechanical state variables which occur in linearly viscoelastic materials, it would be expected that a linear relation between the dielectric properties and the mechanical state variable could be used. The determination of the stress state from observations on the birefringence of materials for which such a relation exist is discussed in Section 4. It is found that the principle axes of stress do not, in general, coincide with the principal axis of polarization as they do in elastic materials. Therefore, the difference in principal stresses

is not determined solely by the difference in the indices of refraction, but also by the angle between the principal axes of polarization and the principal axes of stress. Thus, for practical stress analysis, routine methods of recording both the difference in indices of refraction (relative retardation) and the plane of polarization (isoclinics) as a function of time must be devised.

In the following sections, all quantities are referred to a stationary rectangular cartesian coordinate system $(z^1, z^2, z^3) = (x, y, z)$. Vectors are denoted by subposed tilde. The time is denoted by t. The symbols are defined as they are encountered. Brackets are used in Section 2 to indicate the difference in a quantity on two sides of a surface. The base vectors are denoted by $\underset{\sim}{g}_i$. All indices have the range 1, 2, 3. Repeated indices indicate summation. The symbol $[\underset{\sim}{a}, \underset{\sim}{b}, \underset{\sim}{c}]$ indicates the scalar triple product of the vectors. In Section 2, the dielectric tensor, although dependent on time, is assumed to change slowly compared to the wave speeds and thus can be regarded as constant. The velocity vector is $\underset{\sim}{v}$.

2. Electromagnetic Waves

2.1 Fundamental Equations[1]

The principles of conservation of charge and magnetic flux lead to the following field equations which hold, except on certain singular surfaces:

$$\operatorname{div} \underset{\sim}{J} + \frac{\partial Q}{\partial t} = 0, \tag{2.01}$$

$$\operatorname{curl} \underset{\sim}{E} + \frac{\partial \underset{\sim}{B}}{\partial t} = 0, \tag{2.02}$$

$$\operatorname{div} \underset{\sim}{B} = 0. \tag{2.03}$$

Here, $\underset{\sim}{B}$ is the density of magnetic flux, $\underset{\sim}{E}$ is the electric field, $\underset{\sim}{J}$ is the current density, and Q is the charge density.

These field equations imply the existence of electromagnetic potentials such that

$$\underset{\sim}{B} = \operatorname{curl} \underset{\sim}{A}, \tag{2.04}$$

$$\underset{\sim}{E} = -\frac{\partial \underset{\sim}{A}}{\partial t} - \operatorname{grad} V, \tag{2.05}$$

[1] References are listed at the end of the appendix

$$Q = \text{div } \underset{\sim}{D}, \tag{2.06}$$

$$\underset{\sim}{J} = \text{curl } \underset{\sim}{H} - \frac{\partial \underset{\sim}{D}}{\partial t}. \tag{2.07}$$

Here, $\underset{\sim}{A}$ is the magnetic potential: V is the electric potential; $\underset{\sim}{H}$ is the current potential (usually called the magnetic field intensity); $\underset{\sim}{D}$ is the charge potential (usually called the electric displacement).

The electric field and the magnetic flux density are related to the charge potential and the current potential at all points, inside and outside of the material, by the "aether" relations:

$$\underset{\sim}{D} = \epsilon_0 \underset{\sim}{E}, \tag{2.08}$$

$$\underset{\sim}{H} = \frac{1}{\mu_0} \underset{\sim}{B}. \tag{2.09}$$

ϵ_0 and μ_0 are fundamental constants depending on the units of time, charge, and magnetic flux.

Across a surface of discontinuity, such as the boundary between regions of different material properties, which moves with speed u_n and has the unit normal $\underset{\sim}{\nu}$, the following jump conditions hold:

$$\underset{\sim}{\nu} \times [\underset{\sim}{E}] - u_n [\underset{\sim}{B}] = 0, \tag{2.10}$$

$$[\underset{\sim}{B}] \cdot \underset{\sim}{\nu} = 0, \tag{2.11}$$

$$[\underset{\sim}{J}] \cdot \underset{\sim}{\nu} - u_n [\underset{\sim}{Q}] = 0. \tag{2.12}$$

In addition to these fundamental fields and potentials, constitutive equations defining the electromagnetic nature of the material are required. The formulation of constitutive equations is facilitated by the introduction of certain auxiliary fields and potentials: Let $\underset{\sim}{P}$ be the density of polarization and $\underset{\sim}{M}$ the magnetization field. The polarization current $\underset{\sim}{J}_p$, the bound charge Q_B, and the magnetization current $\underset{\sim}{J}_M$ are given by

$$\underset{\sim}{J}_p = \frac{\partial \underset{\sim}{P}}{\partial t} + \text{curl } (\underset{\sim}{P} \times \underset{\sim}{\nu}), \tag{2.13}$$

$$Q_B = - \text{div } \underset{\sim}{P}, \tag{2.14}$$

$$\underset{\sim}{J}_M = \text{curl } \underset{\sim}{M}. \tag{2.15}$$

The total charge is considered to be made up of the bound charge plus the free charge:

$$Q = Q_B + Q_F \tag{2.16}$$

The total current is the sum of the free, the polarization, and the magnetization currents:

$$\underset{\sim}{J} = \underset{\sim}{J}_F + \underset{\sim}{J}_P + \underset{\sim}{J}_M. \tag{2.17}$$

In terms of the partial potentials $\underset{\sim}{H}'$ and $\underset{\sim}{D}'$ which are defined by

$$\underset{\sim}{H}' = \underset{\sim}{H} - \underset{\sim}{M} - \underset{\sim}{P} \times \underset{\sim}{\nu}, \tag{2.18}$$

$$\underset{\sim}{D}' = \underset{\sim}{D} + \underset{\sim}{P}; \tag{2.19}$$

the free current and free charge are given by

$$\underset{\sim}{J}_F = \text{curl } \underset{\sim}{H}' - \frac{\partial \underset{\sim}{D}'}{\partial t}, \tag{2.20}$$

$$Q_F = \text{div } \underset{\sim}{D}'. \tag{2.21}$$

The jump conditions across a moving surface of discontinuity, with speed u_n and normal $\underset{\sim}{\nu}$ are

$$[\underset{\sim}{D}'] \cdot \underset{\sim}{\nu} = 0, \tag{2.22}$$

$$\underset{\sim}{\nu} \times [\underset{\sim}{H}] + u_n [\underset{\sim}{D}'] = 0. \tag{2.23}$$

2.2 Ideal Dielectrics

An ideal anisotropic dielectric is defined by the equations

$$\begin{aligned} \underset{\sim}{J}_F &= 0, \\ Q_F &= 0, \\ \underset{\sim}{M} &= 0, \\ P_i &= \epsilon_0 p_{ij} E_j. \end{aligned} \tag{2.24}$$

Therefore

$$D_i' = \epsilon_0 K_{ij} e_j, \tag{2.25}$$

where

$$K_{ij} = \delta_{ij} + P_{ij}. \tag{2.26}$$

The fundamental equations for dielectrics are equations (2.25), (2.02), (2.03), and (2.09), combined with equations (2.20) and (2.21) which become

$$\text{curl } \underset{\sim}{H}' - \frac{\partial \underset{\sim}{D}'}{\partial t} = 0, \tag{2.27}$$

$$\text{div } \underset{\sim}{D}' = 0. \tag{2.28}$$

The K_{ij} will be called the dielectric tensor.

2.3 Plane Electromagnetic Wave

Suppose that a dielectric at rest is transversed by a plane electromatnetic wave given by

$$\underset{\sim}{E} = \underset{\sim}{e}\, e^{i\varphi}, \tag{2.29}$$

$$\underset{\sim}{B} = \underset{\sim}{b}\, e^{i\varphi}, \tag{2.30}$$

$$\underset{\sim}{D}' = \underset{\sim}{d}\, e^{i\varphi}, \tag{2.31}$$

$$\underset{\sim}{H}' = \underset{\sim}{h}\, e^{i\varphi}, \tag{2.32}$$

$$\varphi = k\, \underset{\sim}{n} \cdot \underset{\sim}{z} - \omega t. \tag{2.33}$$

The unit vector $\underset{\sim}{n}$ gives the direction of the wave; k is the wave number; ω is the angular frequency; $\underset{\sim}{e}$, $\underset{\sim}{b}$, $\underset{\sim}{d}$, and $\underset{\sim}{h}$ are constant, complex vectors.

Substituting equations (2.29) - (2.33) into equations (2.02) and (2.27) gives

$$k\, \underset{\sim}{n} \times \underset{\sim}{e} = \underset{\sim}{b}\, \omega, \tag{2.34}$$

$$k\, \underset{\sim}{n} \times \underset{\sim}{h} + \omega \underset{\sim}{d} = 0. \tag{2.35}$$

Therefore, $\underset{\sim}{b}$ is perpendicular to $\underset{\sim}{n}$ and $\underset{\sim}{e}$ while $\underset{\sim}{d}$ is perpendicular to $\underset{\sim}{n}$ and $\underset{\sim}{h}$. Equation (2.09) shows that $\underset{\sim}{b}$ is parallel to $\underset{\sim}{h}$ for a dielectric at rest. Thus, $\underset{\sim}{n}$, $\underset{\sim}{d}$, $\underset{\sim}{h}$ are mutually perpendicular and $\underset{\sim}{d}$, $\underset{\sim}{e}$, $\underset{\sim}{n}$ lie in the same plane (Figure B-1).

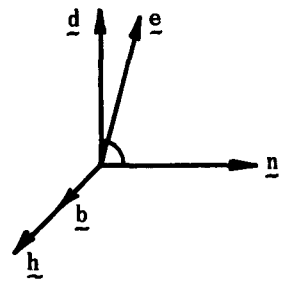

Figure B-1 General Plane Wave

The plane d, h is the wave front. The direction of h is the direction of polarization. The plane n, h is the plane of polarization. The direction of n is the direction of propagation. The direction of e is the direction of vibration.

The constitutive relation for a dielectric, equation (2.25), gives

$$\epsilon_0 e_i = K_{ij}^{-1} d_j. \tag{2.36}$$

Equation (2.36) gives

$$e_i = -\frac{k}{\omega \epsilon_0} K_{ij}^{-1} e_{jrs} n_r h_s. \tag{2.37}$$

Equations (2.09) and (2.35) lead to

$$(\delta_{ik} + N^2 e_{ipq} e_{jrk} K_{qj}^{-1} n_p n_r) h_k = 0. \tag{2.38}$$

Where,

$$N = \frac{kc}{\omega} \tag{2.39}$$

is the index of refraction and

$$c = \sqrt{\frac{1}{\epsilon_0 \mu_0}} \tag{2.40}$$

is the speed of light.

Let us choose z^i to be the principal axes of K_{ij} and consider the case when $\underset{\sim}{n}$ is directed along z. Then equation (2.38) becomes

$$\begin{bmatrix} 1 - N^2/K_2 & 0 & 0 \\ 0 & 1 - N^2/K_1 & 0 \\ 0 & 0 & 1 \end{bmatrix} \begin{bmatrix} h_1 \\ h_2 \\ h_3 \end{bmatrix} = 0 \qquad (2.41)$$

Equations (2.41) and 2.37) show that only two plane waves are possible: Either

$$N = N_1 = \sqrt{K_1},\ h_1 = h_3 = e_2 = e_3 = 0,\ h_2 = N_1 \epsilon_0 e_1, \qquad (2.42)$$

or

$$N = N_2 = \sqrt{K_2},\ h_2 = h_3 = e_1 = e_3 = 0,\ h_1 = -N_2 \epsilon_0 e_2. \qquad (2.43)$$

The direction of polarization coincides with one of the principal axes and the direction of vibration is normal to the wave direction (Figure B-2). Every wave must be a linear combination of these two waves.

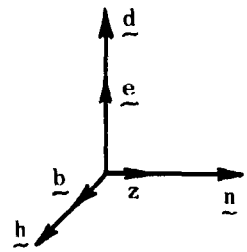

Figure B-2 Plane Wave Propagating Along One Principal Axis, Case 1

In free space $K_{ij} = \delta_{ij}$; therefore N = 1 and $h_3 = e_3 = 0$.

2.4 Plane Polariscope

Suppose a slice of dielectric is bounded by the planes z = 0, h. Consider the case when the coordinate axes are principal axes of the dielectric tensor K_{ij}. By means of a polarizer, a linearly polarized plane electromagnetic wave propagating along the z axis is obtained. Every such wave can be divided into the sum of monochromatic waves and every monochromatic wave can be

decomposed into components, given by equations (2.29) - (2.33), such that the direction of polarizarion of each component coincides with one of the coordinate axes. Let this plane wave be incident on the surface z = 0. In order to satisfy the jump conditions, equations (2.10) and (2.23), there must also be a wave traveling in the opposite direction (reflected).

The electromagnetic field preceding the dielectric, Figure B-3, is therefore the sum of two fields:

$$\underset{\sim}{E} = \underset{\sim}{E}_{(1)} + \underset{\sim}{E}_{(2)} \tag{2.44}$$

where

$$\underset{\sim}{E}_{(1)} = \underset{\sim}{e}_{(1)} e^{i(k_0 z - \omega t)},$$

$$\underset{\sim}{E}_{(2)} = \underset{\sim}{e}_{(2)} e^{i(-k_0 z - \omega t)}.$$

The wave transmitted into the material is itself reflected at the surface z=h. The electromagnetic field in the dielectric material is therefore

$$\underset{\sim}{E} = \underset{\sim}{E}_{(3)} + \underset{\sim}{E}_{(4)} \tag{2.45}$$

where

$$\underset{\sim}{E}_{(3)} = \underset{\sim}{e}_{(3)} e^{i(kz - \omega t)},$$

$$\underset{\sim}{E}_{(4)} = \underset{\sim}{e}_{(4)} e^{i(-kz - \omega t)}.$$

The wave transmitted across the surface z=h gives rise to the electromagnetic field following the dielectric:

$$\underset{\sim}{E} = \underset{\sim}{e}_{(5)} e^{i(k_0 z - \omega t)} \tag{2.46}$$

where

$$k_0 = \frac{\omega}{c}.$$

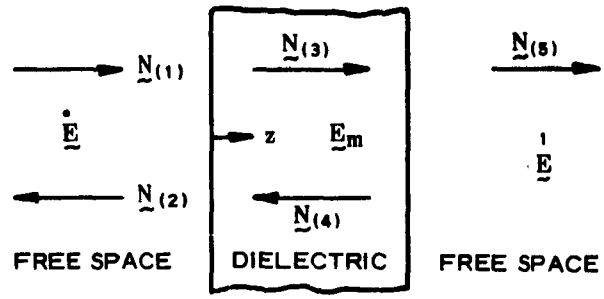

Figure B-3 Directions of Plane Waves

The vectors $\underset{\sim}{e}_{(i)}$ are complex constant vectors which, in the present case, are all directed along the same one of the coordinate lines. The value of k used in equation (2.45) is determined from the appropriate one of equations (2.42) or (2.43). The corresponding magnetic field is determined from equation (2.34).

The jump conditions, applied to the plane z = 0 and to the plane z = h, lead to a set of four vector equations containing the five $\underset{\sim}{e}_{(i)}$ which yield the following result[2]

$$\underset{\sim}{e}(5) = \frac{4N\, e^{-ik_0 h}}{(1+N)^2\, e^{-ikh} - (1-N)^2\, e^{ikh}}\, \underset{\sim}{e}(1) \tag{2.47}$$

If N is of order of magnitude unity, then approximately[3]

$$\underset{\sim}{e}(5) \doteq \frac{4N}{(1+N)^2}\, e^{i(k-k_0)h}\, \underset{\sim}{e}(1). \tag{2.48}$$

The further simplification[4]

$$\underset{\sim}{e}(5) \doteq e^{i(k-k_0)\, h}\, \underset{\sim}{e}(1) \tag{2.49}$$

is also sometimes assumed.

By assigning the appropriate value to k, this result applies to incident waves polarized along either of the coordinate axes.

Consider an incident monochromatic transverse wave obtained by passing monochromatic light through a polarizer:

$$\underset{\sim}{E}_I = (A \cos \alpha \ \underset{\sim}{g}_1 + A \sin \alpha \ \underset{\sim}{g}_2) \ e^{i(k_0 z - \omega t)}. \tag{2.50}$$

where α is the angle between $\underset{\sim}{E}_I$ and the x - axis.

Applying equation (2.47) to each component of the incident wave, the transmitted wave is found to be

$$\underset{\sim}{E}_T = A(c_1 \cos \alpha \underset{\sim}{g}_1 + c_2 \sin \alpha \ \underset{\sim}{g}_2) \ e^{i(k_0 z - \omega t)}; \tag{2.51}$$

where

$$c_1 = \frac{4N_1 \ e^{-ik_0 h}}{(1+N_1)^2 \ e^{-ik_1 h} - (1-N_1)^2 \ e^{ik_1 h}},$$

$$c_2 = \frac{4N_2 \ e^{-ik_0 h}}{(1+N_2)^2 \ e^{-ik_2 h} - (1-N_2)^2 \ e^{ik_2 h}}.$$

Passing this wave through a second polarizer, will give a wave of complex amplitude

$$E = A(c_1 \cos \alpha \cos \beta + c_2 \sin \alpha \sin \beta) \ e^{i(k_0 z - \omega t)} \tag{2.52}$$

where β is the angle between the transmitted wave and the x - axis.

This can be put in the form

$$E = 4 A K_1 \cos \alpha \cos \beta \ e^{i(k_0 z - \omega t - k_0 h + \theta_1)} \tag{2.53}$$

$$+ 4 A K_2 \sin \alpha \sin \beta \ e^{i(k_0 z - \omega t - k_0 h + \theta_2)}$$

where

$$K_n = \frac{N_n}{2\sqrt{4 N_n^2 \cos k_n h + (1 + N_n^2)^2 \sin^2 k_n h}} \tag{2.54}$$

$$\tan \theta_n = \frac{1+N_n^2}{2 N_n} \tan k_n h. \tag{2.55}$$

Either the real or imaginary part of E, equation (2.53), may be regarded as the light transmitted. The imaginary part is

$$I = Q \sin (k_0 z - \omega t - k_0 h - \chi) \tag{2.56}$$

where

$$Q \cos \chi = 4 A K_1 \cos \alpha \cos \beta \sin \theta_1 + 4 A K_2 \sin \alpha \sin \beta \sin \theta_2 ,$$

$$Q \sin \chi = 4 A K_1 \cos \alpha \cos \beta \cos \theta_1 + 4 A K_2 \sin \alpha \sin \beta \cos \theta_2 .$$

Consider the case $\beta = \alpha + \pi/2$, i.e., the first and second polarizers are crossed. Then

$$Q^2 = 4 A^2 \sin^2 \alpha \left[K_1^2 + K_2^2 - 2K_1 K_2 \cos \chi \, n_\pi \right] \tag{2.57}$$

where the fringe order n is defined by

$$n = \frac{\theta_2 - \theta_1}{2\pi} \tag{2.58}$$

Therefore the light intensity is zero where $\alpha = 0, \pi/2$. Lines connecting all such points are called isoclinic lines. The light intensity will be a local minimum where $N_1/N_2 = c_1, c_2, \text{---}$. The lines connecting all such points are called isochromatics.

For the transparent materials used in photoanalysis N_1 is equal to N_2 in the natural state, and both N_1 and N_2 change very little as a result of deformation of the material. In such a case, the minimum values of equation (2.57) occur at integer values of the fringe order n. If N_1 and N_2 are sufficiently close to unity, then equation (2.55) gives

$$n \doteq \frac{h\omega}{2\pi c} (N_2 - N_1). \tag{2.59}$$

Therefore, for materials with an index of refraction which is near unity and which changes only slightly upon deformation, the isochromatic lines occur at definite values of $N_2 - N_1$ as given by equation (2.59).

3. Viscoelasticity

3.1 Fundamental Equations

The principle of conservation of mass leads to the field equation

$$\frac{\partial \rho}{\partial t} + \text{div}\,(\rho \underset{\sim}{v}) = 0 \tag{3.01}$$

where ρ is the density and $\underset{\sim}{v}$ is the velocity vector.

The stress vector $\underset{\sim}{t}$ on a surface with unit normal $\underset{\sim}{n}$ is related to the stress tensor t^{km} by the equation

$$t^{k}_{(\underset{\sim}{n})} = t^{km}\, n_m. \tag{3.02}$$

The principle of conservation of linear and angular momentum leads to the equations of motion:

$$t^{km},_{m} + \rho f^{k} = \rho a^{k}, \tag{3.03}$$

$$t^{km} = t^{mk}, \tag{3.04}$$

where $\underset{\sim}{f}$ is the body force and $\underset{\sim}{a}$ is the acceleration.

In general, the electromagnetic field gives rise to the bory force

$$\underset{\sim}{f} = Q\,\underset{\sim}{E} + \underset{\sim}{J} \times \underset{\sim}{B}.$$

3.2 Constitutive Equations for Deformation[5, 6]

The deviatoric stress σ_{ij} is defined by

$$\sigma_{ij} = t_{ij} - \frac{1}{3}\, t_{kk}\, \delta_{ij}. \tag{3.05}$$

The quantity

$$p = -\frac{1}{3}\, t_{kk} \tag{3.06}$$

is the mean pressure.

The deviatoric strain is defined by

$$\epsilon_{ij} = e_{ij} - \frac{1}{3} e_{kk} \delta_{ij}. \tag{3.07}$$

For small strains, the relative volume dilatation is

$$\frac{dv - dV}{dV} \doteq e_{kk} = e. \tag{3.08}$$

Empirical evidence suggests that, for some materials experiencing isothermal deformation and small displacements, the material is characterized with sufficient accuracy by the relations:

$$\epsilon_{ij} = \int_{-\infty}^{t} \frac{d\sigma_{ij}(x)}{dx} J(t-x)\, dx \tag{3.09}$$

$$e = -\int_{-\infty}^{t} \aleph(t-x) \frac{dp(x)}{dx}\, dx \tag{3.10}$$

The inverse of equations (3.09) and (3.10) has the form

$$\sigma_{ij} = \int_{-\infty}^{t} G(t-x) \frac{d\,\epsilon_{ij}(x)}{dx}\, dx \tag{3.11}$$

$$p = -\int_{-\infty}^{t} K(t-x) \frac{de(x)}{dx}\, dx \tag{3.12}$$

Any material which can be adequately characterized by equations (3.09, 3.10) or by (3.11, 3.12) is called "linear viscoelastic." The kernels of these Duhamel integrals have the names

G(t)	relaxation modulus in shear.
J(t)	creep compliance in shear.
K(t)	bulk relaxation modulus.
$\aleph(t)$	bulk creep compliance.

Alternative notation is

$$G(t) = G_0 + \Phi(t),$$
$$J(t) = J_0 + t/\eta + \Psi(t),$$
etc.

where J_0 is the initial elastic compliance.

η is a Newtonian viscosity coefficient.

Ψ is the creep function, $\Psi(0) = 0$.

G_0 is the equilibrium elastic modulus.

Φ is the relaxation function, $\Phi(\infty) = 0$

This notation has the advantage that the creep function is generally found to be a monotonically increasing function with initial value zero and having monotonically decreasing slope. The relaxation function is then a monotonically decreasing function tending to zero and having monotonically increasing (algebraically) slope.

Each of these quantities is temperature dependent as well as time dependent so that they should be written in the form $G(t, \theta)$, where θ is the absolute temperature. For isothermal deformations, empirical evidence suggests that, for many materials, the temperature dependence can be adequately described with the aid of a "temperature shift function." It is found that, for test at any given temperature, if a reduced time τ defined by

$$\ln\tau = \ln t - f(\theta) \tag{3.13}$$

is introduced; then

$$G(t(\tau)) = \overline{G}(\tau), \tag{3.14}$$

where $\overline{G}(t)$ is the relaxation modulus at a reference temperature θ_0. The function $f(\theta)$ is a monotonically decreasing function of temperature such that $f(\theta_0) = 0$ and is regarded as a material property. The shift factor $a(\theta)$ is defined by

$$\ln a = f(\theta).$$

Then

$$t = a(\theta)\,\tau \tag{3.15}$$

Similar relations are assumed to hold for the bulk modulus. A material characterized by equation (3.14) is said to be thermo-rheologically simple.

Equation (3.14) implies that

$$G(0) = \overline{G}(0) = G_0 + \Phi(0)$$

and

$$G(\infty) = \overline{G}(\infty) = G_0.$$

That is, the initial elastic modulus and final modulus are not affected by temperature changes. Thus, only the relaxation function $\Phi(t)$ need be considered:

$$\Phi(t) = \overline{\Phi}(\tau) \tag{3.16}$$

where $\Phi(t)$ is the relaxation function at the reference temperature θ_0.

Similarly, for the creep compliance:

$$J(t) = \overline{J}(\tau) \tag{3.17}$$

implies J_0 and η are independent of temperature and

$$\Psi(t) = \overline{\Psi}(\tau) \tag{3.18}$$

where $\overline{\Psi}(t)$ is the creep function at the reference temperature θ_0.

3.3 Constitutive Equations for Linear Thermoviscoelasticity

There is a viscous dissipation of energy but if the heat due to this dissipation can be neglected and since the volume changes are small, the temperature distribution is determined by the uncoupled Fourier heat conduction equation.

$$K\theta_{,kk} - \frac{\partial\theta}{\partial t} = 0 \tag{3.19}$$

Thus the temperature may be regarded as a known function of space and time $\theta = \theta(x, t)$. The theory is then rendered complete by specifying a phenomenological relation between stress, strain, and temperature.

The shear creep compliance measured by a creep test at varying temperature is f(t). If the initial and final compliance for a material not experiencing viscous flow are independent of temperature, then $f(0) = \overline{J}(0)$ and $f(\infty) = J(\infty)$, where J(t) is the creep compliance at constant reference temperature θ_0. In this case there is a function $\xi(t)$ called the reduced time such that

$$f(t) = J(\xi(t)) \tag{3.20}$$

and

$$f'(t) = \frac{d\xi}{dt}\overline{J}'(\xi) \tag{3.21}$$

where the prime indicates differentiation with respect to the argument.

The isothermal creep test of a thermo-rheologically simple material (equation 3.17) yields

$$J'(t) = a(\theta)\,\bar{J}'(\tau). \tag{3.22}$$

It is physically appealing to assume that this relation[7] holds also for the creep at non-constant temperature. With this fundamental hypothesis

$$\frac{d\xi}{dt} = a(\theta(t)). \tag{3.23}$$

Therefore

$$\xi(t) = \int_0^t a(\theta(x))\,dx. \tag{3.24}$$

Now suppose that the same temperature field exists, but the load is applied at time τ. The resulting creep compliance is $F(t, \tau)$: The total strain resulting from a continuous distribution of load is then

$$\epsilon_{ij}(t) = \int_0^t F(t, x)\,\frac{d\sigma_{ij}(x)}{d\tau}\,dx. \tag{3.25}$$

With assumption $F(\tau, \tau) = \bar{J}(0)$ and $F(\infty, \tau) = \bar{J}(\infty)$, there exists a function $\xi(t, \tau)$ such that

$$F(t, \tau) = \bar{J}(\xi). \tag{3.26}$$

and

$$\frac{dF(t, \tau)}{dt} = \frac{d\xi}{dt}\,\bar{J}'(\xi). \tag{3.26a}$$

According to the fundamental hypothesis

$$\frac{d\xi}{dt} = a(\theta(t)). \tag{3.27}$$

Since $F(\tau, \tau) = \bar{J}(0)$, $\xi = 0$ at $t = \tau$.

Therefore

$$\xi(t, \tau) = \int_\tau^t a(\theta(\eta))\,d\eta \tag{3.28}$$

$$= \xi(t) - \xi(\tau)$$

and

$$F(t, \tau) = \bar{J}(\xi(t) - \xi(\tau)). \tag{3.29}$$

Introducing the notation

$$\bar{\epsilon}_{ij}(\xi(t)) = \epsilon_{ij}(t) \tag{3.30}$$

$$\bar{\sigma}_{ij}(\ (t)) = \sigma_{ij}(t) \tag{3.31}$$

the constitutive equation becomes

$$\bar{\epsilon}_{ij}\ (\xi) = \int_0^{\xi} \bar{J}(\xi - \eta)\ \frac{d\bar{\sigma}_{ij}\ (\eta)}{d\eta}\ d\eta \tag{3.32}$$

The fundamental constitutive equation for thermoviscoelasticity is therefore equation (3.25) which, under the fundamental hypothesis, can be put into the form (3.32) for thermo-rheologically simple materials.

4. Photothermoviscoelasticity

4.1 Dielectric Constitutive Equations for Isothermal Deformations

Experimental evidence suggests that certain polymers exhibit polarization under isothermal deformations which depend upon the history of deformation. This suggests that a relationship exists between the dielectric tensor and the strain tensor similar to that for linear viscoelasticity.

Let N_{ij} be a tensor called the refraction tensor whose principal axes coincide with those of the dielectric tensor K_{ij}, and such that the principal values N_i of N_{ij} are related to the principal values K_i of K_{ij} by

$$N_i = \sqrt{K_i} \tag{4.01}$$

Denote the deviatoric part of N_{ij} by $\bar{N}_{ij}$ and let $N = \frac{1}{3} N_{kk}$.

Consider the hypothesis

$$\bar{N}_{ij} = \int^{t} \chi(t-\tau)\ \frac{d}{d\tau}\ [\ \epsilon_{ij}(\tau)\ ]\ d\tau\ , \tag{4.02}$$

$$N\ \ = \int^{t} \Delta(t-\tau)\ \frac{d}{d\tau}\ [e(\tau)]\ d\tau\ . \tag{4.03}$$

where $\chi(t)$ is the optical-relaxation function,

$\Delta(t)$ is the optical-volume-relaxation function.

Denote the Laplace transform of a function by a superposed asterisk. Then

$$\overline{N}^{*}_{ij} = p\, \chi^{*}\, \epsilon^{*}_{ij} \tag{4.04}$$

where p is the transform variable. From equation (3.13)

$$\epsilon^{*}_{ij} = pJ^{*}\, \sigma^{*}_{ij}. \tag{4.05}$$

Therefore

$$\sigma^{*}_{ij} = p\, \Gamma^{*}\, N^{*}_{ij}, \tag{4.06}$$

where

$$\Gamma^{*} = \frac{1}{p^{3}\, \chi^{*}\, J^{*}}\ .$$

The inverse transform gives

$$\sigma_{ij}(t) = \int_{0}^{t} \Gamma(t-\tau)\, \frac{d}{d\tau}\, [\overline{N}_{ij}(\tau)]\, d\tau\ . \tag{4.07}$$

Thus, a unique relation between the polarization and the history of deformation implies a unique relation between stress and the history of polarization and inversely.

Both the function $\chi(t)$ and $\Gamma(t)$ may be expected to depend on the temperature. Analogous to the situation for the mechanical state the existence of an optical-temperature shift factor $b(\theta)$ may be supposed such that

$$\chi(t) = \overline{\chi}\, (b\, (\theta)t) \tag{4.08}$$

where $\overline{\chi}(t)$ is the optical-relaxation function at temperature θ_0 and $\chi(t)$ is the optical-relaxation function at temperature θ.

Similarly

$$\Gamma(t) = \overline{\Gamma}\, (b\, (\theta)t). \tag{4.09}$$

4.2 Dielectric Constitutive Equations for Thermal Stress

Consider deformations that occur in the presence of varying temperatures $\theta(t)$. If the polarization at various strain levels but the same temperature history can be superimposed, the constitutive equation for the isothermal deformations (4.02) becomes

$$\overline{N}_{ij} = \int_0^t f(t,\tau)\,\frac{d}{d\tau}\,[\,\epsilon_{ij}(\tau)]\,d\tau\,. \tag{4.10}$$

The function $f(t,\tau)$ may in general depend upon the history of temperature.

In the case of thermo-rheologically simple materials, it may be that a reduced time $\rho(t)$ exists, in general different from that for mechanical case, such that

$$f(t,\tau) = \overline{\chi}\,(\rho(t,\tau)), \tag{4.11}$$

$$\rho(t,\tau) = \int_\tau^t b(\theta\ (t))\ dt. \tag{4.12}$$

In this event, the optical properties are completely characterized by optical-relaxation function at reference temperature θ, $\overline{\chi}(t)$, and the optical-temperature shift factor $b(\theta)$. Equation (4.10) can then be written in a form similar to equation (3.36):

$$\overline{\overline{N}}_{ij}\,(\eta) = \int_0^\eta \overline{\chi}\,(\eta-\tau)\,\frac{d}{d\tau}\,[\overline{\overline{\epsilon}}_{ij}(\tau)]\ d\tau\,. \tag{4.13}$$

where

$$\eta(t) = \int^t b(\theta\ (t)\ )\ dt,$$

$$\overline{\overline{N}}_{ij}\,(\eta) = \overline{N}_{ij}\,(t\,(\eta)\ ),$$

$$\overline{\epsilon}_{ij}\,(\eta) = \overline{\epsilon}_{ij}(t\,(\eta)\ ).$$

If the temperature shift factors $a(\theta)$ and $b(\theta)$ are different, no simple transformation to the form analogous to equation (4.07) exist. But if $a(\theta) = b(\theta)$, then $\eta(t) = \xi(t)$. Taking the Laplace transform with respect to ξ of equation (4.13) and equation (3.36) gives

$$\overline{\overline{N}}^*_{ij} = p\,\overline{\chi}^*\,\overline{\epsilon}^*_{ij}, \tag{4.14}$$

$$\overline{\epsilon}^*_{ij} = p\,\overline{J}^*\,\overline{\sigma}^*_{ij}. \tag{4.15}$$

Therefore

$$\bar{\sigma}^*_{ij} = p\,\Gamma^*\,\bar{\bar{N}}^*_{ij}, \tag{4.16}$$

where

$$\bar{\Gamma}^* = \frac{1}{p^3\,\bar{X}^*\,\bar{J}^*}\ .$$

The inverse transformation gives

$$\bar{\sigma}_{ij}(\xi) = \int_0^{\xi} \bar{\Gamma}(\xi - \tau)\,\frac{d}{d\tau}\,[\,\bar{\bar{N}}_{ij}(\tau)\,]\,d\tau\ . \tag{4.17}$$

4.3 Principal Axes

Let z^i be the fixed rectangular cartesian axis with $z^3 = z$. Consider the plane stress problem and take $z^3 = z$ normal to the plane of the stress field. Suppose that z is a principal axis of σ_{ij}, ϵ_{ij}, and N_{ij}. Let x^i be the principal axis of strain, $x^3 = z^3$, and let α be the angle from z^1 to x^1. Let y^i be the principal axis of stress, $y^3 = z^3$, and let β be the angle from z^1 to y^1. Let x^i be the principal axis of N_{ij}, $x^3 = z^3$, and γ be the angle from z^1 to x^1.

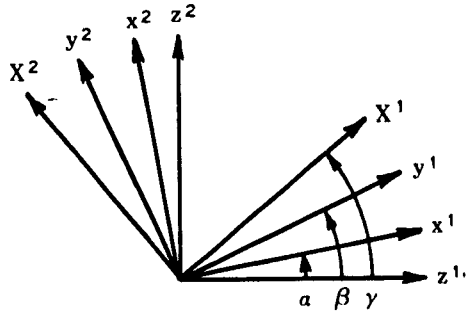

Figure B-1 Principal Axes

In a manner similar to that of Section 3.4, it follows from equation (4.07) that

$$\sigma_{11}(t) - \sigma_{22}(t) = \int_0^t \Gamma(t-\tau)\,\frac{d}{d\tau}\,[\,(N_1(\tau) - N_2(\tau))\cos 2\gamma(\tau)\,]\,d\tau, \tag{4.18}$$

$$\sigma_{12}(t) = \int_0^t \Gamma(t-\tau)\,\frac{d}{d\tau}\,[\,(N_1(\tau) - N_2(\tau))\sin 2\gamma(\tau)\,]\,d\tau\ . \tag{4.19}$$

Using equations (3.32) and (3.33), it is seen that a knowledge of the angle $\gamma(t)$ and the difference $N_1(t) - N_2(t)$, of the principal values of N_{ij}, as a function of time is necessary and sufficient to determine the difference in principal stresses and the principal axes of stress in the isothermal case.

A similar reasoning applies to the transient temperature case when equation (4.17) may be used.

4.4 Experimental Procedure

The model is placed in a standard plane polariscope and subjected to a desired loading and heating sequence. The isoclinic and isochromatic patterns will vary with time. A complete record of the time variation of the fringe order $n(t)$ and the axis of polarization $\gamma(t)$ at a point is made. This will require a more elaborate recording device than is normally used with the polariscope. For a given model thickness h, equations (2.59) and (2.55) determine a value for $N_1(t) - N_2(t)$. Equations (4.18) and (4.19) may then be used in the isothermal case to determine the difference in principal stresses $\sigma_1(t) - \sigma_2(t)$ and the axis of principal stress $\beta(t)$ as functions of time. To determine the material optical properties, this procedure is applied to any configuration for which the stress is known; for example, a creep test.

REFERENCES:

1. C. Truesdell and R. Toupin: "The Classical Field Theories." Encyclopedia of Physics, V. III/1, p. 660-689, Springer-Verlag, Berlin, 1960.

2. J. A. Stratton: Electromagnetic Theory, sect. 9.10, 1st ed., McGraw-Hill, 1941.

3. E. G. Coker and L. N. G. Filon: Photo-Elasticity, sec. 1.33-1.34, 2nd ed., Cambridge University Press, 1957

4. T. J. Dolan and W. M. Murray: "Photoelasticity." Handbook of Experimental Stress Analysis, p. 828-924, ed. by M. Hetényi, John Wiley and Sons, Inc., New York, 1950.

5. A. J. Staverman and F. Schwarzl: "Linear Deformation Behavior of High Polymers." Die Physik der Hochpolymeren, p. 1-125, ed. by H. Stuart, Springer-Verlag, Berlin, 1956.

6. B. Gross: Theories of Viscoelasticity. Publications de l'Institut National de Technologie Brésil, Hermann and Co., Paris, 1953.

7. L. W. Morland and E. H. Lee: "Stress Analysis for Linear Viscoelastic Materials with Temperature Variation." Trans. Soc. Rheology, V. 4, p. 233-263, 1960.

LPC
578-F
10 May '63

UNCLASSIFIED

Lockheed Propulsion Company, P.O. Box 111, Redlands, California
"THERMAL GRAIN STRUCTURAL ANALYSIS," 10 May 1963
Final Report. Period Covered: 6 December 1961 through 28 February 1963. [423] p. 2 tables, 54 figures. Contract No. AF 04(611)-8013)

CONFIDENTIAL REPORT

Volumes 1 and 2 present the formulation, theoretical solution, mathematical analysis, and experimental confirmation of the problem of stress analysis for a real viscoelastic, case-bonded solid propellant grain subjected to an arbitrarily time-varying thermal input. In engineering handbook form Volume 3 presents simplified methods of determining the above, including simplified methods for obtaining the viscoelastic material operators from laboratory data. Volume 3-A (Classified) presents specific solutions for selected large booster motors. A Theoretical treatment of dynamic birefringence (photoviscoelasticity) is given in an appendix to Volume 1.

UNCLASSIFIED

LPC
578-F
10 May '63

UNCLASSIFIED

Lockheed Propulsion Company, P.O. Box 111, Redlands, California
"THERMAL GRAIN STRUCTURAL ANALYSIS," 10 May 1963
Final Report. Period Covered: 6 December 1961 through 28 February 1963. [423] p. 2 tables, 54 figures. Contract No. AF 04(611)-8013)

CONFIDENTIAL REPORT

Volumes 1 and 2 present the formulation, theoretical solution, mathematical analysis, and experimental confirmation of the problem of stress analysis for a real viscoelastic, case-bonded solid propellant grain subjected to an arbitrarily time-varying thermal input. In engineering handbook form Volume 3 presents simplified methods of determining the above, including simplified methods for obtaining the viscoelastic material operators from laboratory data. Volume 3-A (Classified) presents specific solutions for selected large booster motors. A theoretical treatment of dynamic birefringence (photoviscoelasticity) is given in an appendix to Volume 1.

UNCLASSIFIED

LPC
578-F
10 May '63

UNCLASSIFIED

Lockheed Propulsion Company, P.O. Box 111, Redlands, California
"THERMAL GRAIN STRUCTURAL ANALYSIS," 10 May 1963
Final Report. Period Covered: 6 December 1961 through 28 February 1963. [423] p. 2 tables, 54 figures. Contract No. AF 04(611)-8013)

CONFIDENTIAL REPORT

Volumes 1 and 2 present the formulation, theoretical solution, mathematical analysis, and experimental confirmation of the problem of stress analysis for a real viscoelastic, case-bonded solid propellant grain subjected to an arbitrarily time-varying thermal input. In engineering handbook form Volume 3 presents simplified methods of determining the above, including simplified methods for obtaining the viscoelastic material operators from laboratory data. Volume 3-A (Classified) presents specific solutions for selected large booster motors. A theoretical treatment of dynamic birefringence (photoviscoelasticity) is given in an appendix to Volume 1.

UNCLASSIFIED

LPC
578-F
10 May '63

UNCLASSIFIED

Lockheed Propulsion Company, P.O. Box 111, Redlands, California
"THERMAL GRAIN STRUCTURAL ANALYSIS," 10 May 1963
Final Report. Period Covered: 6 December 1961 through 28 February 1963. [423] p. 2 tables, 54 figures. Contract No. AF 04(611)-8013)

CONFIDENTIAL REPORT

Volumes 1 and 2 present the formulation, theoretical solution, mathematical analysis, and experimental confirmation of the problem of stress analysis for a real viscoelastic, case-bonded solid propellant grain subjected to an arbitrarily time-varying thermal input. In engineering handbook form Volume 3 presents simplified methods of determining the above, including simplified methods for obtaining the viscoelastic material operators from laboratory data. Volume 3-A (Classified) presents specific solutions for selected large booster motors. A theoretical treatment of dynamic birefringence (photoviscoelasticity) is given in an appendix to Volume 1.

UNCLASSIFIED